Layered Double Hydroxide-Based Nanomaterials for Biomedical Applications

Tingting Hu,[a] Zi Gu,[b] Gareth R. Williams,[c] Margarita Strimaite,[c] Jiajia Zha,[d] Zhan Zhou,[e] Xingcai Zhang,*[fg] Chaoliang Tan*[dhi] and Ruizheng Liang*[a]

[a] *State Key Laboratory of Chemical Resource Engineering, Beijing Advanced Innovation Center for Soft Matter Science and Engineering, Beijing University of Chemical Technology, Beijing 100029, P. R. China.*
E-mail: liangruizheng2000@163.com

[b] *School of Chemical Engineering and Australian Centre for NanoMedicine (ACN), University of New South Wales, Sydney, NSW 2052, Australia.*

[c] *UCL School of Pharmacy, University College London, 29-39 Brunswick Square, London WC1N 1AX, UK.*

[d] *Department of Electrical Engineering, City University of Hong Kong, 83 Tat Chee Avenue, Kowloon, Hong Kong. E-mail: chaoltan@cityu.edu.hk*

[e] *College of Chemistry and Chemical Engineering, Henan Key Laboratory of Function-Oriented Porous Materials, Luoyang Normal University, Luoyang, 471934, PR China.*

[f] *School of Engineering and Applied Sciences, Harvard University, Cambridge, Massachusetts 02138, USA. E-mail: xingcai@mit.edu*

[g] *School of Engineering, Massachusetts Institute of Technology, Cambridge, Massachusetts 02139, USA.*

[h] *Center of Super-Diamond and Advanced Films (COSDAF), City University of Hong Kong, Kowloon, Hong Kong.*

[i] *Shenzhen Research Institute, City University of Hong Kong, Shenzhen, 518057 P. R. China.*

Against the backdrop of increased public health awareness, inorganic nanomaterials have been widely explored as promising nanoagents for various kinds of biomedical applications. Layered double hydroxides (LDHs), with versatile physicochemical advantages including excellent biocompatibility, pH-sensitive biodegradability, highly tunable chemical composition and structure, and easy of composite formation with other materials, have shown great promise in biomedical applications. In this review, we comprehensively summarize the recent advances in LDH-based nanomaterials for biomedical applications. Firstly, the material categories and advantages of LDH-based nanomaterials are discussed. The preparation and surface modification of LDH-based nanomaterials, including pristine LDHs, LDH-based nanocomposites and LDH-derived nanomaterials, are then described. Thereafter, we systematically describe the great potential of LDHs in biomedical applications including drug/gene delivery, bioimaging diagnosis, cancer therapy, biosensing, tissue engineering, and anti-bacteria. Finally, on the basis of the current state of the art, we conclude with insights on the remaining challenges and future prospects in this rapidly emerging field.

1. Introduction

Layered double hydroxides (LDHs) are a type of host-guest layered material, which consist of positively charged host layers with guest anions and water molecules intercalated in interlayer galleries.[1] The brucite-like host layers consist of edge-sharing $M(OH)_6$ octahedra, and the three-dimensonal (3D) layered structure arises due to the electrostatic attraction between the cationic host layers and the anionic guest molecules. As shown in Fig. 1, the chemical formula of LDHs is generally described as $[M^{2+}_{1-x}M^{3+}_{x}(OH)_2]^{x+}[A^{n-}]_{x/n} \cdot mH_2O$, in which M^{2+} (e.g., Mg^{2+}, Ca^{2+}, Mn^{2+}, Fe^{2+}, Co^{2+}, Ni^{2+}, Cu^{2+} or Zn^{2+}) and M^{3+} (e.g., Al^{3+}, Cr^{3+}, Mn^{3+}, Fe^{3+}, Co^{3+}, Ga^{3+}, In^{3+} or Gd^{3+}) represent divalent and trivalent metal cations located in the host layers, and A^{n-} stands for exchangeable anions (e.g., nitrate ions (NO_3^-), carbonate ions (CO_3^{2-}), chloride ions (Cl^-), *etc.*) present in the interlayer region for neutralizing the positive charge of the layers. *X* is determined by the molar ratio of $M^{3+}/(M^{2+}+M^{3+})$. Typically, *X* falls within the range of 0.2−0.33, in which the M^{2+}/M^{3+} ratio is 2−4 and LDHs with high purity and excellent crystallization can be obtained.[2-4] Rarely, LDHs with M^{2+}/M^{3+} ratio of 5 can also be synthesized.[5] The chemical composition, crystal structure, size, morphology, interlayer spacing and anion exchange capacity of LDHs are tunable by changing the type, charge and ratio of metal cations, the charge and orientation of interlamellar anions as well as the relative content of water molecules.

LDHs were discovered 100 years ago, and have attracted great interest from physicists and chemists since 1960s. In 1842, Hochstetter first discovered natural hydrotalcite minerals from schist.[6] In 1942, Feitknecht *et al.* artificially synthesized MgAl-LDHs for the first time through the reaction of metal salt solution with alkali metal hydroxide, and proposed a layered structure model.[7] This model was confirmed in 1969, when Allmann *et al.* solved the crystal structure of single-crystalline MgAl-LDHs.[8] In the 1970s and 1980s, Miyata *et al.* conducted detailed studies on the structure of MgAl-LDHs and carried out exploratory work on their application as a new type of catalyst.[9] In the 1990s, the widespread application of modern analytical techniques and advanced characterization tools allowed for more detailed research on the structure and properties of LDHs, and the flexibility and variability of their layered structure were fully revealed.

In 1994, Duan *et al.* took the lead in carrying out the engineering and industrialization research of LDHs, realizing their structural innovation and breaking through key preparation technologies.[10] In 1999, they further discovered the intercalation properties of LDHs and then successfully constructed a series of LDH-based advanced functional materials with supramolecular intercalation structures.[11] Since the mid-20th century, LDHs have been extensively explored and shown great potential in a variety of applications, including optics, energy storage and conversion, environmental remediation, and catalysis, by virtue of their special layered structure, tunable chemical composition and appealing physicochemical properties (e.g., light, thermal, magnetic and ultrasonic response).[12-21]

Since Choy *et al.* proposed the concept of "bio-ceramic nanohybrids" in 1999,[22] multifunctional nanomaterials with a layered structure have been greatly explored for biomedical applications. Compared to more widely explored layered nanomaterials (e.g., graphene, transition metal oxides (TMOs), silicate clays, *etc.*),[23-27] LDHs possess many advantages such as excellent biocompatibility, biodegradability, anion exchange capacity, pH-sensitivity response, and easy surface modification.[28-30] The first biomedical application of LDHs was their use as active ingredients in antacids and anti-pepsin agents in the early 2000s.[31-33] MgAl-LDH-contained anti-gastric acid drugs can significantly raise the pH of the stomach to relieve stomach pain, indigestion, heartburn and other symptoms associated with hyperacidity. Since then, the extraordinary properties of LDHs have been exploited to a wide range of biomedical applications including drug/gene delivery, tumor imaging, cancer therapy, biosensing, anti-bacteria, and tissue engineering (Fig. 2).[34-38] The application of LDHs as biocompatible vectors for gene delivery was for the first time reported in 1999 by Choy *et al.* who used MgAl-LDH hybrids to load DNA *via* ion-exchange.[22] Later on, the modification of MgAl-LDH nanoparticles with fluorescein isothiocyanate (FITC) (FITC-LDH) for bioluminescence imaging was reported by the same group in 2000.[39] In 2004, Choy *et al.* described the synthesis of methotrexate (MTX)-incorporated MgAl-LDH (MTX-LDH) for chemotherapy.[40] It was the first time that LDHs were utilized as drug delivery systems. Shortly afterwards, pioneering studies on synthesis of drug-loaded LDHs for

cardiovascular disease (low molecular weight heparin (LMWH)-loaded MgAl-LDH) and bone repair (MgFe-LDHs) were reported.[41,42] In 2011, MgAl-LDH containing DNA vaccines were successfully formulated for immunotherapy for the first time.[43] In the past decade, various new cancer therapies, biosensing, and anti-bacteria based on LDHs have been developed.

Our group has also carried out a series of works in this promising field. For example, in 2014, we first synthesized zinc phthalocyanines (ZnPc)-intercalated MgAl-LDH (ZnPc/LDH) as supramolecular photosensitizers (PSs) for photodynamic therapy (PDT), which displayed high stability, good biocompatibility and excellent anticancer behavior.[44] In 2017, a Mn^{2+}-containing LDH nanoparticle has been described as a superior magnetic resonance imaging (MRI) contrast agent that sensitively respond to a very weakly acidic tumor microenvironment (TME, characterized by the overexpression of H_2O_2 and glutathione (GSH), hypoxia and mild acidity).[45] Subsequently, we first reported an near infrared laser (NIR)-activated PS (isophthalic acid (IPA)-intercalated ZnAl-LDH) with an ultrahigh singlet oxygen ($^1O_2$) quantum yield for two-photon PDT in 2018.[46] In the same year, Gd^{3+}-doped MgAl-LDH nanosheets were prepared as drug carriers to co-load doxorubicin (DOX, a chemotherapy drug) and indocyanine green (ICG, a photothermal agent) with ultrahigh drug loading content (797.36%) and encapsulation efficiency (99.67%).[47] This was the highest drug loading level at nearly 100% encapsulation efficiency among the two-dimensional (2D) drug delivery systems reported at that time. Also, we for the first time reported a peroxidase-like Fe^{2+}-containing LDH nanozyme that was shown to be biodegradable and exhibit high catalytic activity to efficiently generate abundant hydroxyl radicals (·OH) under the acidic TME, thereby selectively killing tumor cells.[48] In 2020, a highly dispersed nanoenzyme (GOD/CoFe-LDHs) with high ·OH generation efficiency was also developed by assembling natural glucose oxidase (GOD) onto CoFe-LDH monolayer nanosheets for tumor-specific therapy.[49] Most recently, we first reported a novel defect-rich CoMo-LDH nanosheet, which was activated *via* acid etching-induced defect engineering, as a highly active inorganic PS for PDT in the third near-infrared (NIR-III) window (1350–1870 nm).[50] The defect-rich CoMo-LDH

exhibited excellent activity for generation of reactive oxygen species (ROS) under 1567 nm laser irradiation, making it a potential PS for NIR-III PDT to efficiently induce cancer cells apoptosis *in vitro* and eliminate tumors *in vivo*. Therefore, LDH-based nanomaterials have been demonstrated to be one of the most promising platforms featured with biodegradability, high drug loading capacity, tunable physiochemical structure, and desirable biosafety for biomedical applications.

Due to recent remarkable progresses in the field, we believe that an up-to-date and well-focused Review on this topic is of great importance for its future development. Although several reviews on the biomedical applications of LDHs have been published, their focus mainly on targeting strategies, or a particular application such as drug delivery, cancer therapeutics, biomedical imaging, or biosensing.[30,34,35,51] For example, in a review reported by Cao *et al.* in 2019,[29] they only focused on LDH-based diagnostic probes and therapeutic agents for biomedical applications. Focusing on biomolecule-intercalated 2D LDHs, they introduced surface engineering strategies for improved stability and targeting strategies for enhanced tumor accumulation, and only discussed their research progress in theranostic and immunotherapy.

In this review, we aim to provide a comprehensive and in-depth summary of the state-of-the-art progress of LDH-based nanomaterials for biomedical applications. Firstly, all the LDH-based nanomaterials used in biomedical field are classified according to their structure and composition, followed by the detailed discussion of their advantages in this field. Then, all their synthesis strategies and surface modification are systematically described. Subsequently, the great potential of LDH-based nanomaterials for various biomedical applications including drug/gene delivery, bioimaging, cancer therapy, biosensing, anti-bacteria and tissue engineering is discussed in depth. Finally, on the basis of the current research status of LDHs, this Review is concluded with insights on the current challenges and future prospects in this rapidly expanding field.

2. Material categories and advantages

2.1. Material categories

To date, a variety of LDH-based nanomaterials with different chemical compositions and diverse morphologies have been prepared by various kinds of synthetic methods.

According to their components, LDH-based nanomaterials can be classified into three broad groups: pristine LDHs, LDH-based nanocomposites, and LDH-derived nanomaterials. Pristine LDHs, which are not modified with any additional materials, can be further categorized into binary, ternary and quaternary subcategories. Binary LDHs, such as MgAl-LDH, CoMn-LDH, and NiFe-LDH, are composed of only one divalent and one trivalent metal cations.[11,52,53] The physicochemical properties of binary LDHs can be customized by introducing a third or fourth cation, resulting in the formation of ternary or quaternary LDHs, such as MgAlGd-LDH, CoFeMn-LDH and MgAlGdYb-LDH.[47,54,55] Considering the charged layered structure of LDHs, they can serve as an ideal platform to construct LDH-based nanocomposites.[4] For example, hybridizing LDHs with other nanomaterials like carbon materials (e.g., graphitic carbon nitride (*g*-C_3N_4), carbon nanotubes, and graphene oxide (GO)), metal-based materials (including metal, metal oxides, metal sulfide and phosphide), organic materials or polymers is a typical way to obtain LDH-based nanocomposites.[56-59] Intercalating guest species, such as drugs and nucleic acids, into LDHs is another way to prepare LDH-based nanocomposites.[22,44,46] Interestingly, LDHs can also be used as sacrificial templates to prepare LDH-derived nanomaterials, including mixed metal oxides (MMOs) and transition metal chalcogenides (TMCs).[54,60]

According to their structures, pristine LDHs can be categorized as bulk LDHs (where each crystal contains many layers), ultrathin 2D nanosheets (which are only several or single-layer(s) thick), and LDHs with hollow structures (where the LDHs have been grown on a sacrificial template, which is then removed). According to the combination modes between LDHs and other materials, LDH-based nanocomposites can be categorized into intercalated LDHs, nanomaterial@LDHs (nanomaterials functionalized with LDHs), and LDHs@nanomaterial (LDHs functionalized with nanomaterials). For LDH-derived nanomaterials, such as MMOs and TMCs derived from LDH precursors through topotactic transformation, their ultrathin 2D morpholoty remains unchanged, thus inheriting the structure of LDH precursors.

2.2. Advantages of LDH-based nanomaterials for biomedical applications

Owning to their tunable chemical composition and physicochemical properties, LDH-

based nanomaterials exhibit some advantages for biomedical applications, which are schematically shown in Fig. 3. These may be summarized as follows:

(1) The high biocompatibility and low cytotoxicity of LDHs ensure the biosafety of LDH-based nanomaterials. As a typical example, MgAl-LDH is one of the major ingredients in commercial anti-gastric oral drugs, i.e., Hydrotalcite Chewable Tablets, proving the excellent *in vivo* biosafety of LDHs. It is worth pointing out that the biocompatibility of LDHs with different chemical compositions and structures/sizes is slightly different. The cytotoxicity of MgAl-LDHs (80–120 nm) on healthy cells has been reported to be relatively low, without significant cytotoxic effect (cell viability ≈ 100%) even at a concentration as high as 0.5 mg mL^{-1}.[61] Rrecently reported CoMo-LDH nanosheets (50–80 nm) showed negligible cytotoxicity against cancer cells with cell viability > 95% at a concentration of 200 μg mL^{-1}.[50] Tb^{3+}-doped MgAl-LDHs (100–200 nm) also exhibited good biocompatibility on cancer cells (cell viability of > 90%) at a concentration of 120 μg mL^{-1}.[62] Overall, LDHs with different chemical compositions and structures/sizes have satisfactory biocompatibility.

(2) The intercalation properties of LDHs as well as their adjustable interlayer spacings (0.73−2.28 nm) and high specific surface area (100−600 m^2 g^{-1}) allow them to be loaded with a variety of functional molecules such as drugs, genes, and biomolecules (e.g., nucleic acids, proteins, polypeptides, *etc.*).[63-66] More interestingly, the grain size and/or interlayer spacing of LDHs can be tuned by the intercalation of functional molecules, which may change their properties and/or optimize their performance in specific applications. The interlayer separation in LDHs can expand and contract, which is an advantage over other host materials such as MOFs which are rigid.

(3) The confinement effect of LDHs can significantly enhance the therapeutic performance of intercalated molecules as well as their stability and dispersibility, avoiding the damage caused by biological, chemical and physical environments. For instance, our group has demonstrated that the NIR-activated PDT performance of IPA/ZnAl-LDH composite formed by incorporating IPA into ZnAl-LDH can be remarkably boosted because of the space-confinement and surface-confinement effects of LDHs toward IPA molecules.[46]

(4) The positive charge of LDHs is conducive to conjugation with negatively charged drugs, and the hydrogen bonds attributed to the abundant hydroxyl groups of LDH hydrotalcite-like layers can further increase drug loading. Moreover, positively charged LDHs can readily interact with negatively charged cell membranes (or bacterial membranes), allowing the effective intracellular delivery of drugs to cells (or bactericidal agents to bacteria). For example, the positively charged ZnAl-LDHs reported by Peng *et al.* were shown to attach to the negatively charged bacterial membranes.[67] This caused a change to the charge distribution of the bacterial membrane, and thus prevented nutrient delivery, producing an anti-bacterial effect.

(5) LDHs are essentially a type of hydroxides, which makes them sensitive to acidic environments. Thus, LDHs can gradually degrade through hydrolysis, and slowly release the loaded drug molecules in acidic environments. Barahuie *et al.* found that ZnAl-LDH loaded with anticancer drug chlorogenic acid (CHA) could be gradually degraded under weakly acidic conditions, leading to the slow and sustained release of CHA and enabling high-efficiency chemotherapy.[68] After the implementation of their therapeutic or diagnostic functions, LDHs can eventually be disintegrated, thereby minimizing the biosecurity risks caused by the long-term accumulation of nanoparticles *in vivo*. Cao *et al.* successfully constructed biodegradable 2D PEGylated FeAl-LDH nanosheets (PEG/Fe-LDH) for nanocatalytic tumor-dynamic therapy. It was found that the PEG/Fe-LDH gradually dissolved in a buffer solution of pH 5.0, and no particles could be observed at 4 h.[48]

(6) The diversity of chemical composition and structure of LDHs enables their use in different biomedical applications. For instance, as a drug carrier, monolayered MgAl-LDH with a lateral size of 70 nm can effectively accumulate at the tumor site through the enhanced permeability and retention (EPR) effect for chemotherapy,[47] while MgAl-LDHs with a diameter distribution of ca. 6 ± 2 μm can successfully modify poly(methyl methacrylate) (PMMA) for bone regeneration.[69] The inclusion of specific metals can make LDHs effective contrast agents in imaging applications. For example, Mn^{2+}-containing LDH nanoparticle has been described as a superior MRI contrast agent due to the paramagnetic susceptibility of Mn^{2+}.[45] Owing to these outstanding advantages,

LDHs were initially explored for their drug/gene delivery applications in cancer chemotherapy, and their applications have been recently extended to a wide range of biomedical applications.

(7) From the perspective of practical application, the characteristics of wide source of raw materials, low cost, and simple synthesis make it easy to achieve ton-level production of LDHs. Promisingly, some enterprises have actively invested in the industrial application of LDHs recently. In addition, monolayer LDH nanosheets with high specific surface area have also been mass-produced in the laboratory.[70] These solid foundations will promote the large-scale preparation of LDHs and their wide application in the biomedical field.

3. Preparation

LDH-based nanomaterials used for biomedical applications can be prepared by a variety of well-established synthetic methods to obtain different structures (such as shape, size, thickness, crystallinity) and physicochemical properties (such as optical and electronic properties) and achieve various functions (e.g., therapy, bioimaging, biosensing, anti-bacteria, *etc.*). In general, the preparation of LDHs with different morphologies (Fig. 4) involves the mixing of a metal salt solution with an alkaline solution, which is affected by the following synthesis conditions: (1) the pH value of the reaction medium; (2) the concentration and nature of the alkaline solution used in synthesis; (3) reaction temperature and time; (4) the total metal cation concentration and their molar ratios. In this section, we will detail the preparation of pristine LDHs (bulk LDHs, nanosheets, LDH hollow nanostructures), LDH-based nanocomposites (intercalated LDHs, nanomaterial@LDHs, and LDHs@nanomaterial), and LDH-derived nanomaterials (i.e., MMOs and TMCs). Finally, the surface modification of LDH-based nanomaterials for biomedical applications is systematically described.

3.1. Pristine LDHs

3.1.1. Bulk LDHs

Bulk LDHs are generally synthesized by well-established methods, including co-precipitation, hydrothermal synthesis, separate nucleation and aging steps, and anion exchange.[71,72]

a) ***Co-precipitation***. Co-precipitation has been the most commonly used method to directly synthesize bulk LDHs in an one-step process with high yields since it was first used to synthesize MgAl-LDHs in 1942.[7] In this method, a salt solution containing divalent and trivalent metal cations is slowly added to a solution containing the target anion. To create the required alkaline environment (pH range of 6−11), sodium hydroxide (NaOH) or urea is added to induce the simultaneous precipitation of cationic hydroxides. An appropriate temperature (60−80 °C) is also required to increase the crystallinity of the obtained LDHs.[73] This method is cheap, simple and does not require any specialist equipment, which is therefore conducive to mass production.

Andrade *et al.* successfully prepared Gd/Dy-doped ZnAl-LDHs by this method.[74] Briefly, an aqueous solution containing hydrated nitrate salts of Zn, Al, Gd, and Dy was titrated with NH_4OH under vigorous stirring. The final pH value of the solution was maintained at 10.0 and the resulting slurry was aged at room temperature for 24 h. The GdDy-doped ZnAl-LDHs were obtained after being washed with deionized water. Similarly, Usman *et al.* synthesized GdZnAl-LDHs by adding a NaOH solution to a Zn/Al/Gd nitrate aqueous solution with vigorous stirring under nitrogen (N_2) atmosphere, followed by aging at 70 °C for 18 h.[75] The GdZnAl-LDHs were finally acquired after centrifugation and washing. It is worth noting that the co-precipitation approach also allows the incorporating various inorganic anions, organic molecules, and large biomolecules into LDHs, which will be introduced in Section 3.2 ("LDH-based nanocomposites").

b) ***Hydrothermal synthesis***. The hydrothermal synthesis of bulk LDHs involves mixing a selected alkali solution with a solution containing divalent and trivalent metal ions followed by the subsequent high-temperature and high-pressure treatment in a hydrothermal reactor. Compared with the co-precipitation method, the most prominent advantage of this method is the improved crystallinity and purity of LDHs. Ultrafine LDHs with controllable size and shape were obtained by adjusting reaction temperature and pressure.[76] For example, CoFe-LDH nanoparticles of 200 nm were prepared by mixing two solutions containing Co/Fe nitrates and $NaOH/Na_2CO_3$ respectively at a constant pH value of 8.0 and then transferring the mixture to a stainless-steel Teflon-

lined autoclave for hydrothermal treatment at 80 °C for 24 h.[77]

c) ***Separate Nucleation and Aging Steps***. Similar to the hydrothermal synthesis method, this method involves hydrothermal treatment but different seed formation process. First, a metal salt solution and an alkali solution are simultaneously added to the colloid mill and mixed at about 3000 rpm for 1-2 min. The colloid mill is used to ensure more even nucleation and therefore a narrower particle size distribution of LDHs. The resulting colloidal suspension is then transferred to an autoclave and placed at high temperature or stirred at room temperature. Bulk LDHs are obtained after aging for a certain period of time. By adjusting the temperature and crystallization time, LDHs with small sizes, high crystallinity and high yields can be easily acquired with this method without complicated operations.[33] Xu *et al.* reported the preparation of CoMn-LDHs by using this method (Fig. 4a).[78] In brief, a solution containing Co/Mn nitrates and a solution containing NaOH/Na_2CO_3 were simultaneously added to a modified colloid mill reactor with a rotor speed of 3000 rpm for 2 min. After aging at 30 °C for 5 h, the resulting suspension was thoroughly cleaned with deionized water and dried at 60 °C overnight to obtain the CoMn-LDHs. The modified method was used to successfully synthesize CoAl-LDHs and MgMn-LDHs.[78]

d) ***Anion-exchange***. This method is an alternative to co-precipitation, especially when the target anions are unstable at high pH values, or there is potential interaction between guest species and metal ions. In the anion exchange process, a pre-formed LDH is added to a concentrated solution of desired anions. The resulting solution is then stirred at room temperature or 50−70 °C for several hours. During stirring, the anions originally present in LDH precursor are gradually replaced by the desired anions. From the thermodynamic point of view, the anion-exchange capacity of LDHs mainly depends on the charge density and molecular size of target anions, the pH value and identity of the medium solution, affinity of original anions in LDH, and the chemical composition of the LDH host layers.[79] In a recent work, Zhan *et al.* synthesized NiFe-LDH-NO_3^- from pre-formed NiFe-LDH-CO_3^{2-} through ion exchange processes.[53] NiFe-LDH-CO_3 was first prepared by hydrothermal synthesis and then dispersed into a NaCl/HCl solution. The resulting suspension was stirred for 36 h under N_2 atmosphere to ensure

the complete replacement of CO_3^{2-} by Cl^-. The resultant NiFe-LDH-Cl phase was collected after centrifugation and washing, and then added to a concentrated $NaNO_3$ aqueous solution to eventually obtain NiFe-LDH-NO_3.

e) ***Atom economy method***. In the industrial production of LDHs, the aforementioned methods will produce low-value sodium salt by-products. Meanwhile, the high-concentration alkaline solution used in the synthesis process requires a large amount of water for washing, resulting in excessive waste of water resources.[80,81] In view of this, Song *et al.* successfully designed a green atom-economic method for various LDHs preparation, such as MgAl-LDHs and MgFeAl-LDHs, etc.[82] Taking MgAl-LDHs as an example, an aqueous solution containing $Mg(OH)_2$ and $Al(OH)_3$ was added with carbonic acid solution under vigorous stirring, and the resulting mixture was aged at 80 °C for 2 days to obtain the pure product without washing. Importantly, this method could achieve 100% atomic utilization without by-product generation.

3.1.2. LDH nanosheets

Although bulk LDHs have widely explored in biomedical fields, in most cases their overall performance is restricted by the stacking of the layers and/or the formation of agglomerates. Exfoliating bulk LDHs into monolayer or few-layer nanosheets can maximize the utilization of 2D LDHs, which can be used either without further functionalization, or as a building block to prepare various functional nanocomposites due to its high specific surface area.[83-86] In the past two decades, the preparation of LDH nanosheets has been extensively studied, and is mainly categorized as top-down (exfoliation) and bottom-up (direct synthesis). Top-down synthesis is the most widely used approach based on the direct exfoliation (driven by pre-modified interlayer environment or mechanical forces) of bulk LDH crystals. Bottom-up synthesis is an attractive method, as it uses a chemical approach to control the diameter and thickness of LDH nanosheets, which omits the need for pre-synthesis of layered bulk LDHs and therefore produces nanosheets in a single step.

a) ***Top-down exfoliation driven by pre-modified interlayer environment***. The layer charge density of LDHs is significantly higher than other inorganic layered compounds, making the direct exfoliation of LDHs more difficult.[87] Therefore, the interlayer

environment needs to be pre-modified, and suitable anionic organic guests, such as amino acids (glycine, serine, and L-asparagine) or surfactants (e.g., dodecyl sulfate (DDS)), should be selected to insert into the LDHs interlayer. These interlayer anions show a high degree of interdigitation, thereby increasing the interlayer distance and weakening the electrostatic force between LDH layers. When LDHs are dispersed in a highly polar (alcohols, formamide) or non-polar solvent (toluene), the attractive interactions caused by the strong hydrogen bond between the dispersant and the intercalated anions will lead to the successful penetration of a large amount of dispersant, resulting in the successful exfoliation.[88,89] Chen *et al.* reported the successful preparation of exfoliated CoAl-LDH using a typical delamination method.[90] The pre-synthesized CoAl-LDH-NO_3^- was firstly mixed with a saturated L-asparagine solution by vigorously oscillating at 45 °C for 48 h. After being stored at 4 °C overnight, the mixture was centrifuged to remove the unexfoliated particles, and a translucent colloidal suspension containing CoAl-LDH nanosheets was obtained.

b) ***Top-down exfoliation driven by mechanical forces***. In this method, LDHs can be successfully exfoliated by formamide *via* mechanical shearing and ultrasonication without the need for pre-modifying LDHs' interlayer environment. As previously reported, the delamination of LDHs in formamide has been verified to be spontaneous and instant without any heat or refluxing, which is therefore regarded as a very effective but simple method. The exfoliation behavior of formamide is closely associated with the type of interlayer anion, and nitrate intercalated LDHs (NO_3^--LDHs) exhibit the best exfoliation efficiency.[91] When NO_3^--LDHs are dispersed in formamide, the interlayer height becomes larger due to the uptake of a large number of formamide molecules into the interlayer region, which may be similar to "osmotic swelling". During continuous application of mechanical shearing or ultrasonication, LDHs can be successfully exfoliated.[92,93] For example, Aziz *et al.* first fabricated NiAl-LDH-CO_3^{2-} by hydrothermal treatment, and then obtained NiAl-LDH-NO_3^- *via* ion exchange treatment.[94] The as-prepared NiAl-LDH-NO_3^- was uniformly mixed in formamide and then placed on a mechanical shaker. The delamination of NiAl-LDH was accomplished after continuous mechanical stirring in formamide for 72 h. The supernatant containing

well-dispersed delaminated NiAl-LDH nanosheets was acquired after centrifugation. However, the disadvantage of this method is that the LDH nanosheets exfoliated in formamide are prone to restack after re-dispersing in water, which limits their further application.

c) ***Other top-down exfoliation methods***. Apart from the aforementioned top-down strategies, other methods such as aqueous miscible organic solvent treatment (AMOST), amino acid reconstruction, water-plasma-enabled exfoliation and dry exfoliation methods can also be applied to prepare LDH nanosheets.[95-99] For instance, Wang *et al.* reported the scale-up synthesis of Zn_2Al-borate LDH nanosheets using the AMOST method.[96] Bulk Zn_2Al-borate LDHs were first synthesized by co-precipitation. Then, the water-washed Zn_2Al-borate LDHs slurry was dispersed in acetone with vigorous stirring at room temperature for 1 h. Finally, Zn_2Al-borate LDH nanosheets were obtained by filtering the LDH slurry and washing it thoroughly with acetone. Remarkably, these nanosheets would not restack together even in the dry phase. Recently, Yu *et al.* synthesized MgAl-LDH nanosheets gel by amino acid reconstruction.[97] Typically, bulk MgAl-LDHs was calcined at 450 °C for 12 h and then mixed with glycine. The mixture was transferred to an autoclave and heated at 100 °C for 48 h to obtain the final nanosheets gel. Since the plasma can destroy the electrostatic interaction between the host layer and the interlayer anions, Liu *et al.* treated the bulk CoFe-LDHs with water plasma to prepare ultrathin CoFe-LDH nanosheets.[98] Briefly, the aqueous solution containing CoFe-LDHs was placed in a dielectric barrier discharge (DBD) plasma reactor for 5 min treatment. After filtration and vacuum drying, water-plasma exfoliated CoFe-LDH nanosheets with a thickness of 1.54 nm were finally obtained. The same group further synthesized CoFe-LDH nanosheets by Ar plasma dry exfoliation.[99] CoFe-LDHs powder was put into the quartz boat in a plasma reactor, followed by pumped in Ar atmosphere. After treatment with Ar plasma for different times, the ultrathin CoFe-LDH nanosheets were successfully prepared.

d) ***Bottom-up direct synthesis***. One route to the direct synthesis of LDH nanosheets is the reverse microemulsion method. This synthetic route introduces the traditional water-based co-precipitation system into the oil phase (isooctane) with sodium dodecyl

sulfate (SDS) as the surfactant and 1-butanol as the auxiliary surfactant to form a reverse micro-emulsion system, in which aqueous droplets containing reactants are surrounded by surfactant and dispersed within the oil phase. These droplets act as nanoreactors to confine the space and nutrient for the nucleation and growth of LDH nanosheets, providing an effective way to control the diameter and thickness of LDH nanosheets.[100]

Recently, another direct synthesis route based on co-precipitation in the presence of formamide was developed. During this synthesis process, formamide molecules are adsorbed on the LDH layer surface to prevent the formation of thick layers, owning to its high dielectric constant and preferential interaction with the LDH surface.[101] As the volume percentage of formamide in the reaction system increases, better result can be observed in terms of the exfoliating degree of LDH and the quality of the exfoliated nanosheets.[102] The simplicity of this method makes large-scale production possible. Gd^{3+}-doped monolayered MgAl-LDH (MLDH) nanosheets were prepared by our group *via* a facile bottom-up synthesis method (Fig. 4b).[47] Solution A (containing Mg/Al/Gd nitrates), solution B (containing $NaNO_3$/formamide), and solution C (containing NaOH) were prepared first. Then, solution A and solution C were added slowly into solution B and stirred at 80 °C for 30 min. The resulting MLDH nanosheets with uniform morphology (ca. 70 ± 9.5 nm) were acquired after centrifugation and washing. With this method, we successfully synthesized a variety of LDH nanosheets, including CoFe-LDH nanosheets,[49] CuFe-LDH nanosheets,[103] CoMn-LDH nanosheets,[52] CoCuFe-LDH nanosheets,[104] and CoFeMn-LDH nanosheets.[54]

Another bottom-up method using phosphonic or phosphate acid terminated polyethylene glycol (PEG) molecules was developed by Cao *et al.* and Zhang *et al.*[48,105] In this method, mixed metal salt and sodium hydroxide was mixed initially to form LDH nuclei. Negatively charged PEG molecules act as layer growth inhibitor are subsequently added to terminate nucleation and facilitate particle growth along the *ab* plane. PEG molecules in this method not only act as a layer growth inhibitor but also a bio-functional surface modifier that increases colloidal stability and prolong blood circulation of LDH nanosheets.

In addition, for the large-scale direct synthesis of LDH nanosheets, H_2O_2-mediated single-step approach and $NH_3 \cdot H_2O$-mediated low-temperature synthesis were proposed in recent years.[70,106,107] In terms of H_2O_2-mediated single-step approach developed by Yan *et al.*,[106] Mg/Al nitrates and urea were dissolved into 30% H_2O_2. The resulting solution was then transferred to an autoclave. After hydrothermal treatment at 150 °C for 24 h, the large-scale MgAl-LDH ultrathin nanosheets were acquired by centrifugation and washing. For the $NH_3 \cdot H_2O$-mediated low-temperature synthesis reported by Zhang *et al.*,[107] a solution containing Mg/Al nitrates and a solution containing $NH_3 \cdot H_2O$ were simultaneously added to a beaker. The mixture was magnetically stirred under N_2 protection, during which the pH was maintained at 10 by controlling the relative dropping rates of two solutions. After stirring for 10 min, the single-layer MgAl-LDH nanosheets were collected by centrifugation and washing. These two methods do not involve layer growth inhibitors such as formamide, which are beneficial for biomedical application.

3.1.3. LDH hollow nanostructures

Template etching. LDH hollow nanostructures can be obtained *via* template etching by using sacrificial templates. Briefly, the synthesis process involves introducing pre-synthesized templates into a metal salt solution to allow the growth of LDHs on the surface, and then removing the template by etching. Metal-organic frameworks (MOFs) and silica (SiO_2) are two commonly used sacrificial templates.[108-111] MOFs are a type of porous material composed of organic linkers coordinated to metal centers. During the synthesis process, the metal salts in aqueous solution introduced to form LDHs are hydrolyzed, and the resulting H^+ ions can destroy the coordination bonds between the metal ions and the ligands in MOFs, thereby gradually corroding MOFs and generating LDHs with a hollow structure (Fig. 4c).[108] SiO_2 possesses a regular and adjustable pore structure as well as large specific surface area. With the growth of LDHs on the surface, SiO_2 gradually dissolves in the alkaline environment generated, eventually forming hollow LDHs.[111] By using templates with different sizes and shapes, hollow structures with different dimensions can be obtained.

Wang *et al.* adopted ZIF-67@ZIF-8 as a template to synthesize hollow-structured

ZnCo-LDHs through an *in-situ* transformation strategy (Fig. 4d).[109] The pre-synthesized ZIF-67@ZIF-8 nanoparticles were added to a $Co(NO_3)_2$ solution with a chosen ethanol-water solvent content. The suspension was mixed thoroughly and aged at room temperature for 10 min. During the hydrolysis of $Co(NO_3)_2$ in aqueous solution, H^+ ions were generated and began etching the ZIF-67@ZIF-8 templates by destroying the coordination bond between Zn^{2+} and hexadecyltrimethylammonium bromide (CTAB) ligands, thus gradually releasing Zn^{2+} ions. Subsequently, Co^{2+} and Zn^{2+} ions co-precipitated on the surface of ZIF-8, accompanied by more H^+ ions generation. Finally, the ZIF-8 template was etched completely by H^+ ions, forming hollow-structured ZnCo-LDHs. It has been found that the etching and growth rates can be adjusted by regulating the concentration of metal precursor, water content of solvent, and morphology of MOF templates, resulting in a variety of LDH hollow nanostructures.

3.2. LDH-based nanocomposites

3.2.1. Intercalated LDHs

Due to their intercalation properties, LDHs can be intercalated with negatively charged drugs, dyes, biomolecules and other functional compounds for various applications.

a) ***Traditional methods*.** Most intercalated LDH nanocomposites can be obtained through the aforementioned co-precipitation, hydrothermal synthesis, separate nucleation and aging steps, or anion exchange method. Unlike the synthesis of pristine LDHs, the target guest molecules must be added into the salt solution or alkali solution and proceed to the co-precipitation process to form LDH nanocomposites. It should be noted that the interest guest molecules must be stable in the reaction solution and not react with any other ions present. For example, our group utilized the co-precipitation method to synthesize IPA-intercalated ZnAl-LDH (IPA/LDH).[46] A solution of metal salts with the required molar ratio of Zn^{2+}/Al^{3+} was prepared. Then, a mixed aqueous solution of NaOH and IPA was added dropwise with vigorous stirring under N_2 flow. The pH of the suspension was maintained at 7.0 before heated to 60 °C for 24 h. After filtering and washing, the IPA/LDH sample was obtained.

In other work, ZnPc-intercalated MgAl-LDH was fabricated by our group *via* a

nucleation/crystallization separation method.[44] In brief, a mixture of Mg/Al nitrate and ZnPc ethanol solution and a NaOH aqueous solution were simultaneously added into a colloid mill and mixed at 3000 rpm for 60 s. The resulting suspension was then heated in a stainless-steel Teflon-lined autoclave at 80 °C for 24 h. The product ZnPc/LDH was acquired after washing with distilled water. Another method is anion exchange, in which pristine LDH particles are firstly prepared and mixed with a solution containing guest ions. In this method, the affinity of guest ions to hydrotalcite-like layers is often stronger than that of host ions. For instance, Usman *et al.* fabricated CHA-intercalated GdZnAl-LDHs through the anion exchange method.[75] GdZnAl-LDHs were first synthesized by a co-precipitation route. Subsequently, the prepared NaOH and CHA solutions were slowly added into the GdZnAl-LDHs suspension simultaneously. The resulting suspension was kept under constant N_2 flow with vigorous stirring until the pH reached 7.0, followed by aging at 70 °C for 18 h. Finally, the CHA-intercalated LDHs were obtained after filtering and washing.

b) ***Reconstruction or rehydration***. Reconstruction or rehydration is another common approach to synthesize intercalated LDHs. This strategy is based on the structural memory effect of LDHs.[112] Briefly, pristine LDHs are calcined at 400−500 °C for dehydration, and then the resulting MMOs are immersed in an aqueous solution containing target anions to recover the original structure of LDHs. Accompanying the reconstruction, guest molecules are intercalated into the LDH interlayer.[113] For example, Kim *et al.* successfully incorporated drug molecules (methotrexate (MTX) and 5-fluorouracil (5-FU)) into MgAl-LDH using the reconstruction route.[114] First, pristine MgAl-LDH was prepared by hydrothermal synthesis and then calcined at 400 °C for 8 h to obtain MMO ($Mg_2AlO_{7/2}$). The calcined LDH powder was then redispersed into MTX or 5-FU solution and vigorously stirred under N_2 atmosphere for 24 h to obtain MTX/MgAl-LDH or 5-FU/MgAl-LDH nanohybrids, respectively. The MTX and 5-FU co-intercalated MgAl-LDH (MTX&5-FU/MgAl-LDH) was also obtained through a similar reconstruction route. However, intercalated LDHs synthesized by this method possess poor dispersibility and crystallinity, and amorphous phases are often generated as by-products.[79] Therefore, this method has fewer applications in the field of

biomedicine.

c) ***Other methods***. In addition to the aforementioned five main strategies, other methods such as water-assisted mechanochemical grinding can also be applied to prepare intercalated LDH nanocomposites. Madhusha *et al.* reported a green synthesis of curcuminoid-incorporated LDH nanohybrids (CC-LDH) through a water-assisted mechanochemical grinding process.[115] Briefly, curcuminoid powder, NaOH pellets, and water were added to the pre-synthesized MgAl-LDH-NO_3^- in a ceramic mortar and manually ground for 1.5 h with a ceramic pestle at room temperature under an inert environment in a glove box. The resulting paste was washed thoroughly with distilled water and dried at 90 °C overnight to obtain CC-LDH nanohybrids.

3.2.2. Nanomaterial@LDHs

Various synthesis methods including *in-situ* growth, template-oriented assembly and exfoliation-reassembly method can be used to synthesize nanomaterial@LDHs.

a) ***In-situ growth***. *In-situ* growth includes *in-situ* electrodeposition, *in-situ* hydrothermal, and *in-situ* etching of metal surfaces. Nanomaterial@LDHs prepared by the *in-situ* growth method are, in most of cases, featured with directionally ordered nanoarray structure.

In-situ electrodeposition is usually carried out in nitrate or sulfate solutions containing the required metal ions. The local pH value on the working electrode is increased by reducing NO_3^- or sulfate ions (SO_4^{2-}) to generate hydroxide ions (OH^-), thus promoting the precipitation of LDHs on electrodes. Various conductive substrates can be used for electrodeposition, such as metals (Au, Fe, Ni, *etc.*), transition metal oxides (CuO, NiO, ZnO, WO_3, TiO_2, *etc.*), TMCs and conductive polymers (polypyrrole (PPy), and polyaniline (PANI)).[116-123] For example, to realize the uniform and direct growth of CoNi-LDHs on the CuO surface (Fig. 4e), An *et al.* utilized the as-prepared CuO/glassy carbon electrode (GCE) (denoted as CuO/GCE) as the working electrode, platinum (Pt) wire as the counter electrode, and Ag/AgCl electrode as the reference electrode.[124] Briefly, an aqueous solution containing $Co(NO_3)_2$, $Ni(CH_3COO)_2$ and $NaNO_3$ was placed in a small-volume single compartment cell. A potential difference of 0.8 V versus Ag/AgCl was then applied at room temperature for 100 s, during which NO_3^-

ions were reduced and the generation of OH^- ions occurred. The resulting local pH increase led to the precipitation of CoNi-LDHs on the CuO/GCE surface, leading to the generation of CuO/CoNi-LDHs.

In-situ hydrothermal involves the introduction of LDH crystals onto the activated substrate surface (e.g., metals, carbon materials, metal oxides, and metal-organic complexes), followed by hydrothermal treatment (Fig. 4f).[109,125-129] The preparation conditions of this method are relatively harsh, usually requiring a high temperature and long reaction time. Lu *et al.* proposed the one-step hydrothermal synthesis of NiFe-LDH nanosheets on Ni foam (Fig. 4g).[130] Ni foams were first pretreated with an HCl solution, and then cleaned by deionized water and absolute ethanol in an ultrasonic cleaner for 10 min each. A homogeneous solution containing Ni/Fe nitrates and urea was then prepared. The cleaned Ni foams were immersed into the above homogeneous solution, and transferred to a stainless-steel Teflon-lined autoclave. The autoclave was sealed and heated at 120 °C for 12 h, and then allowed to cool to room temperature. After washing with deionized water and absolute ethanol respectively, the NiFe-LDH/NF hybrid was obtained.

In-situ etching of metal surface is used to synthesize LDH composites by taking advantages of the metal elements etched from substrates. The added metal ions co-precipitate with the metal ions provided by the etched substrate, thereby allowing *in-situ* growth of LDHs on the substrate surface.[131] For example, Amin *et al.* presented a biosensor design for glucose detection, based on a composite electrode containing nickel nanotube network (Ni-NTNW) loaded with NiCo-LDH nanosheets.[132] The Ni-NTNW acts as a conductive supporting layer, in order to both prevent agglomeration and improve conductivity of the NiCo-LDH nanosheets. They first integrated the Ni-NTNW into the electrode by Ni electrodeposition. Next, the Ni surface layer was chemically etched by nitric acid to improve the diffusion of reagents into the network and achieve the homogeneous coverage of Ni-NTNW by NiCo-LDH nanosheets under electrodeposition. During the growth of NiCo-LDH, NO_3^- ions were reduced by gaining electrons and OH^- ions were generated. Subsequently, these OH^- ions reacted with Ni^{2+} provided by the etched Ni layer and Co^{2+} presented in the electrolyte, forming

NiCo-LDH nanosheets *via* precipitation.

b) ***Template-oriented assembly***. The preparation of nanomaterial@LDHs *via* template-oriented assembly generally follows two steps: (1) the formation of organic self-assembly materials. The special environment provided by the ordered self-assembly material is used as a "microreactor" or template for further chemical reactions; and (2) the assembly of LDHs precursors guided by intermolecular forces and spatial confinement effects to form nanocomposites with controllable composition, morphology, size, orientation and arrangement. In this method, the commonly used organic templates include vesicles, block copolymers, microemulsions formed by surfactants, and MOFs.[133-135] For example, Jung *et al.* successfully synthesized size-controlled hybrids (Gd/MgGa-LDH) of LDH platelets and $Gd(OH)_3$ nanorods using microemulsion as a template.[136] First, to prepare a surfactant-containing microemulsion, 1-butanol and CTAB were added into cyclohexane. Next, the following solutions were prepared: (A) Mg/Ga nitrate solution, (B) Gd-DTPA solution, and (C) NaOH solution. To deprotonate Gd-DTPA, solution B was titrated dropwise with solution C until the pH reached 10. Then, each solution (A, B and C) was added successively into the above microemulsion with an optimal water/surfactant ratio. Finally, after aging for 24 h, the suspension was washed with a water/ethanol solution at 75 °C for 8 h and acetone at 50 °C for 8 h, respectively. The resulting Gd/MgGa-LDH hybrids presented a quasi-core-shell structure, in which $Gd(OH)_3$ nanorods were covered by LDH platelets.

In addition, inorganic materials such as alumina films, porous silica, and carbon nanotubes can also be adopted as templates to guide the assembly of nanomaterial@LDHs.[111,137] For example, Shao *et al.* utilized SiO_2 as a template to fabricate Fe_3O_4@SiO_2@NiAl-LDH microspheres through hydrothermal treatment (Fig. 4h).[58] First, Fe_3O_4@SiO_2 microspheres were prepared by a sol-gel approach, and then added into the pre-prepared AlOOH primer sol with vigorous agitation for 1 h. During this process, a layer of AlOOH microcrystals uniformly grew on the surface of SiO_2 microspheres to form Fe_3O_4@ SiO_2@AlOOH microspheres. The obtained Fe_3O_4@SiO_2@AlOOH microspheres were added to a mixed solution containing $Ni(NO_3)_2 \cdot 6H_2O$ and NH_4NO_3, and then transferred to an autoclave. After crystallization

at 100 °C for 48 h, the resultant Fe_3O_4@SiO_2@NiAl-LDH microspheres were washed with ethanol and separated from the supernatant using a magnet.

c) ***Exfoliation-reassembly***. As an emerging synthetic method of nanomaterial@LDHs, exfoliation-reassembly technique enables the encapsulation of large biomolecules or polymers into LDHs. In this method, bulk LDHs are pre-treated with formamide or reflux in alcohols (e.g., butanol, pentanol, and hexanol) to exfoliate the layers into nanosheets. When the exfoliated positively charged LDH nanosheets are added to a solution containing the desired negatively charged species, the reassembly reaction under vigorous stirring will produce nanocomposites, and the large-size molecule encapsulated LDHs can be obtained.[2] Two kinds of double-stranded DNA (AA′ and BB′) have been successfully encapsulated by LDH nanosheets *via* exfoliation-reassembly.[138] Briefly, NO^{3-}-intercalated MgAl-LDHs were first prepared, and then treated in formamide solvent to delaminate the layers into nanosheets. After that, the colloid of MgAl-LDH nanosheets was blended with DNA solution. The electrostatic interaction between LDH nanosheets and DNA molecules gave rise to self-reassembly, resulting in DNA(AA′)@LDH and DNA(BB′)@LDH. The LDH host matrix was proved to protect the DNA strands from degradation and enhance their bioavailability. Besides, the exfoliated LDH nanosheets can also assemble with organic molecules to fabricate LDH-based films through layer-by-layer assembly technique. For example, Zhang *et al.* reported the preparation of well-ordered films composed of CoNi-LDH nanosheets and iron porphyrin (Fe-PP).[139] CoNi-LDHs was first synthesized by hydrothermal method and then exfoliated by formamide *via* mechanical shearing. Subsequently, the pre-treated indium-tin-oxide (ITO) glass substrate was dipped into CoNi-LDH nanosheets suspension for 10 min, followed by immersed into Fe-PP solution for another 10 min. After repeating this operation *n* times, the LDH-based films were obtained. Similarly, Dou *et al.* successfully fabricated ultrahigh films by the assembly of XAl-LDH nanosheets (X=Mg, Zn, Co, Ni) and polyacrylic acid (PAA) using the same method.[140] The synthesis procedure followed two steps: (1) dipping the pretreated quartz glass substrate to XAl-LDH nanosheets suspension for 10 min; (2) immersing the above substrate into PAA solution for another 10 min. Finally,

multilayer films were obtained after *n* cycles.

3.2.3. LDHs@nanomaterial

Surface coating or deposition. Surface coating or deposition is a common method to coat LDHs with other nanomaterials, such as SiO_2 nanodots (Fig. 4i), Fe_3O_4 nanoparticles, quantum dots (QDs), or carbon dots (CDs) to synthesize LDHs@nanomaterial.[141-144] Among these nanomaterials, SiO_2 has become the most widely used nano-coating owning to its advantages of simple functionalization, high porosity, excellent hydrophilicity and good biocompatibility.[145,146] Therefore, LDHs can be decorated with SiO_2 for drug/gene delivery and sustained release.[147,148] Noble metal elements including Ag, Pt, Au cannot act as metal centers within LDH layers due to their large ionic radius, so they are usually anchored on LDHs *via* surface deposition (Fig. 4j).[149,150] Due to the large specific surface area and abundant Lewis base sites of LDHs, the dispersity of active noble metals can be improved and their agglomeration can be effectively inhibited.

Jia *et al.* developed an intelligent biocatalyst by coating FeMn-LDH with upconversion nanoparticles (UCNP), which are themselves coated with SiO_2 and the photosensitizer chlorin e6 (denoted as UCSP).[151] In brief, Na_2CO_3 and pre-fabricated UCSP were mixed in a three-necked flask. To this, a solution of Mn and Fe chloride salts as well as a NaOH solution were added slowly under vigorous mixing. The pH value of the mixture was maintained at 10 by controlling the dropping rate of NaOH solution. After the Mn and Fe chloride salt solution was added completely, the mixture was aged at room temperature for 1.5 h. The suspension was then transferred to an autoclave and crystallized at 90 °C for 16 h. After washing with deionized water, the final UCSP-FeMn-LDH product was obtained.

An alternative method to produce LDHs@nanomaterial is the surfactant-assisted sol-gel coating method. For example, Wang *et al.* prepared MgAl-LDH core@mesoporous silica shell (LDH@MS) as a drug carrier through the surfactant-assistant sol-gel coating method (Fig. 4k).[152] First, the MgAl-LDH obtained by co-precipitation was added to a solution containing CTAB, $NH_3.H_2O$ and ethanol to form a homogeneous dispersion in an ultrasound bath for 60 min. Next, tetraethyl orthosilicate (TEOS) was added

dropwise into the dispersion under vigorous stirring. After aging for 6 h, the LDH@MS was obtained by centrifugation and washing with distilled water. Finally, the dried LDH@MS samples were extracted with a mixed solution of ethanol and hydrochloric acid for 24 h to remove the surfactant, and then dried at room temperature.

3.3. LDH-derived nanomaterials

Topological transformation. In crystallography, a topological property is defined as a relationship between the arrangement of atoms in the crystal lattice which is invariant during continuous spatial transformation. In the case of LDHs, continuous transformation across any of the lattice dimensions (i.e. change of constituent atoms and therefore atomic spacing within the layers, or a change in the spacings between the layers) still results in a topologically equivalent layered structure. Based on this concept, MMOs or TMCs can be obtained through topotactic transformation from LDH precursors (Fig. 4l).[60,153] In this process, the arrangement and relative position of metal ions in layers remain unchanged, and the migration only occurs in the direction perpendicular to the layers.[154] Topotactic transformations of LDHs are usually performed under high-temperature calcination or hydrothermal conditions. The topotactic transformation products MMOs or TMCs also inherit the characteristics of LDHs associated with their structure (i.e. large specific surface area, high stability and good dispersion of metal atoms, abundant active sites).[104,155,156]

Our group proposed the fabrication of ultrathin CoFeMn dichalcogenide nanosheets (CFMS NSs) based on CoFeMn-LDH nanosheets.[54] Lamellar CoFeMn-LDH precursor was first synthesized *via* a bottom-up method. Subsequently, thioacetamide (TAA) was dissolved in ethanol and then added to the CoFeMn-LDH precursor in a Teflon-lined autoclave. After hydrothermal treatment at 120 °C for 12 h, the resulting CFMS NSs were collected by washing and centrifugation. More recently, we also prepared CoCuFe-selenide (CCFS) NSs by the *in situ* selenylation of CoCuFe-LDH nanosheets.[104] Briefly, a NaHSe solution (obtained by introducing $NaBH_4$ into Se powder) was mixed with the CoCuFe-LDH suspension under N_2 flow. Then, the suspension was transferred to a Teflon-lined autoclave and heated at 180 °C for 12 h. After several times of water and ethanol purification, the CCFS NSs product was

acquired.

4. Surface modification of LDH-based nanomaterials

The methods discussed above provide the basis for the preparation of pristine LDHs, LDH-based nanocomposites and LDH-derived nanomaterials. However, similar to most nanomaterials in biomedicine, LDHs often suffer from instability under complex physiological conditions and tend to rapidly aggregate in biological media. Therefore, surface modification of LDH-based nanomaterials with other functional agents is needed to improve the stability and dispersity of LDHs in physiological environments. Moreover, surface modification not only allows convenient attachment of targeting ligands, but also renders LDHs flexibility in versatile functionalities.[157-159] Surface modification also plays an extremely important role in enhancing LDHs' cellular uptake, biocompatibility and bioavailability. In general, the chemical modification to obtain functionalized LDH-based nanomaterials can be realized mainly through two strategies: non-covalent covering and covalent conjugation.

a) ***Non-covalent covering***. In this strategy, the surface of LDH-based nanomaterials can be modified with certain biomolecules, fluorophores or polymers (e.g., PEG and polyvinylpyrrolidone (PVP)) through non-covalent interactions (electrostatic interactions, hydrogen bonds and van der Waals forces) to adjust the physicochemical properties of LDH-based nanomaterials.[104,160-162] For example, coating LDHs with PEG and its derivatives by physical mixing can improve the stability and dispersity affected by steric and electrostatic factors, thereby prolonging their circulation time and increasing their accumulation in tumors by protecting LDH-based nanomaterials from immune effects.[163] Recently, bovine serum albumin (BSA) has also been used to prevent the aggregation of LDHs and increase their stability and cellular uptake.[164,165]

b) ***Covalent conjugation***. Unlike non-covalent coating, this strategy uses covalent conjugation of the hydroxyl groups of LDHs with specific functional groups on desired moieties, such as targeting ligands or fluorescent probes. Park *et al.* found that the terminal amine groups of 3-aminopropylsilane could covalently bind to the hydroxyl groups on the LDHs surface without changing their layered structure.[166] The resulting reactive silane functional groups could then be used as attachment points for further

functionalization, such as with fluorescent dyes or disease-specific ligands. Oh *et al.* used a similar process, in which instead of silane they introduced amino groups onto the surface of MgAl-LDHs, and subsequently grafted folic acid (FA) onto the particles for cancer cell targeting function.[167] The biocompatibility of MgAl-LDHs was also shown to be significantly improved due to the FA coating. Kuo *et al.* coated cyanine-5.5 (Cy 5.5) and PEG-5000 onto amine-modified LDHs by covalent conjugation.[168] The obtained LDHs-PEG-5000 exhibited improved blood circulation time with high fluorescence intensity in the tumor.

5. Biomedical applications

5.1. Controlled release of drugs

The aim of controlled drug release is to keep the drug concentration in the blood more constant by means such as controlling the release rate, prolong the plasma half-life of drugs, or increasing their bioavailability. It has been widely reported that LDHs can be internalized by cancer cells *via* clathrin-mediated endocytosis and subsequently stored in endosomal vesicles (pH = 5–6).[169,170] In this case, LDHs can partially dissolve to release metal ions, resulting in a large number of water molecules being pumped from the cytoplasm into the endosome driven by osmotic forces. This process will cause the swelling of the endosomal vesicles, leading to their eventual rupture and release of LDHs into the cytoplasm.[171] The unique "endosomal escape" capability of LDHs allows loaded drugs to escape from the endosome, which can protect drugs to retain their function and deliver them to functional place: the perinuclear region of the cytoplasm.[172] Therefore, LDHs as nanocarriers for controlled drug release have become increasingly popular in the biomedical field in recent years.[34,37]

5.1.1. Advantages of LDH-based nanomaterials for drug release

Based on the large specific surface area and adjustable interlayer spacing of LDHs, high-efficiency loading of drug molecules can be achieved through various methods such as ion exchange, co-precipitation and physical adsorption. Intercalation of drugs into LDHs confers a number of advantages when compared to free drugs: (1) LDHs can protect drug molecules from the influence of the complex physiological environment to prevent or slow their degradation and the loss of efficacy;[173] (2) the hydroxyl groups

on the LDHs layers can interact with drug molecules to improve their stability;[64] (3) the surface/space confinement effect of LDHs can reduce the aggregation of drug molecules and allow them to exert the optimal therapeutic effect;[46] (4) the layered structure of LDHs enable poorly soluble drugs to be loaded in LDH carriers to increase drug solubility, thereby enhancing the bioavailability and absorption efficiency of drugs;[174,175] (5) the positive charge of LDHs is conducive to their combination with negative cell membranes to improve the uptake of LDHs and promote the uptake efficiency of drugs by cells;[167] (6) the acid-responsive degradation property of LDHs is not only beneficial to the control of drug release rate, but also to the eventual removal of LDHs in the body, thereby ensuring biological safety.[176] Therefore, LDHs have potential applications in controlled release of drugs.

5.1.2. Drug release mechanisms

The mechanism by which drug release from LDHs occurs can be mainly divided into two categories:[64] (1) corrosion, in which the weakly alkaline LDHs are partially dissolved in an acidic microenvironment and then the drug molecules can be released, and (2) ion exchange, where LDH nanocomposites intercalated with drugs enter an organism, and the drug molecules can be slowly released through ion exchange with phosphate in physiological environments.

a) ***Corrosion mechanism.*** As an important mechanism of drug release, the corrosion mechanism has been extensively studied. For example, with the aim to increase the half-life and anticancer activity of methotrexate (MTX, a negatively charged anticancer drug), Yan *et al.* designed a type of aqueous dispersible MgAl-LDH nanosheets to load MTX.[177] MTX displayed a pH-responsive release behavior. In phosphate-buffered saline (PBS) solution (pH 7.4), less than 65% of the MTX was released within 24 hours. When the pH dropped to 5.0 (the pH of endosomes/lysosomes), 100% release of MTX was observed within 2 hours, indicating that MTX could be efficiently released after endocytosis. Similarly, DOX-loaded MgAl-LDH nanosheets with ultrahigh drug loading (734%) and prolonged blood circulation were developed by Zhang *et al.* for cancer therapy.[178] The release behavior of LDH-DOX was investigated under different pH environments, and the results showed that DOX was easily released at pH 5.4 with

an accumulative release of 92.7%, while the accumulative release was only 21.3% at pH 7.4 after 24 h. Such a pH-responsive release behavior could facilitate the release of DOX at the tumor site, optimizing its cancer therapeutic effect. Bao *et al.* synthesized a drug delivery system for bladder cancer by intercalating ethylene diamine tetraacetic acid (EDTA, a metal ion chelator) into neurotensin (NT)-modified ZnAl-LDH interlayer.[179] EDTA could deprive Ca^{2+} from intercellular connexin through EDTA-Ca^{2+} chelation, leading to tumor disaggregation (Fig. 5a), which is an unprecedented tumor therapy strategy. In a weakly acidic environment at pH 6.5, the release of EDTA from LDH was rather rapid within the first hour and sustained thereafter, reaching 25.8 wt % within 16 h (Fig. 5b). Such a sustained EDTA release guaranteed biosafety and provided sufficient EDTA molecules for Ca^{2+} capture, ultimately effectively eradicating bladder tumors (Fig. 5c,d).

Encouraged by the drug release performance of LDHs, it is expected that the modification of LDHs with other nanomaterials will promote the release of drugs. Zheng *et al.* employed MgAl-LDHs to simultaneously load selenium (Se) and small interfering RNAs (siRNAs) *via* electrostatic interactions.[180] The obtained Se@LDHs/siRNA effectively overcame the drug resistance mediated by class III β-tubulin (β-tubulin III) and P-glycoprotein (P-gp) in breast cancers. In this work, Se@LDHs not only protected siRNA from degradation, but also enhanced siRNA cellular internalization. The introduction of Se reduced the surface charge of LDHs and weakened the electrostatic interaction between siRNA and Se@LDHs. The weaker electrostatic force had little effect on the intercalation of siRNA and Se@LDHs, but facilitated the release of siRNA. Thus, the release rate of Se@LDHs was faster than LDHs alone. More importantly, Se@LDHs/siRNA exhibited pH-sensitive release performance, with a cumulative siRNA release of 78.9% within 8 hours at pH = 5.2 and only 13.8% at pH = 7.4.

Drug release behavior from LDHs may also be mediated by exogenous stimuli such as light or heat. Our group fabricated monolayered MgAl-LDH (MLDH) nanosheets through a bottom-up method (Fig. 5e), and then co-loaded DOX and ICG with a drug loading content (797.36%) and encapsulation efficiency (99.67%) (Fig. 5f-j).[47] The

DOX&ICG/MLDH exhibited pH-responsive and NIR-induced DOX release (Fig. 5k). The release amount of DOX at pH 7.4, 6.5 and 5.0 was 3%, 9.05% and 21.01%, respectively. After NIR laser irradiation, a remarkable increase in drug release was observed (52.01% at pH 7.4, 61.62% at pH 6.5, and 82.37% at pH 5.0), which could be attributed to the partial dissolution of MLDH at pH 5.0, ICG-mediated photothermal effect and the NIR-induced disruption of the interaction between DOX and ICG.

b) ***Ion exchange mechanism.*** The earliest research on the ion exchange drug release mechanism from LDHs started in 2001 when Ambrogi *et al.* synthesized ibuprofen (IBU)-intercalated LDHs (HTlc-IBU) to study a new controlled release formulation.[181] As a non-steroidal anti-inflammatory drug (NSAID), IBU can relieve the symptoms of rheumatoid arthritis and osteoarthritis. However, the high plasma levels after the administration of conventional formulations bring significant side effects such as indigestion, gastric ulcer, gastrointestinal bleeding. To address this difficulty, LDHs were explored to control the release of IBU. The results of dissolution tests demonstrated that 100% IBU in commercial Neo-Mindol® was released immediately in simulated intestinal fluid (pH 7.5), while 60% IBU was released from HTlc-IBU within 20 min and 100% within 100 min. This difference is due to the diffusion rate-limited release of IBU from HTlc-IBU through the ion exchange between IBU ions and phosphate in the buffer. In another study, Gu *et al.* investigated the effect of particle aggregation and hydrothermal treatment on the release behaviors of NSAID agents (i.e., naproxen, diclofenac, ibuprofen) from LDH nanoparticles.[182] They also prepared low molecular weight heparin (LMWH)-intercalated MgAl-LDHs *via* a coprecipitation method,[183] and demonstrated that the sustained release of LMWH from LDHs helped to increase the short half-life of LMWH. Gao *et al.* designed vitamin C (VC)-intercalated CaAl-LDHs in the same way.[184] *In vitro* release results showed that the release time of VC in phosphate buffer was significantly prolonged.

To investigate the effect of anion types (chloride, acetate and phosphate) of release media on ion exchange drug release behavior, Rojas *et al.* synthesized IBU-incorporated MgAl-LDH and then carried out dissolution tests.[185] The results showed that compared with Cl^- and AcO^-, the release of IBU from MgAl-LDH increased

significantly in the presence of $H_2PO_4^-$ or HPO_4^{2-}, indicating that IBU release was highly dependent on the anion nature of the release media. Later, Senapati *et al.* found that different interlayer anions could also affect drug release ability.[186] They synthesized three kinds of raloxifene hydrochloride (RH)-intercalated MgAl-LDHs (RH-LDHs), with three interlayer anions (NO_3^-, CO_3^{2-} and PO_4^{3-}) respectively. Controlled drug release was achieved with fast release observed in phosphate-based LDHs and sustained release found in nitrate-based LDHs, which could be explained by the interactions between RH and LDHs (which is related to the charge density of the interlayer ions) along with the order-disorder structure of RH molecules in the LDH layers. Nitrate-based LDHs exhibited stronger interaction with RH that showed an ordered arrangement in the LDH layers, leading to sluggish release, while phosphate-based LDHs displayed relatively weak interaction with RH which showed a disordered arrangement in the LDH layers, resulting in fast release. In addition, Zhang *et al.* reported that captopril (Cpl)-intercalated MgAl-LDHs (Cpl-LDHs) could realize controlled release through a combination of both the corrosion mechanism and ion exchange mechanism.[187] *In vitro* release studies showed that the release percentage and release rate increased significantly with the decrease of medium pH value. At pH 7.45, the slower and sustained release process was interpreted as the ion-exchange between Cpl and phosphate in buffer. At pH 4.60, the release behavior involved corrosion mechanism caused fast release within 1 min, followed by ion exchange mechanism release after 1 min.

Drug-loaded LDH can also be controlled by H_2O_2 gradient, temperature, and light irradiation. For instance, Zhang *et al.* presented a catalytic nanomotor based on ferrous-containing LDH (Fe-LDH) nanosheets with chemotaxis properties for controlled drug delivery toward the TME.[105] The Fe-LDH nanomotor exhibited high catalytic activity to convert H_2O_2 to O_2, enabling responsive, sustained, and relatively long-distance movement. Moreover, this Fe-LDH nanomotor showed directional motion toward high gradient H_2O_2, demonstrating excellent chemotactic behavior. By using DOX as a model drug delivered by the Fe-LDH nanomotor, they found the fast DOX release rate when the nanoparticles diffuse quickly in the TME, due to the exchange of the loaded

DOX with the ions in the solution and diffusion from LDH surface into the medium solution. In another study, Li *et al.* demonstrated a heat-enhanced chemotherapy in response to the NIR irradiation by constructing 5-FU-loaded Cu-LDH nanoparticles.[188] *In vitro* and *in vivo* HCT-116 colon tumor models showed that enhanced anti-tumor effects under the NIR trigger, partly due to faster on-demand release of 5-FU at higher temperature.

In conclusion, LDHs have potential applications in the controlled and sustained release of various drug molecules. Apart from those described above, other therapeutic agents which can be released from LDHs based on these two mechanisms are summarized in Table 1.[189-198] Despite the promising commercial prospects, LDHs as carriers still have some deficiencies in controlled drugs release. Regarding the corrosion mechanism, in addition to the degradability of LDHs in acidic environments, new endogenous and exogenous stimuli need to be exploited to promote drugs release. For the ion exchange mechanism, whether the existence of other ions in complex physiological environments will interfere with the ion exchange process between drug molecules and phosphate is worthy of further investigation. Therefore, a considerable amount of research is still required into the use of LDHs as controlled release systems in a commercial setting.

5.2. Tumor imaging

Cancer imaging diagnosis is another popular area of LDH-based biomedical applications. As an integral part of clinical cancer therapies, medical imaging plays a vital role in all stages of cancer management, including cancer screening, therapeutic effect monitoring, and tumor recurrence detection.[199-201] An ideal imaging modality are typically featured with minimal or no invasiveness, convenient imaging, real-time monitoring, and the ability to provide sufficiently detailed information about the target tissues. For instance, this can include the structure of organs and blood vessels, physiology of dynamic bioprocess, and bio-distribution of drugs, ranging from the molecular to cellular and/or organ to organism levels.[202-205]

Significant advances have been made over the years in a range of cancer imaging modalities (such as MRI, fluorescence imaging (FLI), computed tomography (CT), ultrasound (US), and photoacoustic imaging (PAI)) which provide structural

information. In addition, more modern methods such as positron emission computed tomography (PET) and single-photon emission computed tomography (SPECT), have been developed, which provide additional information such as physiological characterizations of organs and tissues.[206-208] To date, LDH-based imaging contrast agents (ICAs) have been extensively studied for FLI, MRI, CT, PAI, PET and SPECT by virtue of their tunable host composition and versatile intercalation chemistry. Imaging contrast ability in LDHs can be achieved either by loading imaging functional agents or altering the metal elements of layers. Currently, LDH-based ICAs can be divided into single-mode and multi-mode ICAs.

5.2.1. Single-mode imaging

FLI is a widely studied imaging method with relatively high imaging contrast due to its good planar resolution and high sensitivity.[209] The early attempt in loading guest molecules into LDHs for FLI applications was reported by Choy *et al.* in 2000, who constructed fluorescein FITC-modified MgAl-LDH hybrids (FITC-LDH) to monitor the drug delivery behavior of LDHs.[39] Since then, a variety of other imaging functional agents including organic fluorescent molecules (ICG, Cy 5.5 and rhodamine B (RB)), inorganic fluorescent agents (QDs, CDs, up-conversion nanoparticles (UCNPs), carbon nitride (CN), and gold nanoclusters/nanoparticles (Au NCs or Au NPs)) have been utilized to modify LDHs for FLI.[47,144,168,210-212]

Yan *et al.* designed and fabricated versatile fluorescent nanohybrids by incorporating RB molecules and MTX into ultrathin MgAl-LDH nanosheets (MTX/LDH-RB).[177] The MTX/LDH-RB nanosheets retained strong fluorescence in both liquid and dry powder forms owning to the protective effect of LDHs. *In vitro* fluorescent images showed that MTX/LDH-RB could penetrate cell membranes easily, making it promising for bioimaging applications. Our group employed exfoliated MgAl-LDH nanosheets to localize Au NCs through electrostatic force and hydrogen bonds for enhanced FLI.[213] Benefiting from the surface confinement effect of LDH, the fluorescence performance of Au NCs was significantly boosted with a promoted quantum yield (QY) and prolonged fluorescence lifetime (both ~7 times improvement relative to Au NCs). Accordingly, Au NCs/LDH exhibited a strong fluorescence imaging contrast and good

biocompatibility, which were further confirmed by *in vitro* assays. CN is a good candidate for optical applications due to its inherent fluorescence properties derived from the C-N conjugated structure. Our group synthesized MgAl-LDH-based carbon nanomaterials (CN/LDH) by triggering the interlayer condensation of citric acid (CA) and urea for up-conversion fluorescence imaging.[214] CA was first intercalated into the LDH, and then submerged in urea, during which a reaction between urea and CA in the interlayer space occurred and produced LDH-CN. The obtained CN/LDH emitted strong cyan light under ultraviolet (UV)-light irradiation with the highest solid-state quantum yield (SSQY: 95.9 ± 2.2%) of carbon-based fluorescent nanomaterials reported so far, by virtue of the 2D confinement effect of LDH. Moreover, CN/LDH showed enhanced luminescence stability to temperature and environmental pH value relative to free CN. Experimental studies revealed that the host-guest electrostatic interactions between LDH and CN made a predominant contribution to this unprecedented SSQY.

In addition to FLI, the combination of LDHs with some imaging contrast agents (e.g., CuS nanodots, Fe_3O_4 and $CoFe_2O_4$ nanoparticles) can also be used for other single-mode imaging, such as PAI and MRI. Liu *et al.* prepared PAI contrast agents LDH-CuS NCs *via* the *in situ* growth of CuS nanodots on MgAlCu-LDH nanosheets.[215] The LDH-CuS NCs demonstrated the capacity to act as contrast agents for real-time *in vivo* PAI of tumors because of the NIR absorption capacity of CuS. Zhang *et al.* constructed a novel T_1-weighted (positive contrast) MRI contrast agent based on MgAl-LDH.[216] In this nanosystem, ultrasmall Fe_3O_4 nanoparticles were stabilized on the surface of LDH, followed by the loading of hyaluronic acid (HA) and DOX (Fig. 6a). The obtained LDH-Fe_3O_4-HA/DOX nanohybrids displayed a 10-fold higher r1 relaxivity than pristine Fe_3O_4 nanoparticles (4.38 mM^{-1} s^{-1} *vs* 0.42 mM^{-1} s^{-1}). *In vivo* experiments demonstrated that LDH-Fe_3O_4-HA/DOX could effectively penetrate into the tumor for enhanced MRI signal (Fig. 6b-d). Similarly, $CoFe_2O_4$/ZnAl-LDH nanocomposites have also been reported to possess T_1-weighted MRI effect.[217]

Apart from the imaging agent-modified LDHs for single-mode imaging, LDHs may also exhibit inherent single-mode imaging contrast capacity by inclusion of particular

metal elements within the host layers. It has been reported that a variety of high magnetic moment metal ion-doped LDHs (e.g., Gd^{3+}, Mn^{2+}, Fe^{3+}, Cu^{2+}, Yb^{3+} and Dy^{3+}) possess superior MRI contrast performance.[218-223] For example, Li *et al.* devised Mn-doped MgAl-LDH (Mn-LDH) through the isomorphic substitution of partial Mg^{2+} with Mn^{2+} ions for T_1-weighted MRI.[45] The Mn-LDH nanoparticles demonstrated sensitive response to weakly acidic environments (pH 6.5−7.0, the pH range in the TME) and exhibited a ultra-high longitudinal (r1) relaxivity (9.48 mm^{-1} s^{-1}). *In vivo* evaluations showed clear MR imaging of tumor tissues in mice after intravenous injection, showing great potential for accurate and precision tumor diagnosis.

Further to this study, Zuo *et al.* investigated the theranostic function of the Mn-LDH nanoparticles by loading therapeutic siRNA in the Mn-LDH particles.[218] The high delivery efficacy and ultrasensitive pH-responsive MRI contrast effect make dual-functional Mn-LDH particles a potential theranostic agent for cancer diagnosis and therapy. Furthermore, the same group constructed a cancer cell membrane (CCM)-coated Mn-LDH biomimetic particle to realise cell-specific targeting and improve tissue penetration for enhanced MRI diagnosis of cancers.[219] The favorable cell-specific targeting and tissue penetration capabilities were unveiled using 2D cell cultures, 3D spheroid cultures, and mouse models of breast cancer. *In vivo* MR imaging of the CCM-coated nanoparticle showed clear images of tumor tissues with significantly enhanced contrast in the central region. Moreover, *in vitro* and *in vivo* biosafety evaluations have verified the desirable biocompatibility of this Mn-LDH-based biomimetic nanoparticle. We envisage that such a biomimetic nanoparticle will further serve as a promising MRI contrast agent for precise cancer diagnosis.

Wang *et al.* manufactured a T_1-weighted MRI contrast agent consisting of an Fe^{3+}-doped MgAl-LDH nanoring *via* a coprecipitation-acid etching approach.[221] The doped Fe^{3+} dispersed in the LDH crystalline structure causes a decrease in the volume magnetic anisotropy, and ultimately reduces T_2-weighted MRI performance. After acid etching, the Fe^{3+} content on the LDH surface increased substantially, which enhanced the T_1-weighted MRI effect. Likewise, the paramagnetic susceptibility of Gd^{3+} and Dy^{3+} enable their application as MRI contrast agents, and most currently used MRI CAs are

Gd based. Andrade *et al.* prepared ZnAlGdDy-LDH with different Gd^{3+}/Dy^{3+} doping ratios ($Zn_{2.0}Al_{0.75}Gd_{0.125}Dy_{0.125}$-LDH and $Zn_{2.0}Al_{0.5}Gd_{0.25}Dy_{0.25}$-LDH) to evaluate their efficiency as contrast agents.[74] Relaxometry assessments showed that the best T_1-weighted contrast was achieved with the former (r_2/r_1 ratio is 7.9), while the highest T_2-weighted contrast was achieved with the latter (r_2/r_1 ratio is 22.5). Both of them displayed higher r1 relaxivity than a commercial reference, indicating their potential to construct bimodal MRI contrast agents.

In addition, the introduction of radioisotopes (e.g., ^{64}Cu, ^{44}Sc, and Co-57) into LDHs has been shown to be a feasible strategy to obtain PET or SPECT contrast agents.[222,223] Shi *et al.* proposed chelator-free labeling of MgAl-LDH by mixing with PET isotopes (^{64}Cu and ^{44}Sc) to assess the labeling yield and PET imaging contrast effect.[222] After modification with BSA, LDH was successfully labeled by $^{64}Cu^{2+}$ and $^{44}Sc^{3+}$ with excellent labeling efficiency (16.6% and 41.4%, respectively). PET imaging demonstrated that prompt and persistent tumor uptake was achieved with ^{64}Cu-LDH-BSA through passive targeting (EPR effect), supporting LDHs as a feasible platform for PET image-guided cancer therapy.

5.2.2. Multi-mode imaging

The rationale of developing multimodal imaging is to combine different imaging contrast modalities into a single system for collaborative imaging, since each individual imaging technique possesses its inherent features, strengths and weaknesses. For example, FLI exhibits good planar resolution (≈100 nm) and high sensitivity; however, it is difficult to obtain satisfactory imaging depth and 3D information. MRI has the advantages of high resolution with the limitation of long scanning time. CT shows fast scanning and high accessibility; unfortunately, its spatial resolution and sensitivity are relatively low. Although PAI possesses high spatial resolution and low acoustic scattering, it can be easily disturbed by acoustic absorbing objects.[51,206,224] Thus, to maximize functionalities of diagnostic imaging, the paradigm of ICAs is shifting from a single modality to multimodality. Compared with single-mode imaging, multi-mode imaging can provide more accurate and comprehensive diagnostic information. For instance, the trimodal MR/CT/FLI allows deep tissue imaging *via* MRI/CT, while FLI

ensures superior planar resolution. At present, CT/MRI, MRI/FLI, PAI/MRI, NIR thermal imaging/MRI/PAI *etc.* have been developed based on LDHs.

Recently, Jung *et al.* synthesized size-controlled hybrids (Gd/MgGa-LDH) of LDH platelets and $Gd(OH)_3$ nanorods *via* the reverse micelle method for dual-modal CT/MRI.[136] Based on the high X-ray attenuation coefficient of Gd, its oxides or hydroxides possess inherent CT contrast capability. Meanwhile, the paramagnetic properties of Gd^{3+} in $Gd(OH)_3$ enable MRI contrast. More interestingly, the r_1 values of Gd/MgGa-LDH at pH 7 and pH 5 were 2.9 and 7.3, respectively, enabling pH responsive MRI contrast ability depending on the surrounding physiological conditions. In another study, our group designed a supramolecular nanomaterial (FITC/FA-DOX/Gd-LDHs), in which FA and DOX were co-intercalated into Gd-LDHs interlayer, followed by surface adsorption of FITC.[225] The obtained FITC/FA-DOX/Gd-LDHs exhibited excellent T_1-MRI and FLI behavior due to the intrinsic fluorescence of FITC and the longitudinal relaxivity triggered by high-spin Gd^{3+} in the LDH host layers. Satisfactory dual-modal (MRI/FLI) imaging ability was demonstrated by *in vitro* assays performed with KB cells (oral cancer).

With the aim to further enhance spatial resolution, our group successfully developed a PAI/MRI contrast agent by synthesizing CoFe-LDH monolayer nanosheets through a bottom-up method.[49] The presence of Co and Fe elements in the LDH matrix endowed the CoFe-LDH nanosheets with T_2-MRI contrast ability, owing to the unpaired 3d electrons of Co^{2+} and Fe^{3+}. The CoFe-LDH nanosheets also exhibited a concentration-dependent PA signal enhancement, proving the great potential for PAI. *In vivo* tests demonstrated the complete visualization of the tumor site with the help of PAI/MRI after the injection of CoFe-LDH nanosheets. Encouraged by this work, Wang *et al.* fabricated a PA/MR/NIR imaging contrast agent (CoFe-500) by heating CoFe-LDH nanosheets at 500 °C under Ar atmosphere.[77] The CoFe-500 contrast agent absorbed light energy strongly at NIR wavelengths and re-emitted it as heat, giving rise to NIR thermal imaging ability (Fig. 6e). Therefore, CoFe-500 showed trimodal PA/MR/NIR imaging performance, which was verified by *in vitro* and *in vivo* assays (Fig. 6f-j).

5.2.3. Summary of LDH-based nanomaterials for bioimaging

LDHs have received attention as potential contrast agents for various imaging modalities, such as FLI, MRI, CT, PET, and SPECT by virtue of their tunable chemical composition and ion exchange ability. Compared with the application of LDHs in controlled drug release, the development of LDHs as *in vivo* imaging contrast agents is relatively new and still in its infancy. Given that multiple imaging modalities can be integrated into a single LDHs nanoplatform, it is possible to rationally design LDHs to exhibit a combination of feature to acquire more comprehensive biological information than traditional single-modal imaging contrast agents. Therefore, there is still a lot of room for exploring new and advanced LDH-based imaging contrast agents.

5.3. Cancer therapy

Cancer is one of the leading causes of death globally, with high and increasing morbidity and mortality rates.[226,227] Towards optimizing diagnosis and treatment, researchers have explored a number of nanomaterials,[228-236] among which LDHs allow the development of more effective anti-tumor therapy by virtue of their switchable 2D layered nanostructures, excellent biocompatibility and the controllable chemical composition. To date, LDHs and their nanocomposites have been extensively explored in a variety of cancer treatments, including traditional chemotherapy, emerging phototherapy (photothermal therapy (PTT) and PDT), gene therapy, immunotherapy, chemodynamic therapy (CDT), and combination therapy. In this section, we will mainly focus on the most recent advancements of LDH-based nanoplatforms for cancer therapy.

5.3.1. Chemotherapy

Chemotherapy, a widely applied cancer treatment, often suffers from problems of instability, poor solubility and low absorption efficiency of chemical drugs, as well as nonspecific targeting of cancer cells, leading to obvious side effects caused by non-specific uptake of normal cells.[229] Nanomaterial-based drug delivery systems have been exploited to improve the stability, solubility and load efficiency of therapeutic drugs, and control drug release kinetics.[237-242] LDHs and their nanocomposites can meet the requirements of advanced drug delivery systems owning to their excellent biocompatibility, high specific surface area and pH-dependent biodegradability. As early as 2004, LDHs were first explored as drug delivery systems for chemotherapy.

Choy *et al.* synthesized MTX-loaded MgAl-LDH by incorporating MTX into LDH interlayer through ion-exchange.[40] MTX-LDH could be internalized into tumor cells and *in vitro* results proved that compared with free MTX, MTX-LDH effectively inhibited cancer cells proliferation without cytotoxic effects on normal cells. Thereafter, LDH-based drug delivery systems have become increasingly popular.

The synthesis of LDH-based drug delivery systems is generally based on the ion-exchange method, through which therapeutic drugs are intercalated into LDHs interlayer. For example, Qin *et al.* developed podophyllotoxin (PPT)-intercalated MgAl-LDH (PPT-LDH) for cancer therapy, which could overcome the poor solubility and low bioavailability of PPT.[243] *In vivo* experiments demonstrated an enhanced anti-tumor efficacy of PPT-LDH compared with that of free PPT. Applying a similar principle, Zhu *et al.* intercalated chemotherapeutic agent etoposide (VP16) into MgAl-LDH for inhibiting A549 cell migration and invasion.[244] *In vitro* test results confirmed that LDH-VP16 exhibited a desired sustained-release behavior and had a stronger inhibitory effect on cell migration than VP16 alone. On the basis of this research, the same group further studied the performance of SiO_2@MgAl-LDH-VP16 (Fig. 7a).[245] Transwell migration assay showed that SiO_2@MgAl-LDH-VP16 displayed a narrower migration distance and fewer migratory cells compared with LDH-VP16 and free VP16 (Fig. 7b,c), suggesting the heightened anti-metastatic activity. In particular, the core-shell structure of SiO_2@LDH brought satisfied drug loading efficiency and improved the efficiency of VP16 as an anti-metastasis agent.

Apart from the above-mentioned ion-exchange method, chemotherapeutic drugs or biomolecules can also be loaded onto LDHs through co-precipitation or physical adsorption. Since chemotherapeutic agent dacarbazine (DAC) is limited by its poor solubility and severe side effects, Asiabi *et al.* intercalated DAC into NaCa-LDHs *via* co-precipitation to overcome these problems.[246] The prepared DAC-loaded LDHs showed a decent drug loading capability (38% wt%) and pH-sensitive drug release, with an anticancer efficacy against breast cancer cells stronger than that of free DAC. Similarly, positively charged DOX, a DNA-targeting anticancer agent, was intercalated into MgAl-LDH (DOX@LDH) through a one-pot co-precipitation synthesis for pH-

responsive drug release.[247] DOX@LDH exhibited excellent tumor targeting, enhanced cellular uptake and effective release triggered by acidic TME. Superior *in vivo* tumor suppression with DOX@LDH was observed with decreased side effects compared with free DOX.

To further improve the DOX absorption ability of cancer cells, Ge *et al.* prepared electronegative poly(styrenesulfonate) (PSS)-modified NiTi-LDH to load DOX by physical mixing at 37 °C.[248] DOX could be internalized by cancer cells through endocytosis rather than passive diffusion with the assistance of PSS, thereby enhancing drug absorption. Li *et al.* designed a hyaluronidase (HAase)-modified MgAl-LDH nanoplatform to physically load DOX (DOX/LDH-HAase) for enhanced tumor penetration and augmented chemotherapy (Fig. 7d).[249] Owning to the catalytic activity of HAase in digesting HA nearby the cancer cells, the obtained DOX/LDH-HAase enabled more significant cell uptake and tumor penetration than enzyme-free DOX/LDH, therefore exhibiting much better antitumor efficacy, as evidenced by *in vitro* and *in vivo* therapeutic activity assessments (Fig. 7e).

In addition, it has been reported that pristine LDHs without drug loading can function as anticancer agents for chemotherapy. Recently, pure CaAl-LDH synthesized by Saha *et al.* through co-precipitation route exhibited a significant growth inhibition effect on human colon carcinoma (HCT116) and human breast adenocarcinoma (MCF-7), since the excessive Ca^{2+} released by CaAl-LDH degradation under acidic TME would impair cellular functions and eventually induce cell death.[250] Furthermore, the same group investigated the apoptotic pathway mediated by pure CaAl-LDH on MCF-7 and HCT116 cells.[251] The innate anticancer activity of CaAl-LDH was verified by assessing the calcium calmodulin protein kinase II α (CAMKII α) expression and associated superoxide dismutase (SOD) activity in cancer cells. The results indicated that pure CaAl-LDH could significantly down regulate CAMKII α and SOD gene at cellular level, resulting in cell apoptosis. Similarly, Wang *et al.* found that a pH-sensitive film consisting of $Ni(OH)_2$ and Ni-Ti LDH with Ni/Ti ratio (7:1) released large amounts of nickel ions in acidic environments, ultimately inhibiting cancer cells growth without adverse effects on normal cells.[252] High intracellular nickel ions content was detected

in vitro, demonstrating that excessive intake of nickel ions could induce cancer cell death.

5.3.2. Gene therapy

Gene therapy is a promising treatment for gene-related diseases (e.g., cancers, neurodegenerative disorders and some infectious diseases), which refers to the use of negatively charged nucleic acid molecules with therapeutic functions, such as DNA, siRNA, short hairpin RNA (shRNA) and microRNA (miRNA).[65,253-256] Unfortunately, the low delivery efficiency, easy degradability, high toxicity and poor anticancer specificity of nucleic acids hinder their clinical application.[257] With a view to overcome these limitations, many studies have been carried out utilizing LDHs as biodegradable gene delivery vectors since the 2000s. Positively charged LDHs can protect genes from degradation through the confinement effect, and potentially enhance the gene delivery efficiency and targeting ability of nucleic acids.

Research on the application of LDHs as biocompatible vectors for effective gene delivery was started in 1999, as Choy *et al.* utilized MgAl-LDH hybrids to load DNA *via* ion-exchange.[22] The DNA molecules stabilized within the LDHs interlayer space maintained their chemical and biological integrity without any degradation in the physiological environment. In 2008, Thyveetil *et al.* demonstrated the first proof-of-concept study of LDH-based gene therapy by delivering DNA molecules into cancer cells *via* LDHs vectors.[258] When DNA/LDHs nanocomposite penetrated into tumor, LDHs gradually dissolved under the acidic microenvironment, allowing the slow release of DNA molecules that originally stabilized in LDHs interlayer to exert therapeutic effects. More recently, Li *et al.* utilized MgAl-LDH to load the pEGFP-N1 DNA plasmid to transfect mouse motor neuron (NSC 34) cells.[259] Cytotoxicity assessment assay preliminarily demonstrated the minimal cytotoxic effect of DNA-loaded LDH on cellular viability. Based on the pH-responsive degradation ability of LDHs, the released pEGFP-N1 DNA plasmid could effectively transfect NSC 34 cells, showing a good potential for the treatment of cellular neurological diseases.

Wong *et al.* investigated the efficiency of LDH-mediated nucleic acid delivery into neurons and mouse fibroblasts (NIH3T3s).[260] They found that the delivery efficiency

of double-stranded DNA (dsDNA) or siRNAs was determined by the nucleotide sequence (11% of dsDNA *vs* 60% of siRNAs), which led to the conclusion that LDHs would be more suitable for siRNA delivery. In view of this, the same group further demonstrated that dsDNA/siRNA could be more effectively intercalated into smaller LDHs (e.g., a Z-average diameter is approximately 45 nm) to transfect human embryonic kidney cells (HEK 293T).[261] They engineered MgAl-LDH with an average particle size of about 45 nm for gene therapy, of which the cellular delivery efficiency (88% *vs* 58%, at a dsDNA concentration of 10 μg mL^{-1}) was markedly enhanced compared to large LDHs (approximately 100 nm). Yu *et al.* also engineered ultrasmall LDHs (approximately 60 nm) to load peptide nucleic acid (PNA) for efficient gene therapy of pancreatic cancer (Fig. 8a).[262] The developed PNA-loaded LDHs platform (LDHs/PNA) allowed selective targeting of intranuclear mutant sequences (oncogenic $KRAS^{G12D}$ gene) due to the proton sponge effect of LDHs. It was found that LDHs/PNA successfully silenced $KRAS^{G12D}$ gene and induced its inactivation, ultimately significantly inhibiting the growth of pancreatic cancer xenografts (Fig. 8b-g).

Functionalization of and nanocomposite formation with LDHs can further enhance their gene delivery efficiency and therapeutic efficacy. For example, Park *et al.* designed FA-modified MgAl-LDH (LDHFA) to delivery survivin siRNA (siSurvivin, an inhibitor of apoptosis (IAP) gene that can induce cancer cell death) for FA receptor-mediated active targeting uptake by cancer cells.[263] *In vivo* assays demonstrated that the prepared LDHFA/siSurvivin achieved 3-fold higher inhibition rate of tumor growth than LDH/siSurvivin with passive targeting function, which was attributed to the 1.2-fold higher selective accumulation of LDHFA/siSurvivin at tumor site than other organs. Recently, mannose-conjugated SiO_2 coated MgAl-LDH (Man-SiO_2@LDH) was reported by Li *et al.* for targeted delivery of cell death siRNA (CD-siRNA) to enhance cancer therapy.[143] The surface modification of MgAl-LDH with mannose and SiO_2 endowed it with good colloidal stability and excellent biocompatibility. Cellular uptake studies showed that CD-siRNA could be more efficiently delivered to osteosarcoma (U2OS) cells by Man-SiO_2@LDH compared with unmodified MgAl-LDH due to the targeting ability of mannose (targeting lectin-like receptors on tumor cells), thereby

promoting cancer cell apoptosis.

The gene delivery efficiency of exfoliated LDH nanosheets has been shown to be higher than that of unexfoliated or bulk LDHs. Wang *et al.* synthesized Mg-Al-lactate and Mg-Al-acetate LDH nanosheets (LDH-lactate, LDH-acetate) as non-viral vectors for the delivery of salmon DNA to 293T cells.[264] The DNA adsorption capacity of LDH-lactate and LDH-acetate were evaluated, and results suggested that the former had higher adsorption capacity due to more LDH surface exposure caused by its larger delamination degree. Cytotoxicity studies verified that LDH-lactate was less toxic than LDH-acetate, since a smaller dose of LDH-lactate was required to deliver the same amount of DNA. Hence, the greatly delaminated LDH nanosheets have more potential to deliver genes than bulk LDHs.

In order to enhance therapeutic performance, two or more therapeutic agents have been simultaneously loaded in a LDH nanoplatform, demonstrating that LDH is an ideal drug nanocarrier for combination therapy. For example, Li *et al.* employed MgAl-LDHs to load allstars CD-siRNA and 5-FU (an anticancer drug) for enhanced cancer therapy.[265] By intercalating 5-FU into LDHs interlayer and loading CD-siRNA on LDHs surface, the obtained CD-siRNA-5-FU/LDHs exhibited significantly higher cytotoxicity on MCF-7, U2OS and HCT-116, compared to CD-siRNA/LDHs and 5-FU/LDHs. Similarly, Ma *et al.* assembled LDHs with chalcone (a p53 activator, used to activate p53 for regulating the cellular response to cisplatin) and disuccinatocisplatin (DSCP, a Pt(IV) prodrug) into a nanoplatform (Pt(IV)-chalcone/LDH).[266] The *in vitro* anticancer activity of Pt(IV)-chalcone/LDH was dramatically increased compared to cisplatin and Pt(IV)/LDH, due to the synergistic effect of p53 protein promoted cell apoptosis and necrosis initiated by the platinum drug.

5.3.3. Immunotherapy

Immunotherapy is a form of cancer treatment that targets the immune system rather than the tumor itself, in which adjuvants are usually involved to potentiate the immunogenicity of antigens (e.g., epitope peptides, recombinant proteins, DNA plasmids or message RNA) and activate antigen-presenting cells (APCs).[267-269] The increasing complexity of cancer is a challenge faced by immunotherapy, requiring

adjuvants to simultaneously stimulate humoral and cellular immune responses by enhancing their activity or more efficiently carrying antigens to APCs or lymphoid organs.[270-272] Notably, LDHs have been reported as ideal adjuvants, since the layered structure, positively charged host layers, and adjustable interlayer space enable them to load large amounts of antigens and interact with APCs or lymphoid organs, thereby achieving potent and durable immunity.[169,273,274]

In 2011, Li *et al.* successfully formulated DNA vaccines using MgAl-LDHs as vaccine adjuvants to activate dendritic cells (DCs).[43] It was the first attempt to synthesize LDHs as useful vectors for promoting vaccine delivery in immune cells. Thereafter, LDH adjuvants were extensively investigated to formulate vaccines for immunotherapy. During this period, the relationship between the adjuvanticity of LDHs and their chemical composition was explored, and it was found that the physicochemical properties of LDH adjuvants regulated by their composition, particle size and crystal structure could determine the immunological responses.

Williams *et al.* reported that LDHs with different cations and anions exhibited varying degrees of adjuvanticity.[275] Their study showed that ovalbumin (OVA, an antigen)-loaded Ca_2Al-NO_3-LDH induced a high level of antibody production, whereas OVA-loaded Mg_2Al-NO_3-LDH did not. The intercalated anions also influenced adjuvanticity. Compared with Mg_2Al-NO_3-LDH, Mg_2Al-CO_3-LDH showed dramatically enhanced adjuvanticity, leading to both cellular and immune response. Li *et al.* prepared a series of Mg_xAl-LDHs composed of different Mg/Al ratios (x = 1, 2 and 3) to further investigate their effect on immune response.[276] Results clarified that the ratio of metal cations directly affected their adjuvanticity. For instance, MgAl-LDH (x = 1) displayed higher expression of pro-inflammatory cytokines (TNF-α, IL-12, CD86 and CD40) in DCs than MgAl-LDH (x = 2 and 3). Moreover, only MgAl-LDH (x = 1) promoted DCs to express NF-κB, resulting in a more intense immune response. In short, the ion composition of LDHs is an important factor that determines the adjuvanticity of LDHs, which not only affect the maturation and activation of DCs, but also regulate the intensity of the immune response.

The particle size and structure of LDH adjuvants are also important factors in affecting

immune response. For example, Chen *et al.* prepared intimin β (IB, a bacterial antigen)-loaded MgAl-LDH vaccine adjuvants with three average sizes (115, 243 and 635 nm, respectively).[170] The immunological data indicated that LDHs with an average diameter of 115 nm induced the highest level of antigen-specific antibody production, which was 2- and 1.5-fold higher than that induced by 243 nm and 635 nm LDHs, respectively. Yan *et al.* further compared the immune induction of MgAl-LDH nanosheets (about 177 nm in size) and MgAl-LDH nanoparticles (average diameter of 110 nm).[277] They combined the two kinds of nano-LDHs with the antigen OVA through physical adsorption. It was found that the former showed stronger adjuvanticity for stimulating specific antibody responses than the latter. LDHs with smaller particle size (ca. 110 nm) were shown to migrate into the subcutaneous tissues, followed by penetration into the draining lymph nodes (dLNs) for rapid activation of APCs and B/T lymphocytes. Larger sized LDHs (ca. 177 nm) on the other hand could circulate through the bloodstream into the spleen, the largest secondary lymphoid organ, thereby effectively triggering an immune response. Zhang *et al.* recently reported that the strength of anti-tumor immunity induced by bioadjuvant CPG and antigen OVA co-loaded MgAl-LDH nanovaccines (CO-LDH) was highly dependent on size, with 215 nm sized LDHs exhibiting the strongest immunotherapeutic effect due to its highest enrichment efficiency in the spleen (Fig. 9a-c).[278]

Another feature of LDH adjuvants is their rapid endosomal escape ability. LDHs can be efficiently internalized by APCs *via* clathrin-mediated endocytosis, and rapidly escape from endosomes within 15−30 min through the “salt osmotic effect”, releasing antigens into the cytoplasm and maximally maintaining the antigen integrity.[279] Antigens located in the cytoplasm after endosomal escape can be presented through MHC I, MHC II or cross-presentation pathway, thereby eliciting effective humoral and cellular immunity.[169,280]

It is worth noting that LDH adjuvants have been shown to have higher adjuvanticity than conventional adjuvants such as Alum and QuilA. A recent work showed that IB-loaded MgAl-LDH adjuvant had excellent biocompatibility and induced 2-fold more IFN-γ secreted splenocytes than Alum.[274] Such a significant enhancement could be

attributed to the loose structure of LDHs (Fig. 9d), which promoted LDHs to release more antigens (50 ~ 60%) than Alum (< 10%) within 35 d. Meanwhile, compared to Alum with tightly held together structure, LDHs caused less local inflammation and were easier to degrade in an acidic environment. Zhang *et al.* found that the amount of tyrosinase-related protein 2 (Trp2)-specific cytotoxic T cells induced by MgAl-LDH was 4-fold higher than that induced by Alum, showing superior melanoma immunotherapy efficacy.[281] In another study, Chen *et al.* reported that MgAl-LDH stimulated a higher level of IB-specific antibodies than QuilA.[282]

The adjuvanticity of LDHs can be enhanced even further by combining them with bioadjuvants to create nano-adjuvants with a synergistic effect on immunogenicity. In 2011, Li *et al.* prepared the first LDH-based synergistic nano-adjuvant by combining MgAl-LDHs with CpG, a bioadjuvant approved by the FDA, and further loaded pcDNA3-OVA plasmid that could transfect cells to produce OVA antigens (pcDNA3-OVA/LDHs-CPG).[43] Immunological assays indicated that the antitumor immune response induced by pcDNA3-OVA/LDHs-CPG was faster and stronger than that of pcDNA3-OVA/LDHs, resulting in effective tumor growth inhibition. In another study, Yan *et al.* employed LDH-CpG adjuvant to load OVA for melanoma immunotherapy.[283] Conjugation of CpG to MgAl-LDHs significantly enhanced the antibody response. Besides LDH-CpG, other synergistic nano-adjuvants such as LDH-siIDO (consisting of LDHs and indoleamine 2,3-dioxygenase (IDO) siRNA) have also been studied to alleviate the immune tolerance of DCs. Zhang *et al.* prepared Trp2-loaded MgAl-LDH-siIDO synergistic nano-adjuvant for melanoma immunotherapy.[281] It was found that Trp2 assisted by LDH-siIDO could induce a higher level of Trp2-specific cytotoxic T cells than pristine LDHs adjuvant, which was attributed to the fact that siIDO down-regulated the expression of IDO genes in DCs and transformed DCs from immune tolerance to immune activation, thus enhancing the antigen presentation of DCs and inducing more Trp2-specific cytotoxic T cells to suppress melanoma growth.

Another recent advance in the field is the development of LDH based immunogenic cancer cell death amplifier. Li *et al.* reported a FeOOH@STA/Cu-LDH nanohybrid amplifier that consists of Cu-LDH, FeOOH nanodots (ROS inducer), and heat shock

protein inhibitor (STA) (Fig. 9e).[284] Using *in vitro* and *in vivo* 4T1 tumor models, the FeOOH@STA/Cu-LDH demonstrated efficient photothermal effect at fever-type temperature (40−42 °C) which enhanced the generation of ROS catalyzed by FeOOH nanodots in the TME, thus efficiently boosting calreticulins (CRT) membrane translocation, inducing cancer cell apoptosis, and stimulating cytotoxic T lymphocytes (CTLs) to activate systemic anti-tumor immunogenicity. Remodeling the immunoenvironment is also a desirable strategy to enhance immunotherapy in solid tumors. Yang *et al.* developed microRNA-155 (miR155)-loaded MgAl-LDH (LDH@155) nanoparticles to modulate the immunosuppressive tumor microenvironment (ITM) by repolarizing tumorigenic M2 subtype macrophages (TAMs) to antitumor M1 subtype (Fig. 9f).[285] It was found that LDH@155 could be passively swallowed by tumor associated TAMs to achieve repolarization, which could elevate T-cell infiltration and activation, thereby promoting therapeutic efficiency of programmed cell death-1 (α-PD-1) antibody immunotherapy.

5.3.4. Phototherapy

Phototherapy, mainly including PDT and PTT, has attracted increasing attention recently due to its non-invasive or minimally invasive nature, high selectivity, and reduced side effects.[286-290] Phototherapy is a clinically applied therapeutic approach. In phototherapy, phototherapeutic agents absorb visible/NIR light, and consequently hyperthermia or cytotoxic substances such as ROS (containing $^1O_2$, superoxide radicals ($\cdot O_2^-$) and ·OH), are generated to induce cancer cell damage. Unfortunately, most phototherapeutic agents are highly hydrophobic and tend to aggregate in a physiological environment, considerably reducing their therapeutic efficiency *in vivo*.[291-293] The use of nanocarriers to increase the hydrophilicity, dispersibility and bioavailability of phototherapeutic agents (i.e., PSs and photothermal agents) is highly preferred. In the past decade, LDH-based nano-systems have been intensively studied for enhanced PDT and PTT.

PDT:

PDT relies on PSs to produce ROS, mainly through two main mechanisms: type I and type II. Initially, PSs in the ground state can be transformed into excited singlet state by

absorption of light, and then changed to activated triplet state through intersystem crossing. In the type I mechanism, the activated PSs (e.g., TiO_2, g-C_3N_4, Ti_3C_2 nanosheets) undergo an electron transfer process with cellular substrates to generate free radicals (i.e., $\cdot O_2^-$ and ·OH) without O_2 dependence. In the type II mechanism, the activated PSs (e.g., zinc phthalocyanine (ZnPc), chlorin e6 (Ce6), methylene blue (MB), rose bengal (RB)) produce $^1O_2$ *via* energy transfer with surrounding O_2 and is therefore highly dependent on O_2.[294-297] Currently, the majority of the LDH-based PSs usually implement PDT through the type II mechanism. For example, in 2014, our group established a supramolecular PS for PDT by intercalating ZnPc into MgAl-LDHs interlayer.[44] The incorporated ZnPc presented a highly dispersed monomeric state in LDHs, endowing ZnPc/LDH with increased $^1O_2$ production efficiency. *In vitro* and *in vivo* assays demonstrated that ZnPc/LDH with a rather low dosage of ZnPc showed a superior PDT performance compared with free ZnPc. Moreover, the improved stability and high biocompatibility of ZnPc/LDH guaranteed its practical application.

In the same year, Li *et al.* incorporated Zn^{2+} phthalocyanine tetra-α-substituted with 4-sulfonatophenoxy groups ($ZnPcPS_4$, a type II PS) into MgAl-LDH *via* electrostatic interaction to fabricate a pH-responsive PS system (LDH-$ZnPcPS_4$) for efficient PDT.[298] The photoactivity of $ZnPcPS_4$ was quenched after combination with LDH due to the host-guest interactions. The as-prepared LDH-$ZnPcPS_4$ was essentially stable against releasing ZnPc at pH 7.4, while in weakly acidic environments (pH 6.5 or 5.0), $ZnPcPS_4$ was released from LDH, resulting in the restoration of photoactivity. *In vitro* results exhibited that the IC_{50} value of LDH-$ZnPcPS_4$ was 24-fold lower than that of pristine $ZnPcPS_4$, whilst showing satisfactory $^1O_2$-based photodynamic activity.

Ce6, a commonly used PS, is known to suffer from problems of low solubility, poor photostability, and low intracellular delivery efficiency.[299] To improve its applicability in PDT, Yan *et al.* covalently conjugated Ce6 to PEG-modified MgAl-LDHs for enhanced anticancer PDT.[174] After being anchored onto LDH matrix, Ce6 exhibited significantly improved photostability and intracellular delivery efficiency. *In vitro* and *in vivo* studies revealed that the PDT performance of Ce6-loaded LDH was stronger than that of free Ce6. Similar to Ce6, phthalocyanines PSs also have some obstacles

like low bio-compatibility, hydrophobicity and non-targeting ability. To overcome the limitations, Wang *et al.* intercalated folic acid-linked $ZnPcG_4$ ($ZnPcG_4$-FA) PS into MgAl-LDH through co-precipitation for a highly efficient PDT (Fig. 10a).[175] The prepared $ZnPcG_4$-FA/LDHs displayed high photostability, enhanced solubility and superior *in vitro*/*in vivo* PDT efficacy without any apparent toxic side effects (Fig. 10b-e). Based on this principle, other sophisticated LDH-based PS systems, such as octasulfonate-modified Zn^{2+} phthalocyanine ($ZnPcS_8$)/MgAl-LDH, curcumin/MgAl-LDH and ICG/Cu-LDH, have also been developed by Li *et al.* Khorsandi *et al.* and Liu *et al.*[300-302]

Apart from poor hydrophilicity and photostability, the limited tissue penetration depth of visible light (1−6 mm) and low $^1O_2$ production efficiency of PSs impede their PDT application.[303] The low penetration depth can be attributed to the absorption of visible light by endogenous chromophores such as hemoglobin and cytochromes in biological tissues, as well as light scattering, diffusion and disorientation caused by the heterogeneous structure of biological tissues.[299] Given that NIR light (including NIR I (700–1000 nm), NIR II (1000–1350 nm) and NIR-III (1350–1870 nm) region) is the "optical window" of biological tissue that minimizes the extent of tissue scattering,[304] our group fabricated an NIR-I-activated PS for two-photon PDT by assembling IPA into LDHs interlayer.[46] The obtained supramolecular PS (IPA/LDH) exhibited dramatically enhanced anti-cancer ability compared to free IPA (Fig. 10f,g), which was attributed to the superior tissue penetration of the 808 nm laser (exceeding 1 cm) and surface/space confinement-promoted $^1O_2$ quantum yield (up to 0.74). *In vivo* tests further verified its significant tumor ablation capabilities without toxic effect on normal tissue (Fig. 10h,i). More importantly, compared with traditional two-photon systems that absorb two photons and then transfer the energy to a second PS, this work achieved two-photon PDT using a single material.

Given that light in NIR-III window has longer penetration depth than the light in NIR-I and NIR-II windows, our group further reported a novel CoMo-LDH nanosheets, which was activated *via* defect engineering, as highly active inorganic PSs for NIR-III PDT.[50] The defect-rich CoMo-LDH exhibited excellent activity for ROS generation

under 1567 nm laser irradiation, making it a potential PS for NIR-III PDT to efficiently induce cancer cells apoptosis *in vitro* and eliminate tumors *in vivo*. This is the first case of highly efficient NIR-III PDT using 2D inorganic nanomaterials as PSs, which effectively overcome the problem of inadequate light penetration in current visible PDT. In addition, since the generation of ROS requires the presence of local O_2, overcoming tumor hypoxia is another important strategy to improve the efficiency of PDT. Ruan *et al.* successfully synthesized FeMn-LDH nanosheets to load MB (a type II PS) for O_2-evolving PDT.[305] FeMn-LDH nanosheets exhibited catalase-like activity, which enabled them to facilitate the decomposition of H_2O_2 into O_2. As a result, FeMn-LDH/MB could significantly alleviate tumor hypoxia and enhance the efficiency of O_2-dependent PDT. *In vivo* assays showed that FeMn-LDH/MB almost completely eliminated tumor tissues.

PTT:

PTT commonly applies photothermal agents to convert NIR light into heat, causing localized hyperthermia and thermally-driven cell death. Therefore, if the photothermal agent is concentrated within a tumor, PTT can be used to ablate cancer cells within the tumor. However, traditional photothermal agents including dopamine, ICG, polythiophene, polypyrrole, *etc.*, have poor photothermal conversion efficiency (η), short half-life and rapid clearance in physiological environment.[306,307]

To address the issues, LDH-based photothermal agents have been developed. For instance, our group synthesized a targeted photothermal agent by co-intercalating ICG and folic acid (FA, a cancer targeting agent) into MgAl-LDHs.[308] The intercalation of ICG into the LDH interlayer prevented aggregation of ICG, which in turn improved it's stability, thereby increasing the photothermal conversion efficiency. The resulting ICG-FA/LDH displayed the functional capabilities of high stability, cancer cells targeting, and high biocompatibility. *In vitro* assays performed with KB cells revealed that ICG-FA/LDH exhibited a largely-enhanced PTT effectiveness compared to free ICG at an ultra-low drug dosage (ICG: 8 μg mL^{-1}), which was attributed to the enhancement of ICG-induced photothermal efficiency and the FA-elevated cellular uptake. We also developed a supramolecular photothermal agent by the co-incorporation of ICG and

DOX into Gd^{3+}-doped MgAl-LDHs.[309] In this nano-system, the homogeneous dispersion of ICG and DOX molecules within the MgAl-LDHs was shown to significantly improve the ICG-mediated phototherapeutic efficiency and DOX-mediated chemotherapeutic efficiency.

In addition to the organic photothermal agents mentioned above, inorganic NIR absorbing nanomaterials (e.g. gold, carbon nanoparticles) have also been complexed with LDHs for PTT.[288,289] The combination of LDHs and inorganic photothermal agents can effectively enhance their photothermal conversion efficiency. For example, Wang *et al.* fabricated GNRs-modified and butyrate (an anticancer agent)-loaded NiTi-LDHs films (Au@LDH/B) on the surface of nitinol alloys for combined chemotherapy and PTT.[310] When Au@LDH/B was exposed to NIR, the photothermal effect induced by GNRs increased the temperature of NiTi-LDHs films, resulting in the eventual release of butyrate. The *in vitro* temperature of Au@LDH/B rose to 50 °C within 10 mins under NIR irradiation (808 nm), 12 °C higher than free GNRs. The distinct synergistic effect of Au@LDH/B in chemothermal therapy was further verified by *in vivo* experiments. Later on, Ma *et al.* took GNRs as seeds, followed by the formation of MgAl-LDHs surrounding GNRs to manufacture a core-shell photothermal agent (GNR@LDH), whose nanostructure ensured the high dispersion of GNRs (Fig. 11a,b).[311] GNR@LDH showed a significantly high photothermal conversion efficiency (60%) in the reported GNRs-based PTT with NIR (808 nm) irradiation, since the interaction between GNRs and LDHs caused electron defects on the Au surface, inducing more thermal energy conversion. *In vitro* and *In vivo* assessments demonstrated the excellent PTT performance of GNR@LDH with a low dosage of Au (Fig. 11c-f).

In addition to being used as a carrier for phototherapeutic agent, LDH itself has also shown potential photothermal properties. Wang *et al.* designed a series of LDH-based photothermal agents (CoFe-*x*) by calcining CoFe-LDH nanosheets at different temperatures (*x*: 200-800 °C) under Ar atmosphere for the exploitation of Co^{2+} defects to enhance photothermal performance.[77] Density functional theory (DFT) calculations and experiments provided strong evidence that Co^{2+} defects modified the electronic structure of CoFe-*x* by narrowing their bandgap, this is why the photothermal efficiency

of CoFe-*x* is dependent on the amount of Co^{2+} defects. As a result, CoFe-500 containing the highest Co^{2+} defect concentration exhibited the most effective photothermal performance under NIR irradiation (808 nm), which was further verified by *in vitro* and *in vivo* assays.

Similarly, Li *et al.* constructed a new theranostic nanoplatform based on defect-rich Cu-doped MgAl-LDH (Cu-LDH) nanoparticles for acid-enhanced PTT.[188] Cu-LDH possessed a large amount of OH defects around Cu^{2+}, enabling a higher photothermal transduction efficiency (53.1%) than that of reported Cu-containing photothermal agents (e.g., $Cu_{2-x}S$, $Cu_{2-x}Se$ and $Cu_{2-x}Te$) under NIR irradiation (808 nm). Moreover, more defects were generated by exposing Cu-LDH to acidic environments, leading to a significant acid-enhanced photothermal conversion (53.1% at pH 7.0 *vs* 81.9% at pH 5.0), by virtue of which the tumors (characterized by acidic microenvironment) treated with Cu-LDH were completely eliminated. Liu *et al.* also verified that the incorporation of Cu into MgAl-LDHs was responsible for photothermal conversion owning to the presence of Cu-related defects (Fig. 11g,h).[312] This nanomedicine effectively eliminated tumors *in vivo* under 808 nm laser irradiation (Fig. 11i-k). In another study, Xie *et al.* prepared Mn-LDH nanoparticles and demonstrated their excellent PTT performance coupled with simultaneous T_1-weighted MRI enhancement ability.[313] *In vivo* studies showed that MRI-guided PTT for tumor elimination has been achieved using the Mn-LDH without additional photothermal agents.

Exploiting the topotactic transformation properties of LDH to convert it into TMCs is also a strategy for preparing LDH-based photothermal agents. Our group prepared CoFe-selenide (CFS) ultrathin nanosheets through a topotactic transformation process from CoFe-LDH precursor, followed by surface modification with PEG.[155] The obtained CFS-PEG nanosheets inherited the finely controlled and ultrathin structure of LDH, displaying an outstanding PTT performance with the photothermal conversion efficiency reaching 74.5%, which is the first level of TMC nanosheets reported at present. *In vitro* and *in vivo* analyses respectively confirmed the superior anticancer activity of CFS-PEG with significant PTT-induced cancer cell apoptosis and complete tumor elimination.

Subsequently, our group synthesized CoCuFe-selenide (CCFS) ultrathin nanosheets by *in situ* selenylation of CoCuFe-LDH precursor for pH-sensitive PTT.[104] The PTT efficiency of CCFS was controlled by Cu doping ratio and pH value, with an optimal photothermal conversion efficiency of 81.0% at a 30% Cu molar content at pH 5.4. *In vivo* investigations demonstrated complete tumor elimination after treatment with CCFS and 808 nm irradiation. Based on these works, we further prepared ultrathin $CuFe_2S_3$ nanosheets *via* CuFe-LDH sulfurization for NIR-II PTT to induce cancer cells apoptosis (1064 nm irradiation).[156] The PEG-modified $CuFe_2S_3$ nanosheets ($CuFe_2S_3$-PEG) exhibited broadband NIR-II absorption with a satisfactory photothermal conversion efficiency of 55.86% under 1064 nm laser irradiation.

5.3.5. Chemodynamic therapy

CDT is an emerging therapeutic approach that is tumor-specific and non-invasive. CDT relies on the metal ions-initiated (e.g., Fe^{2+}, Co^{2+}, Ni^{2+}, Cu^{+}, Ti^{3+} and Mn^{2+}) Fenton or Fenton-like reactions to specifically induce tumor cells apoptosis by catalyzing intracellular H_2O_2 into toxic ·OH within TME.[314-318] Initially, several iron-containing nanomaterials, such as γ-Fe_2O_3 and Fe_3O_4 nanoparticles, were explored as CDT agents.[319] Currently, LDH-based CDT agents have also been implemented due to their adjustable metal element composition.

In 2018, LDH-based CDT was introduced by Cao *et al.* for highly efficient tumor therapy by designing biocompatible and biodegradable 2D PEGylated ferrous-containing LDH nanosheets (PEG/Fe-LDH), which are able to *in situ* catalyze ROS generation in response to the specific TME based on a typical catalytic Fenton reaction (Fig. 12a).[48] The elaborately designed PEG/Fe-LDH nanocatalysts with high biodegradability and biocompatibility as constructed by a toxic solvent-free, bottom-up approach towards concurrent nanosheet delamination and PEGylation, exhibit obvious tumor suppression effect in 4T1 breast tumor xenografts without the use of additional catalysts or any inherently toxic substances or agents, concurrently with high therapeutic biosafety. In this work, PEG/Fe-LDH nanosheets catalyzed endogenous H_2O_2 to generate ROS. Nevertheless, the intrinsic H_2O_2 level in TME is not adequate. Supplying exogenous H_2O_2 to the tumor site would be an effective strategy to promote

the efficacy of CDT.

In 2020, our group fabricated a highly dispersed LDH-based nano-enzyme (GOD/CoFe-LDHs) by immobilizing glucose oxidase (GOD) onto CoFe-LDHs nanosheets for H_2O_2 self-supplied CDT.[49] CoFe-LDHs nanosheets displayed an enhanced capability to convert H_2O_2 into ·OH, and the rate constant (3.26×10^{-4} s^{-1}) is 1-3 orders of magnitude higher than other Fe-based CDT agents. By virtue of the generation of massive H_2O_2 triggered by GOD (catalyzing the decomposition of glucose to H_2O_2), GOD/CoFe-LDHs exhibited efficient ·OH production under acidic conditions, thus leading to remarkable catalytic therapeutic performance *in vitro* and *in vivo* (Fig. 12b,c). Taking into account that heating can increase the rate of chemical reactions, we further developed a multifunctional nanosystem (GOD/CuFe-LDHs) for heat-facilitated CDT.[103] CuFe-LDHs not only possessed acid-enhanced PTT property, but also exhibited pH-responsive CDT performance. More importantly, the hyperthermia from PTT significantly enhanced the rate of ·OH production. Therefore, GOD/CuFe-LDH demonstrated synergistic anticancer activity with complete tumor elimination.

In the same year, our group synthesized CoMn-LDH nanosheets through a bottom-up method for TME-responsive CDT.[52] Co^{2+} in LDH host layer served as a Fenton catalyst for inducing ·OH generation under acidic conditions. Reaction activity assessments showed that the CDT performance of CoMn-LDH was superior to CoAl-LDH with more ·OH generation under simulated TME (H_2O_2 and GSH were present). This is because Mn^{4+} could consume GSH through redox reaction, avoiding further reaction between GSH and ·OH. Additionally, the introduction of Ce6 endowed CoMn-LDH with PDT performance. As a result, Ce6/CoMn-LDH was shown to be capable of acting as a multifunctional therapeutic agent for CDT/PDT synergistic therapy.

Nanocomposites or TMCs obtained from LDHs as precursors have also been adopted as CDT agents. For example, Liu *et al.* presented the fabrication of LDH-CuS nanocomposites (LDH-CuS NCs) as a biodegradable CDT platform through an *in situ* growth strategy.[215] MgAl-LDH nanoplates were first synthesized, followed by the replacement of partial Mg^{2+} and Al^{3+} with Cu^{2+} *via* isomorphic substitution. After

sulfurization, CuS nano-dots were grown *in situ* on the LDH host layers. The obtained LDH-CuS NCs efficiently accumulated in lysosomes, accompanied by the NIR-induced copper ion (Cu^{2+} and Cu^{+}) release, which could catalyze Fenton-like reaction, causing lysosomal membrane permeabilization (LMP) pathway-associated cell apoptosis (Fig. 12d). *In vitro* and *in vivo* assessments demonstrated the prominent anticancer efficacy of LDH-CuS NCs (Fig. 12e-h). Recently, PVP-modified CoFeMn dichalcogenide nanosheets (CFMS-PVP NSs) were developed by vulcanizing CoFeMn-LDH precursors.[54] The presence of metal ions (Co^{2+}, Fe^{2+}/Fe^{3+}) enabled the effective conversion of H_2O_2 into ·OH. Besides, CFMS-PVP NSs possessed an outstanding photothermal performance with the highest photothermal conversion efficiency (89.0%) reported for TMCs to date. The temperature rise also accelerated the disproportionation of H_2O_2, thus achieving PTT-enhanced CDT. Remarkable therapeutic outcomes were observed both *in vitro* and *in vivo*.

5.3.6. Combination therapy

Although the above-mentioned cancer therapies are effective to a certain extent, the outcome of monotherapy generally remains suboptimal. This deficiency has been taken into account in the development of combined regimens that complement one's weaknesses with another's strengths, giving rise to therapeutic synergy. We have already briefly discussed how bimodal systems (e.g., chemo/PTT, CDT/PDT) can outperform single mode therapies. In this section we will explore combination therapies in more detail, including dual-mode (e.g., chemo/PDT, chemo/gene, gene/PTT, PTT/PDT, PTT/CDT) and triple-mode (e.g., chemo/PTT/PDT, PTT/PDT/CDT) treatment.[316,320-322]

Heating can accelerate the release of drugs from nanocarriers or increase the Fenton reaction rate, thus the combination of PTT and chemotherapy or gene therapy or CDT has gained continuous attention. For example, Komarala *et al.* successfully fabricated Fe_3O_4-conjugated MgAl-LDH (MNHs) to delivery DOX for thermo-chemotherapy.[323] The hyperthermic effect of Fe_3O_4 increased the temperature of LDH, facilitating the release of DOX. *In vivo* experiments showed that DOX-loaded MNHs almost completely eliminated tumors due to the synergistic thermo-chemo effect. Wang *et al.*

developed CCM-cloaked MgAl-LDH nanomedicine for heat-facilitated PTT/chemotherapy by co-loading ICG and abraxane (Fig. 13a).[324] The obtained CCM-LDH delivery system enhanced the drug accumulation in tumor tissues thanks to the homologous targeting ability of CCM, and significantly inhibited tumor growth under 808 nm laser irradiation due to the synergistic effect of ICG-induced heat and abraxane-mediated chemotherapy. The heat generated by PTT further accelerated the fluidity of cancer cells, thereby promoting cellular uptake of therapeutic agents.

Liu *et al.* devised siRNA-loaded Cu-LDHs coated with pH-sensitive charge-reversible polymer (siRNA/Cu-LDH@PEG-PA/DM) for synergistic gene/PTT.[325] The charge-reversible polymer mitigated cell uptake at pH 7.4 and facilitated cell internalization at pH 6.8, which led to 6.0% accumulation of siRNA/Cu-LDH@PEG-PA/DM in tumor tissue. More significantly, the hyperthermia from Cu-LDH also sped up siRNA release, resulting in >95% inhibition of tumor growth based on the synergistic thermo-gene performance. Our group manufactured Ce-doped CuAl-LDH nanosheets to high-efficiently load ICG, and the prepared ICG/CAC-LDH was adopted as a photothermal agent and Fenton-catalyst for PTT/CDT.[326] ICG/CAC-LDH induced intracellular GSH depletion by the reduction of Cu^{2+} and Ce^{4+}, and the resulting Cu^{+} and Ce^{3+} further reacted to decompose H_2O_2 into cytotoxic ·OH though the Fenton reaction. Moreover, ICG/CAC-LDH efficiently converted NIR light to heat, which not only afforded PTT performance but also increased the Fenton reaction rate. As a consequence, a remarkable synergistic PTT/CDT effect was obtained with complete apoptosis of cancer cells *in vitro*.

The combination of PDT and chemotherapy or PTT has also been utilized to enhance therapeutic efficiency. Our group prepared a drug delivery system (ZnPc-DOX/LDH) by incorporating ZnPc into MgAl-LDHs interlayer and loading DOX on its surface.[327] The embedded ZnPc endowed LDH with an enhanced PDT efficiency, while the physically adsorbed DOX provided a chemotherapeutic effect. *In vitro* assays substantiated a synergistic anticancer performance of ZnPc-DOX/LDH comparison to pristine DOX, ZnPc, DOX/LDH, and ZnPc/LDH. Ruan *et al.* synthesized FeMn-LDH as a photothermal agent due to the presence of oxygen deficiency, followed by loading

MB (a type II PS) through physical mixing (denoted as FeMn-LDH/MB).[305] Since the $^1O_2$ production of type II PDT is highly O_2-dependent, the hypoxic environment of the tumor may greatly hinder the therapeutic effect of PSs. Fortunately, the catalase-like activity of FeMn-LDH catalyzed the decomposition of H_2O_2 to O_2, efficiently increasing the local O_2 concentration and reinforcing O_2-dependent PDT performance. *In vivo* tests performed with HepG2 tumor-bearing mice indicated a synergistic PDT/PTT effect of FeMn-LDH/MB as well as excellent biocompatibility.

Triple-mode combination therapy is highly effective to further optimize anticancer efficacy and minimize side effects. For instance, our group designed Gd^{3+}-doped monolayered MgAl-LDH (MLDH) nanosheets *via* a bottom-up method, and then co-loaded DOX and ICG to obtain DOX&ICG/MLDH.[47] The as-prepared DOX&ICG/MLDH exhibited pH-responsive and NIR-induced DOX release, NIR-induced PTT performance, as well as a large amount of ROS production originating from ICG. *In vivo* therapeutic evaluation demonstrated a complete tumor ablation owning to the synergistic chemo/PTT/PDT effect. Liu *et al.* also reported a trifunctional LDHs nanosystem (ICG/Cu-LDH@BSA-DOX) composed of ICG-intercalated Cu-LDH and BSA-DOX for combined chemo/PTT/PDT (Fig. 13b).[302] It was found that ICG/Cu-LDH@BSA-DOX exhibited acid-triggered DOX release and simultaneously generated hyperthermia and ROS under 808 nm laser irradiation, synergistically inducing cancer cell apoptosis.

Recently, Zhang *et al.* manufactured a multifunctional therapeutic agent by co-loading ICG, DOX and CpG onto LDH nanoparticles, which exhibited efficient photothermal conversion and quick DOX release to execute synergistic Chemo/PTT (Fig. 13c).[328] The CpG/LDH adsorbed tumor-associated antigens induced by Chemo/PTT, thus stimulating the *in situ* antitumor immunity. As a result, this therapeutic agent efficiently eradicated the primary tumor, inhibited distant tumor growth, and prevented tumor recurrence and metastasis in a 4T1 tumor mouse model (Fig. 13d-i). Jia *et al.* fabricated FeMn-LDH as a photothermal nanocarrier to load Ce6/SiO_2 co-coated UCNP (denoted as UCSP) for synergistic PTT/PDT/CDT.[151] FeMn-LDH could release Fe^{3+} and Mn^{2+} under acidic TME, thus initiating a Fenton-like reaction for CDT. Moreover, Fe^{3+}

facilitated the decomposition of H_2O_2 to O_2, improving PDT guided by Ce6-coated UCSP. By virtue of the intrinsic PTT properties of FeMn-LDH, the CDT effect was further enhanced. *In vitro* and *in vivo* experiments conducted with HeLa cells and tumor-bearing mice respectively indicated an overall strong synergistic therapeutic effect.

5.3.7. Targeting Strategy

Increasing the accumulation of LDHs at tumor sites is critical for improving their therapeutic efficiency and alleviating systemic toxicity. The blood vessels of tumor tissue generally feature with abnormalities, such as 10-1000 nm endothelial pores formed by poorly aligned endothelial cells.[329-331] Nanomaterials with a size range of 50-200 nm are prone to penetrate and remain in tumor tissue, known as the EPR effect.[332-334] Most of LDHs used for biomedical applications meet the EPR effect criteria, which enables them to selectively accumulate in tumors through passive targeting with desirable outcomes. However, from biodistribution studies, it is found that LDHs can accumulate in both tumor tissues and major organs such as heart, liver, spleen, lung, and kidney. Particularly, the accumulation of LDHs in liver and kidney is significant.[47,335,336] Thus, the accumulation of LDHs at tumor sites through passive targeting is limited.

Since active targeting is beneficial to increase nanomaterials accumulation at tumor sites through interactions between characteristic receptors and targeting ligands, some LDH-based targeting systems have been constructed in recent years. Park *et al.* developed a siSurvivin delivery system (LDHFA/siSurvivin) by conjugating FA onto the surface of MgAl-LDH to facilitate FA receptor-mediated active targeting uptake by cancer cells.[263] FA surface modification of LDHs grafted with (3-aminopropyl)-triethoxysilane (APS) was achieved through a coupling reaction with APS and 1-ethyl-3-(3-dimethylaminopropyl)-carbodiimide (EDC). The prepared LDHFA/siSurvivin exhibited 1.2-fold higher selective accumulation at tumor site than other organs, resulting in 3-fold higher inhibition rate of tumor growth than LDH/siSurvivin with passive targeting function. In addition to covalent coupling, FA can also be attached to LDHs surface *via* electrostatic adsorption or chelation interactions.[147,225,337]

Recently, Li *et al.* reported mannose-conjugated SiO_2 coated MgAl-LDH (Man-SiO_2@LDH) for targeted delivery of CD-siRNA to enhance tumor accumulation and anticancer efficacy.[143] Cellular uptake studies showed that CD-siRNA could be more efficiently delivered to U2OS cells by Man-SiO_2@LDH compared with unmodified MgAl-LDH due to the targeting ability of mannose (targeting lectin-like receptors on tumor cells), thereby promoting cancer cell apoptosis. Another paradigm was illustrated by Wang *et al.*, who developed CCM-cloaked MgAl-LDH nanomedicine by co-loading ICG and abraxane.[324] The obtained CCM-LDH delivery system enhanced the drug accumulation in tumor tissues thanks to the homologous targeting ability of CCM, and significantly inhibited tumor growth due to the synergistic PTT/chemotherapy.

Prior to reaching cancer cells, biological barriers such as blood-brain barrier (BBB), peritumoral or intratumoral blood vessels, and extracellular matrix, may affect the transport of nanomaterials and hinder their tumor accumulation.[338-340] Considering this constraint, biomolecules complementary to the target site can combine with LDHs to facilitate passage through these barriers. Zuo *et al.* proposed a new target delivery system by conjugating rabies virus glycoprotein (RVG) and angiopep-2 (Ang2) to MgAl-LDHs surface.[341] This LDH-based delivery system was found to penetrate through BBB with high selectivity, since the receptors for RVG and Ang2 are overexpressed in brain endothelial cells. *In vivo* assays confirmed the higher accumulation of RVG&Ang2-conjugated MgAl-LDHs in mouse brain than pristine MgAl-LDHs. Vascular endothelial growth factor (VEGF), which is overexpressed in tumor tissue, has also become an important target for tumor-targeted therapy. Zhu *et al.* designed bevacizumab (Bev, an anti-VEGF antibody)-modified SiO_2@MgAl-LDHs (SiO_2@LDH-Bev) for targeted delivery of DOX.[342] Compared with SiO_2@LDH-DOX, the as-prepared SiO_2@LDH-Bev-DOX showed enhanced cellular uptake and neuroblastoma targeting due to the interaction between Bev and VEGF, dramatically improving anti-tumor performance of DOX.

5.3.8. Summary of LDH-based nanomaterials for cancer therapy

All in all, LDHs can stabilize various bioactive molecules with therapeutic properties either through intercalation pathways (e.g., co-precipitation, ion-exchange, exfoliation-

recombination) or simple adsorption routes by physical mixing. Essentially, LDH-based nanocomposites offer several advantages for a variety of therapeutic applications, such as excellent biocompatibility, efficient drug loading, pH-responsive release, intracellular delivery, and targeted transport of biomolecules. However, to realize the clinical application of LDHs in the biomedical market in the future, more detailed and in-depth studies on the drug delivery process, mechanism of action, toxicological properties and metabolic pathways of LDHs in organisms are required.

5.4. Theranostics

Theranostics is a cutting-edge biomedical technology that combines the diagnosis or monitoring of diseases with the treatment. Specifically, theranostics show great application potential in personalized medicine, for the monitoring of nanomedicines treatment process as well as the treatment effects.[343,344] With the rapid development of bioimaging technology and cancer therapy in recent years, researchers have developed a series of nanomedicines that can realize theranostics.[345-350] Among them, LDHs have great potential in this field due to their controllable metal composition, large specific surface area, and exchangeable interlayer anions. So far, many LDH-based multifunctional theranostic nanoplatforms have been developed, including single-imaging mode theranostics and more recently multi-imaging mode theranostics.

LDH-based single-mode theranostic reagents have been successfully applied in chemotherapy, CDT, PDT and PTT. For example, Usman *et al.* synthesized a theranostic system (ZAGC) by using GdZnAl-LDHs as nanocarrier, with intercalated CHA as a chemotherapeutic drug. The Gd^{3+} centers within the LDH provided MRI contrast capacity, therefore allowing simultaneous therapeutic and diagnostic functions.[75] The contrast of MRI was further enhanced with AuNPs, which were coated on the surface of the ZAGC nanohybrid. The final product ZAGCAu was shown to be an effective multifunctional theranostic agent, with pH-controlled drug release and stronger MRI contrast ability than pure $Gd(NO_3)_3$. Similarly, Kim *et al.* chose LDH as drug carrier with radioisotope (RI) Co-57 labeling to load anticancer MTX (Co-57@MTX-LDH) for SPECT-guided chemotherapy.[223] It was found that the diagnostic component (Co-57) and therapeutic moiety (MTX) generated a synergistic effect

without adversely affecting each other, making Co-57@MTX-LDH an excellent theranostic nanoplatform. *In vivo* assays revealed the high tumor suppression performance and SPECT diagnostic ability of Co-57@MTX-LDH.

Our group prepared ultra-thin LDH nanosheets onto which they immobilized Ce6 and CDs (CD-Ce6/LDH) for FLI-guided PDT.[144] Fluorescence spectroscopy indicated that the emission intensity of the CD-Ce6/LDH was ca. 90 times higher than that of pristine Ce6, implying an ultrahigh Forster resonance energy transfer (FRET) efficiency. The excellent fluorescence imaging and PDT performance of CD-Ce6/LDH were confirmed *in vitro* using HeLa cells. Subsequently, Zhao *et al.* fabricated MgMnAl-LDH with MoS_2 doping in its surface and interlayer (LMM) to load Ce6 (LMM@Ce6) for MRI-guided PDT/PTT (Fig. 14a).[349] In this formulation, MoS_2 suppressed the cancer cell proliferation *via* NIR-induced hyperthermia, Mn element provided MRI and catalase-like properties to catalyze the decomposition of endogenous H_2O_2 to produce O_2. The generated O_2 alleviated tumor hypoxia to improve the ROS production during Ce6-mediated PDT. *In viv*o assays verified the remarkable MRI-guided PTT/PDT anticancer outcome of LMM@Ce6 (Fig. 14b-d). Our group designed high-quality multicomponent CoFeMn dichalcogenide nanosheets (CFMS NSs) by vulcanization of CoFeMn-LDH for PAI-guided PTT/CDT (Fig. 14e-g).[54] The as-prepared CFMS NSs exhibited excellent PAI capabilities with an extremely low detection limit. Moreover, complete cancer cell apoptosis and tumor elimination substantiated the remarkable PTT/CDT synergistic effect of CFMS NSs (Fig. 14h-j), offering great promise in cancer theranostics.

To acquire more accurate and comprehensive imaging diagnostic information, multi-mode theranostics have also been under development. Our group reported that the incorporation of Ce6 and AuNCs onto the surface of Gd-doped MgAl-LDH monolayer nanosheets (Ce6&AuNCs/Gd-LDH) resulted in a largely enhanced fluorescence QY compared with pristine AuNCs (18.5% *vs* 3.1%), as well as superior T_1-MRI performance to commercial MRI contrast agent Gd-DOTA (17.57 mM^{-1} s^{-1} *vs* 3.4 mM^{-1} s^{-1}).[351] The loading of Ce6 gave LDH an efficient anticancer behavior using PDT. *In vitro* and *in vivo* investigation revealed that Ce6&AuNCs/Gd-LDH exhibited an

excellent FLI/MRI-guided PDT performance, especially the synergetic enhanced FL/MR visualization of tumors.

We further developed Gd^{3+} and Yb^{3+} co-doped MgAl-LDH monolayer nanosheets with the loading of ICG (a fluorescent photothermal agent and PS) and chemotherapeutic drug (SN38) for synergetic theranostic.[55] The Gd&Yb-LDH nanosheets demonstrated MR/CT dual-mode imaging functionality and achieved an ultrahigh loading of hydrophobic SN38 (LC: 925%). The obtained SN38&ICG/Gd&Yb-LDH displayed a pH/NIR-stimulated drug release behavior and significantly enhanced PTT/PDT performance. *In vitro* and *in vivo* assessments verified a MR/CT/FL tri-mode visualization ability and synergistic chemo/PTT/PDT anticancer activity of SN38&ICG/Gd&Yb-LDH. Similarly, Weng *et al.* fabricated CDs and ICG co-incorporated LDHs (CDs/ICG-uLDHs) for FL/PA/two-photon imaging guided PTT.[352] CDs possess both FL and two-photon fluorescence imaging properties, and ICG allows PAI performance. Therefore, CDs/ICG-uLDHs showed great potential application as a multi-mode theranostic agent.

In summary, LDH-based nanocomposites have considerable application prospects in theranostics. Considering that therapeutic agents and multiple imaging modalities can be combined into a single LDHs nanoplatform, rational design of theranostic agent to concurrently obtain the desirable therapeutic effect and comprehensive biological information is made possible. In addition, it is necessary to explore new LDH-based *in vivo* diagnostic probes and synergize them with other more promising therapies to achieve optimal theranostic outcomes. Another research direction should be to evaluate whether LDH-based theranostic reagents have side effects when acting on organisms for a long time, and to investigate their clinical application potential through different toxicological parameters.

5.5. Biosensing

Biosensors play a vital role in disease diagnosis, safety and effectiveness evaluation of new drugs, disease risk prediction, and clinical screening of high-risk groups.[353] With the expansion of their applications in medical care, food detection and environmental monitoring, biosensors are required to possess high sensitivity, good stability during the

detection process, and low cost.[354-356] The properties of nanomaterials (such as conductivity, magnetism, redox, acidity and alkalinity) allow them to interact with biomolecules, which can accelerate the transfer of interface electrons and promote catalytic reactions on the electrode surface, effectively improving the performance of biosensors.[357-359] Therefore, nanomaterial-based biosensors have sparked a wealth of interest to researchers.[360-363]

LDHs have great potential in the construction of high-performance biosensors due to the following characteristics: (1) Positively charged LDHs can combine with active biological enzymes through electrostatic interactions to ensure the even distribution of the enzyme, which effectively avoids the aggregation of biological enzymes and greatly improves their catalytic activity. (2) LDHs, when used in biosensors, can serve as electrocatalysts, adsorbents as well as carriers for the immobilization of biomolecules or other modifiers to prolong the action time between analyte and electrode. (3) The excellent permeability and porosity of LDHs can increase the mobility of analytes and other reaction products. (4) The interlayer of LDHs can provide a good microenvironment for chemical reactions and protect them from external interferences. Currently, the functions of LDH-based biosensors mainly focus on the detection of conventional biomarkers e.g., H_2O_2, glucose, dopamine (DA) and protein components.

5.5.1. H_2O_2 detection

H_2O_2, as a gesturing molecule utilized to accurately and quickly recognize oxidative stress related to various disorders, is dangerous to accumulate in a large amount in organisms, which can be triggered by disturbed mitochondrial functions, enzymes-involved metabolic reactions, and partially reduced oxygen in living cells.[364] It is worth mentioning that excessive H_2O_2 can cause accelerated aging, gastrointestinal damage, heart disease and cancer.[365] H_2O_2 is also widely used as an industrial chemical in the medicinal setting, environmental analysis and other fields, but its overuse is also extremely detrimental to organisms.[353] Therefore, it is crucial to monitor the exact level of H_2O_2 associated with different biological species and to identify its pathophysiological functions.

The detection of H_2O_2 is generally based on enzymatic biosensors where electrodes are

fabricated by using different enzymes e.g., horseradish peroxidase (HRP) and glucose oxidase (GO_X).[35,366] LDHs can serve as a support to incorporate biomolecules or other modifiers due to its large surface area, intercalation features and exchangeable interlayer anions. In view of this, LDH-based enzymatic biosensor systems can be developed for H_2O_2 detection to improve the stability of enzymes without denaturation. Initial H_2O_2 biosensors require a mediator to enhance the electrical conductivity between the enzyme and the electrode surface. For example, Shan *et al.* synthesized 2,2'-azinobis(3-ethylbenzothiazoline-6-sulfonate) (ABTS)-intercalated ZnCr-LDH for the co-immobilization of GOx and HRP to detect H_2O_2.[367] The electrochemical transduction step of HRP/[ZnCr-ABTS] biosensor corresponded to the enzymatic reduction of intercalated mediator ($ABTS^+$) in the presence of H_2O_2, with the detection limit and sensitivity of 10 nM and 443 mA M^{-1} cm^{-2}, respectively.

Later on, H_2O_2 biosensors based on direct electron transport between the enzyme and the electrode without any mediator were developed. Zhang *et al.* reported for the first time that GOx-immobilized MgAl-LDH nanosheets could achieve H_2O_2 detection through a direct electron transfer process.[366] To accelerate the electron transfer of enzymes, some carbon nanomaterials (e.g., graphene, nitrogen doped carbon nanotubes (CNTs), carbon nanodots (C-Dots)) have been introduced to form LDH-based hybrid materials for better analytic performance. Wang *et al.* immobilized HRP on C-Dots-modified CoFe-LDHs (C-Dots/LDHs), and then coated the composite onto a glassy carbon (GC) electrode to manufacture a H_2O_2 biosensor.[368] The electrochemical behavior and practical application of HRP/C-Dots/LDHs/GC biosensor were then investigated. It was found that HRP immobilized by C-Dots/LDHs retained its catalytic activity, and displayed reversible redox behavior and enhanced electron transfer between the HRP and the electrode. The linear range of HRP/C-Dots/LDHs/GC biosensor was 0.1-23.1 μM with the detection limit of 0.04 μM, exhibiting satisfactory stability, good selectivity, high sensitivity and acceptable reproducibility.

The aforementioned enzymatic H_2O_2 biosensors present the advantages of enhanced sensitivity, high selectivity, and low operational potential, but still suffer some disadvantages such as complex immobilization, chemical and thermal instability, and

poor reproducibility. Non-enzymatic H_2O_2 biosensors have therefore sparked increasing interest due to the simpler synthesis and promising capabilities seen in *in vitro* testing.[369] In non-enzymatic biosensors, host materials such as LDHs can act as electrocatalysts in the redox processes. Due to their high specific surface area, the reactant molecules can more easily contact the active sites, thereby improving catalytic activity.

Sun *et al.* prepared ultrathin NiMn-LDHs nanosheets with peroxidase-mimicking performance using the coprecipitation method.[370] With increasing Mn content, the catalytic activity of NiMn-LDHs was seen to improve, which is attributed to the low redox potential and strong Lewis acidity of Mn sites. NiMn-LDHs nanosheets were shown to be stable over a wide pH range (2.6 to 9.0), exhibited excellent substrate affinity and high catalytic activity with the detection limit of 0.04 μM, which is superior to that of HRP. Moreover, disposable paper bioassays utilizing the NiMn-LDHs nanozyme were fabricated. The detection limit of this assay was estimated to be 0.01 mM in the H_2O_2 concentration range of 0.02 mM to 0.228 mM, which is lower than the H_2O_2 level prescribed by the US FDA (0.015 mM).

Since noble metals possess a fast sensing response, noble metal decorated LDHs are useful for designing H_2O_2 biosensors. Habibi *et al.* successfully prepared Ag NPs inserted NiAl-LDH nanocomposite through co-precipitation method.[369] The nanocomposite modified carbon-paste electrode (NiAl-LDH/Ag NPs/CPE) held peroxidase-mimetic activity and functioned as a renewable electrode for the detection of H_2O_2. NiAl-LDH/Ag NPs/CPE displayed good stability and high reproducibility, excellent electrocatalytic activity and fast response time, with a detection limit of 6 μM and sensitivity of 1.863 μA mM^{-1} cm^{-2} in the H_2O_2 concentration range of 10 μM to 10 mM. However, noble metals are rare and costly, and ideally would be replaced by more cost-effective metals with good catalytic efficiency.

Asif *et al.* fabricated n-type (majority carriers are electrons) CuO-intercalated p-type (majority carriers are holes) MnAl-LDHs (CuO@MnAl-LDHs) towards the nonenzymatic sensing of H_2O_2.[59] Their findings demonstrated that CuO could accelerate electron transfer of p-n junction (space charge layer), resulting in excellent

electrocatalytic activity. CuO@MnAl-LDHs modified electrode could be exploited for real-time monitoring of H_2O_2 from human serum, urine, and different live cells, with a low detection limit of 0.126 μM and a broad linear range of 6 μM-22 mM. Considering that unmodified LDHs are weak conductors, a major challenge in developing LDH-based catalysts is to increase their conductivity, which can be achieved by integrating LDHs with conductive materials such as CNTs, conductive polymers or GO.[371,372] Zhou *et al.* proposed a facile synthesis of NiMn-LDHs assembled GO (NiMn-LDH@GO) for H_2O_2 monitoring.[56] The inserted GO greatly enhanced the electron transfer ability of LDH and promoted the distribution of active sites within the composite, thereby improving the electrochemical performance of the NiMn-LDH/GO electrode. As a result, NiMn-LDH/GO hybrids exhibited a significant sensitivity (96.82 μA mM^{-1} cm^{-2}) for H_2O_2 reduction, along with a low detection limit (4.4 μM).

5.5.2. Glucose detection

As a vital biomolecule, glucose provides necessary energy for cells. Disorders related to the management of blood glucose levels are considered as an important indicator in several chronic metabolic diseases, most notably diabetes. Various cardiac, nervous, and renal diseases are also closely linked to elevated blood glucose levels.[373,374] Therefore, it is of great significance to develop biosensors for real-time and accurate monitoring of blood glucose levels in human biological fluids. Traditional enzymatic glucose biosensors are based on the reaction of glucose and O_2 under the catalysis of GO_X to produce gluconolactone and H_2O_2.[375] Williams and Korosi took the lead in developing a GO_X-based biosensor to measure glucose levels in 1970.[376] Since then, enzymatic glucose biosensors based on nanomaterials have been extensively studied, which present low detection limits, high selectivity and sensitivity, as well as high reproducibility.[377-379] Among them, LDHs have been shown to effectively combine with active enzymes to improve catalytic activity on account of its large specific surface area and positive charge.

Cosnier *et al.* reported for the first time that GO_X could be successfully immobilized on LDHs using the surface adsorption method, and a GO_X/LDHs/GC electrode with excellent catalytic performance was obtained for glucose detection.[380] By comparing

different kinds of substrate materials such as polypyrrole, alginate, synthetic latex, and LDHs, it was determined that LDHs maintained the activity of immobilized GO_X. Even with low GO_X loading, the GO_X/LDHs/GC electrode exhibited significant analytical abilities. Experimental results showed that the maximum sensitivity of this enzymatic glucose biosensors was 55 mA M^{-1} cm^{-2}. Recently, Shen *et al.* constructed a multimodal catalytic platform for the detection of glucose, where GOx was functionalized with oligonucleotides and then chemisorbed onto LDHs.[381] Nanoflower-like LDHs acted both as enzyme immobilizers and peroxidase mimics for tandem catalysis, effectively improving the catalytic activity of the whole system. The practical application of this biosensor was evaluated by detecting glucose in human serum and sweat. The results showed that the enzymatic glucose biosensors displayed reliable detection results. The above research demonstrates that LDH is a promising nanomaterial for immobilizing active enzymes, which provides a general method for preparing high-performance enzyme complexes and has broad application prospects in biosensors.

In the past decade, much research has focused on GOx-based glucose biosensors. Although great progress has been made, the application of enzymes is limited by the complex immobilization process, poor stability, and the low temperature storage requirement.[382,383] Therefore, the development of non-enzymatic glucose biosensors with high sensitivity, high stability and simple preparation has attracted much attention.[384] It is found that nanomaterials possessing large surface area and enhanced roughness factors can increase faradaic currents of glucose oxidation in the process of non-enzymatic glucose detection.[385] To this end, LDHs are a promising class of nanomaterials as they possess both a large surface area and high roughness coefficient.[386] In particular, nickel-containing LDHs have been applied in non-enzymatic glucose biosensors because Ni^{3+} centers can react as an oxidant.

For example, Lu *et al.* directly synthesized ultrathin NiFe-LDH nanosheets on porous Ni foam (NF) through hydrothermal synthesis to prepare NiFe-LDH/NF electrode.[130] The obtained NiFe-LDH film was used as a glucose biosensor without further modification, exhibiting excellent sensitivity (3680.2 μA mM^{-1} cm^{-2}), low detection

limit (0.59 μM) and fast response time (< 1s). The outstanding electrochemical catalytic activity could be attributed to the abundant active sites, high electron transfer rate and rapid diffusion of the electrolyte. Similarly, Amin *et al.* presented standalone electrodes based on Ni-NTNWs loaded with NiCo-LDH (NiCo-LDH@Ni-NTNW) for non-enzymatic electrochemical glucose detection.[132] The NiCo-LDH@Ni-NTNW hybrid provided a superior sensitivity of 4.6 mA mM^{-1} cm^{-2} with a low detection limit (0.2 μM) as well as fast response time (5.3 s), showing high selectivity.

Recent studies have shown that the introduction of electroactive noble metals (e.g., Au, Pd), transition metal oxides (e.g., CuO, NiO, MnO_2) and metal complexes can improve the electrocatalytic activity of LDH-based glucose biosensors.[124,387-389] An *et al.* constructed a unique nanostructured electrocatalyst by first fabricating copper oxide (CuO) and then growing CoNi-LDHs on the CuO surface (CuO/CoNi-LDHs) *via* the electrodeposition method (Fig. 15a).[124] Due to the unique structure and synergistic effect of the two materials, the optimized CuO/CoNi-LDHs displayed excellent non-enzymatic electrocatalytic performance, with a detection limit of 0.065 μM and a reliable linear range of 0.1 μM-0.384 Mm (Fig. 15b-d). Moreover, the CuO/CoNi-LDHs sensor was verified to detect glucose in human serum, demonstrating a high tolerance for the presence of interfering species and implying broad application prospects for glucose monitoring (Fig. 15e).

The electrocatalytic activity and sensitivity of LDH-based glucose biosensors can be improved by immobilizing LDHs onto conductive carbon materials (e.g., CNTs, graphene and its derivatives) owning to the high stability, large surface area, and abundant surface active sites of these materials. Moolayadukkam *et al.* proposed NiFe-LDH/reduced graphene oxide (rGO) composites for electrochemical glucose sensing (Fig. 15f).[57] The results show that the NiFe-LDH biosensor exhibited a sensitivity of 20.43 μA mM^{-1} cm^{-2} within the linear range of 0-4 mM concentration. The NiFe-LDH/rGO composites showed an enhanced sensitivity of 176.8 μA mM^{-1} cm^{-2} due to the charge transfer interaction and high conductivity caused by rGO, giving rise to great potential for glucose detection (Fig. 15g-j).

Since it is difficult for a mono-electrochemical biosensor to simultaneously achieve

both fast response and a visible color change, combining it with a colorimetric sensor to construct a dual-function glucose biosensor can overcome these difficulties to achieve higher sensitivity and selectivity for glucose detection. Based on this, Cui *et al.* successfully prepared a bifunctional flexible glucose biosensor by directly growing CoFe-LDHs nanosheet array (LDH-NSA) on Ni wire (Ni/CoFe-LDH-NSA).[390] High-efficiency colorimetric and electrochemical detection of glucose were achieved using Ni wire as a micro-substrate. The obtained Ni/CoFe-LDH-NSA exhibited remarkable activity and long-term durability in both colorimetric (the employed 3,3',5,5'-tetramethylbenzidine (TMB) as a chromogenic reagent could be catalyzed by CoFe-LDHs from colorless to sky blue in the presence of H_2O_2 generated by glucose oxidation) and electrochemical glucose detection, with linear ranges of 1~20 μM and 10~1000 μM, respectively. The bifunctional glucose biosensor synergized the advantages of electrochemistry and colorimetry, providing an effective strategy to fabricate a new generation of high-performance glucose biosensors.

5.5.3. Dopamine detection

Dopamine (DA), one of the most important catecholamine neurotransmitters, plays crucial roles in regulating mammalian brain circuits and controlling the stress response of the kidney system.[391] DA dysregulation can lead to parkinsonism, schizophrenia, attention deficit hyperactivity syndrome and pituitary tumors.[392] Therefore, there is an emerging need for extremely accurate and ultra-sensitive DA detection methods for clinical diagnosis, pathological analysis and neuronal function perception. Electrochemical biosensors have attracted considerable attention from researchers in biological applications due to their low cost, high sensitivity, and strong portability.[393] The modification of electrodes by nanomaterials (such as LDHs and its derivatives) can further improve the sensitivity and selectivity of DA biosensors. For instance, a carbon ionic liquid electrode modified with NiAl-LDH and a GC electrode coated by FeMn-LDHs have been reported to exhibit excellent electrochemical response towards DA detection,[394,395] with detection limits of 5.0 μM and 5.3 nM, respectively. The heightened electrochemical performance of modified electrodes can be attributed to the reduced resistance of coated electrodes, improved ion exchange ability, and the inherent

catalytic performance of the ionic liquids.

In view of the inherently weak conductivity of LDHs alone, to improve the sensing performance of LDHs modified electrodes, graphene and its derivatives with high conductivity have been integrated into LDHs to form composite materials for efficient electrochemical detection of DA. Li *et al.* synthesized NiAl-LDH through coprecipitation method, and then reduced the support GO to obtain NiAl-LDH/graphene (NiAl-LDH/G) hybrid for DA detection.[396] Electrochemical assays indicated that NiAl-LDH/G hybrid modified GC electrode exhibited improved electrochemical properties of DA electrooxidation compared with the pristine LDH modified GC electrode. It was found that the NiAl-LDH/G hybrid exhibited two different linear responses when the DA concentration was in the range of 5.0×10^{-7} ~ 1.2×10^{-4} M (for the reduction peak current) and 8.0×10^{-5} ~ 4×10^{-4} M (for the oxidation peak current). The sensitivities were 0.0156 μA μM^{-1} and 0.022 μA μM^{-1}, respectively, and the corresponding detection limits were 2.0×10^{-7} and 9.6×10^{-6} M. Likewise, Asif *et al.* prepared ZnNiAl-LDH/rGO by integrating positively charged ZnNiAl-LDH and negatively charged rGO through electrostatic interaction.[397] The ZnNiAl-LDH/rGO modified GC electrode exhibited excellent electrocatalytic activity towards DA, owning to a high number of active sites and synergistic effects of interfacial conductivity imparted by the interaction between rGO and LDHs. The DA biosensor showed outstanding selectivity, sensitivity and durability, with a broad linear range of 0.001-1 μM and a low detection limit of 0.1 nM.

5.5.4. Summary of LDH-based nanomaterials for biosensing

Apart from H_2O_2, glucose and DA, several other biomolecules including uric acid (UA), ascorbic acid (AA), L-cysteine (CySH), GSH and DNA have also been detected by LDH-based biosensors,[397-404] as shown in Table 2. In this part, we comprehensively summarize the recent research progress of LDHs and LDH-based nanocomposites as electrocatalysts and biosensors for the detection of metabolic molecules. In general, LDHs have shown excellent performance in immobilizing active enzymes, improving the dispersibility of loaded substances, and promoting the catalytic activity of electroactive materials, which significantly improves the sensitivity, selectivity and

stability of biosensors. Nevertheless, there are still some challenges. For example, the detection of most biomolecules still suffers from insufficient sensitivity and selectivity. Secondly, the deposition of active species or reaction intermediates in solution may block the surface of the working electrode, which is also a disadvantage of sensor operation. Additionally, portable and inexpensive detection equipment is needed to ensure higher availability of testing. With the development of LDH-based biosensors and the progress of sensor devices, the performance of biosensors is expected to be further improved, which will open up a reliable new way for *in vitro* clinical analysis of small molecular metabolites.

5.6. Anti-bacterial applications

To date, bacterial infections remain a growing health problem worldwide, plaguing millions of people. However, the current treatment of bacterial infections mainly relies on antibiotics, which are inefficient and increasingly prone to drug resistance. With the development of nanotechnology, nanomaterial-based antimicrobial agents have been used in antimicrobial therapy to improve drug utilization, enhance antibacterial activity, and reduce biological toxicity and antimicrobial resistance.[405-408] LDHs' good biocompatibility, pH-sensitive biodegradability, and bacteria adsorption ability driven by electrostatic interaction have laid a solid foundation for the preparation of high-efficiency antibacterial agents.

The antibacterial mechanisms of LDHs include: (1) LDHs themselves as antibacterial agents. Since the metal elements in LDHs matrix are adjustable, transition metal ions (Zn^{2+}, Mn^{2+}, Cu^{2+}, Ni^{2+}, Co^{2+}, *etc.*) with antibacterial activity can be introduced into LDHs.[409,410] During the interaction between LDHs and pathogenic bacteria, metal ions in the LDHs are slowly released as the layers dissolve to inhibit the growth and reproduction of bacteria. At the same time, the photocatalytic performance of specific LDHs (e.g., Zn-LDHs, Ti-LDHs) and the large number of hydroxyl groups on the surface also lead to ROS generation, which can destroy the physiological structure of bacteria and ultimately cause their death.[411] (2) LDHs as antibacterial agent carriers. Antibacterial agents can be loaded on LDHs either in the interlayer space or onto the surface of LDHs, and release in a sustained manner from LDH carriers at the biological

target to achieve desirable antibacterial effects.

In recent years, Zn^{2+} has been widely reported to exhibit excellent antimicrobial activity against a variety of microbes, including Gram-positive bacteria (e.g., *Staphylococcus aureus* (*S. aureus*), *Streptococcus pyogenes*, *Staphylococcus epidermidis*), Gram-negative bacteria (e.g., *Escherichia coli* (*E. coli*), *Pseudomonas aeruginosa* (*P. aeruginosa*), *Klebsiella pneumoniae*), and fungi (*Aspergillus fumigatus*, *Candida albicans*, *Trichophyton mentagrophytes* and *Geotricumcandidum*).[412,413] Peng *et al.* prepared four types of LDH (MgAl-LDH, ZnAl-LDH, MgFe-LDH and ZnFe-LDH) *via* coprecipitation to explore their antibacterial properties against *S. aureus* and *E. coli*.[67] It was found that ZnAl-LDH and ZnFe-LDH showed superior antibacterial activity in comparison to MgAl-LDH and MgFe-LDH, and the two bacteria were less resistant to ZnAl-LDH and ZnFe-LDH, indicating the strong antimicrobial performance of Zn^{2+}. Several mechanisms have been proposed to explain these bactericidal effects. The first is the destruction of the bacterial membrane function. Zn^{2+} attached to the negatively charged bacterial membrane changes its charge distribution, thereby blocking the transport of vital nutrients. The second is the denaturation of proteins and enzymes. Zn^{2+} can coordinate with the N and O elements in the bacterial proteins or replace the metal ions in the enzyme active site to inactivate it. The third is nucleic acid damage. Zn^{2+} can bind to nucleic acid to inhibit bacterial proliferation. Moaty *et al.* found that the antibacterial activity of ZnFe-LDH was better than that of TiO_2, ZnTi-LDH and Ag/AgCl-LDH nanocomposite, with the minimum inhibitory concentration (MIC) ranging from 0.49 to 15.60 μg mL^{-1} depending on bacterial species.[414] It could be attributed to the conversion of hydroxyl groups on the surface of LDHs to ·OH, and the increased positive charge of ZnFe-LDH promoted the adsorption of bacteria, thus enhancing the antibacterial performance.

Apart from relying on the inherent antibacterial properties of metal ions, antibacterial treatment can also be achieved with the help of LDHs to generate ROS under photocatalysis. Zhao *et al.* synthesized ZnTi-LDH nanosheets with diameters in the range of 40 ~ 80 nm *via* reverse microemulsion method to investigate the effect of particle size on bactericidal activity.[415] During the photocatalytic process, LDH

containing Ti^{3+} defects could produce $\cdot O_2^-$ and ·OH under visible light, effectively inhibiting the growth of *E. coli*, *S. aureus* and *Saccharomyces cerevisiae* (*S. cerevisiae*). It was found that the concentration of Ti^{3+} was size-dependent. With the decrease of LDH particle size, the density of Ti^{3+} defects increased, and more active free radicals were generated. Therefore, 40 nm ZnTi-LDH exhibited the strongest virulence to bacteria with the antibacterial rate of 95%, which was significantly better than WO_3 and TiO_2.

Metal oxides (such as ZnO, MgO and TiO_2) that can produce ROS species also possess bactericidal effects.[416-418] However, individual oxides are prone to agglomeration, which greatly reduces ROS production capacity. Using LDHs as precursors to prepare MMOs is suggested to overcome this issue. The effective bactericidal components in MMOs are highly dispersed and less likely to agglomerate, thus exhibiting prominent antibacterial activity. For example, Chen *et al.* adopted CoV-LDH as precursors to prepare Co-V MMOs ($Co_3V_2O_8/Co_3O_4$) through calcination.[419] The highly active Co-V MMOs provided large specific surface area, evenly distributed composite structure, and abundant surface active sites (Co^{3+} and oxygen defect), which enhanced their peroxidase/oxidase (POD/OXD)-like activity, resulting in superior bactericidal performance on *E. coli* by generating $\cdot O_2^-$. It can be seen that LDHs and derived MMOs can be utilized as photocatalysts or nanozymes to directly exert effective bactericidal effects, showing broad antibacterial applications.

Due to the layered structure of LDHs, it is also an effective strategy to introduce antibacterial agents (e.g., vancomycin (Van), gentamicin, oxazolidinone and ciprofloxacin) into the interlayer or surface of LDHs for sterilization purposes with the help of pH-responsive release behavior. Sun *et al.* successfully prepared Van and terephthalate (TA) co-modified Eu-doped LDHs (Van-TA-Eu-LDHs) through a two-step method.[420] Since Van has a high affinity to inhibit bacterial cell wall synthesis, Van-TA-Eu-LDHs achieved high-efficiency growth inhibition against *S. aureus* and *E. coli*. The fluorescence property supplied by TA also enabled efficient bacterial labeling. Similarly, Mishra *et al.* intercalated benzoate and its two derivatives para-hydroxybenzoic acid (p-BZOH) and 2-chloro-5-nitrobenzoic acid (BZCN) into the

ZnAl-LDH interlayer respectively by ion exchange.[421] The results showed that all these nanocomposites showed satisfactory bactericidal effects against *S. aureus* and *E. coli* (antibacterial rate up to 99%).

Our group constructed a multifunctional antibacterial composite (DHAD/ZnAlTi-LDH) by loading dehydroabietic acid derivative (DHAD) onto ZnAlTi-LDH nanosheets.[422] The prepared DHAD/ZnAlTi-LDH showed outstanding ROS production ability, and both *S. aureus* and *E. coli* were killed under visible light irradiation with antibacterial rate of 94% and 91%, respectively. Cheng *et al.* incorporated *p*-hydroxybenzoic acid (PHBA) into ZnAl-LDHs to inhibit the growth of *S. aureus* and *Candida albicans*.[423] It was found that PHBA/ZnAl-LDHs continuously released PHBA in acidic environment, which could be attributed to the enhanced solubility of PHBA by protonation. Likewise, Tang *et al.* embedded DL-mandelic acid (MA) into ZnAl-LDHs through an ion exchange reaction.[424] The obtained ZnAl-MA-LDH showed sustained-release property at pH 4.0, which is beneficial for avoiding allergic reactions caused by a sudden and high concentration of MA. This controlled release system demonstrated superior antibacterial activity against *S. aureus*, *E. coli* and *Candida albicans* compared to pure MA.

In addition to pH-responsive antimicrobial release, H_2O_2-responsive release can also be achieved by virtue of the specific crystalline phase and chemical composition of LDHs. Wang *et al.* manufactured a butyrate-inserted NiTi-LDH film (LDH/Butyrate) on the surface of nitinol alloy by a hydrothermal method.[425] LDH/Butyrate with valence-variable Ni elements could convert H_2O_2 to OH^- that would exchange with interlamellar butyrate ions, leading to H_2O_2-responsive butyrate release (Fig. 16a). Moreover, the reaction of the film with H_2O_2 might cause the change of LDHs lattice, which is conducive to the further release of butyrate. *In vitro* and *in vivo* experiments indicated that LDH/Butyrate significantly inhibited bacterial infection without toxicity to normal tissues (Fig. 16b-d). Recently, Du *et al.* fabricated a triboelectric nanogenerator patch for the healing of infected wounds (Fig. 16e),[426] which consisted of a flexible polymer substrate, polytetrafluoroethylene (PTFE), and a minocycline-loaded electrode fabricated by *in situ* growth of MgAl-LDH nanosheets on Al foils. It

was found that antibacterial agent minocycline could be released under electrical stimulation. *In vitro* and *in vivo* tests showed that the skin patch could fit the wounds, inhibiting the growth of *S. aureus* (~ 96.7%) and facilitating skin tissue repair (Fig. 16f,g).

Aside from the above-mentioned organic antibacterial agents, inorganic antibacterial agents such as Ag, Zn and Cu nanoparticles have also received widespread attention due to their durable antibacterial effect and avoidance of drug resistance issues. The antibacterial mechanism can be explained as follows: during the antibacterial process, metal ions gradually dissolved from Ag, Zn and Cu nanoparticles can react with functional groups (such as sulfhydryl and amino) existing in proteins or nucleic acids in microorganisms, thereby reducing enzymatic activity and inhibiting bacterial proliferation.[64] Among them, Ag nanoparticles (AgNPs) have the strongest reported antibacterial effect with the relatively less harm to the human body. Therefore, loading AgNPs onto LDHs to form composites can be an effective strategy to develop new antibacterial formulations.

Chen *et al.* synthesized AgNPs-deposited LDHs (Ag-LDH) by *in-situ* growth method for antimicrobial therapy.[150] Using *S. aureus*, *E. coli*, *P. aeruginosa*, and *Bacillus subtilis* (*B. subtilis*) as experimental models, the antibacterial activity of Ag-LDH was studied. The results showed that Ag-LDH exhibited excellent and long-lasting bactericidal efficacy against four bacteria, killing more than 99% of the bacteria even at the 4th recycle. In another work by Mishra *et al.*, AgNPs-loaded ZnAl-LDH was prepared through co-precipitation, followed by high temperature calcination at 800 °C.[427] The formed Ag_2O-spinel composites showed outstanding antibacterial activity against both *S. aureus* and *E. coli*.

Because of the high price and limited availability of Ag, it is also worth exploring strategies to improve the bactericidal activity while reducing the amount of Ag used. The combination of Ag-LDH and organic antibacterial agents can fully synergize the advantages of both to achieve efficient sterilization. Sun *et al.* fabricated AgNPs and Van co-modified LDH antibacterial composites (Van-Ag/ZnAL-LDH).[428] Compared with Ag/LDH, Van-Ag/ZnAL-LDH presented stronger antibacterial activity against *S.*

aureus and *E. coli*. The combined effect of AgNPs and Van not only overcame the limitation of Van to kill only Gram-positive bacteria, but also conquered the disadvantages of poor dispersion and low stability of AgNPs. Additionally, based on the antibacterial properties of ruthenium complexes, Xiao *et al.* manufactured an antibacterial agent (AgRu-LDH) by inserting a ruthenium complex into LDHs interlayer and loading AgNPs onto the surface.[429] Benefiting from the dual antibacterial activity of Ru and AgNPs, AgRu-LDH displayed effective synergistic inhibition on the growth of *E. coli* and *S. aureus* under illumination.

In conclusion, by virtue of their structure and physicochemical properties, LDHs not only possess inherent antibacterial activity, but can also combine with organic/inorganic antibacterial agents to construct more effective composite antibacterial materials. The above-mentioned studies indicate that LDHs and their composites have significant effects in the field of antibacterial treatment. Although there are some challenges in the synthesis process and *in vivo* safety assessment, currently LDHs remain the better choice compared to many other inorganic ingredients. More collaborative research and commercialization efforts will help to fulfil the potential of LDHs as antimicrobial agents.

5.7. Tissue engineering

Tissue engineering, also known as "regenerative medicine", was defined by Langer and Vacant in 1993 as: applying the principles of engineering science and life science to develop bioactive substitutes for restoring, maintaining and improving the function of damaged tissues and organs.[430] Since then, an increasing number of biomaterials for tissue engineering have been developed, including metals, inorganic ceramics, polymer materials, composites, *etc.*[431-438] In the past few years, LDHs have emerged as a potential candidate for tissue engineering applications. Significant achievements have been made in bone repair, wound healing, nerve regeneration, dental restoration and cardiac repair, greatly promoting the development of tissue engineering.[36,432]

In general, LDH-based tissue engineering materials have two main functions as follows: (1) The combination of LDHs and scaffold materials overcomes the limitation of insufficient biological activity of pristine scaffold materials, and can replace or repair

human tissues without immune rejection. Meanwhile, the composite scaffolds can be endowed with osteogenic properties by adjusting the composition of metal ions in LDHs. (2) As excellent drug carriers, LDHs can achieve sustained release of drugs/growth factors, which not only prolongs the action time of drugs in human tissues, but also effectively avoids the side effects caused by drug burst release.

Scaffold materials are required by most damaged tissues and organs for their formation from cells, whose major function is to assist cell proliferation, differentiation, and biosynthesis.[439,440] To fulfil the function of a scaffold, the following requirements should be met. (1) Scaffolds should have interconnected micropores to allow for seeding numerous cells and the formation of blood vessels, with an optimal pore size between 100 and 500 mm. (2) They must also have optimal mechanical strength and porosity with high surface area. (3) The absorption kinetics of the scaffold should be adequate, which depends on the tissue to be regenerated. Up to now, some polymeric scaffolds (e.g., polyglycolide (PGA), poly(ε-caprolactone) (PCL), lactide-glycolide copolymer (PLGA), poly(L-lactide) (PLLA), lactide-ε-caprolactone copolymers (LA-CL cop), chitosan (CS)) and inorganic scaffolds (e.g., hydroxyapatite (HAP), β-tricalcium phosphate (TCP), Mg alloys, Ti alloys) have been employed in tissue engineering, specifically for bone tissue.[441-443] Presently, composite scaffolds composed of LDHs and the above-mentioned pristine scaffolds, such as Ag-MgSrFe(LDH)/CS, LDH-hyaluronic acid (HA)/Gel, LDH-CS-PFTα, PCL/LDH, have been introduced into bone repair, osteogenic implants, corneal stroma tissue regeneration, dental restoration, and wound dressings.[431,432]

In 2011, a pioneering study on direct growth of MgFe-LDH coatings on pure Mg substrates was conducted by Lin *et al.*[42] It was found that MgFe-LDH coating effectively improved the hydrophilicity of the pure Mg surface. *In vitro* corrosion assays and cell adhesion tests demonstrated that Mg substrates coated with MgFe-LDH exhibited higher corrosion resistance, better cell spreading and growth, as well as stronger cell-cell interaction behavior than pure Mg substrates. It is known that Mg ions play a vital role in balancing osteoblasts (the main functional cells of bone formation)/osteoclasts (the main functional cells of bone resorption) differentiation, and

the lack of Mg in bone tissues can easily cause bone remodeling disorders and increase the risk of osteoporosis.[444]

Kang *et al.* explored the role of Mg-based LDHs in osteogenic differentiation and found that MgAl-LDHs could activate the c-Jun N-terminal kinase (JNK) and the extracellular signal-regulated kinase (ERK) signaling pathway to up-regulate the expression of osteocalcin (OCN) and osteogenic related genes (runt-related transcription factor-2, Runx-2), fully demonstrating the excellent performance and great application potential of Mg-LDHs in osteogenic differentiation.[445] Since then, many composite scaffolds based on Mg-LDHs have been developed in tissue engineering, specifically for bone tissue applications. For example, Li *et al.* fabricated MgFe-LDHs films on acid-etched pure titanium surfaces by the hydrothermal method.[446] *In vitro* assays proved that the MgFe-LDHs-modified titanium exhibited excellent biocompatibility and osteogenic activity compared to pure titanium, since the MgFe-LDHs films formed an appropriate alkaline environment for the proliferation and osteogenic differentiation of stem cells, providing a new method for the design of hard tissue bioactive implant materials. Zhang *et al.* developed MgMn-LDH-modified Mg alloy implants for bone regeneration, osteosarcoma therapy and bacteria killing.[447] The LDH film not only enhanced the corrosion resistance and osteogenic differentiation of Mg alloy implants, but also endowed them with superior chemodynamic/photothermal effects due to the CDT-mediated ROS generation and NIR absorption abilities of black MgMn-LDH. *In vitro* and *in vivo* assays fully demonstrated the excellent antitumor and bone regeneration properties as well as bactericidal activity of LDH-modified Mg alloy implants.

Apart from the inorganic scaffolds, LDHs also exhibit excellent bioactivity in combination with polymer scaffolds. Chu *et al.* utilized CS as matrix and prepared La-doped MgAl-LDH (La-LDH) nanohybrid scaffolds *via* a freeze-drying method.[448] The obtained La-LDH nanohybrid scaffolds possessed the bi-directional regulation functions on the inhibition of osteoclastogenesis and the activation of osteogenesis for osteoporotic bone regeneration (Fig. 17a-c). More importantly, the La^{3+} dopants endowed the nanohybrid scaffolds with enhanced osteogenic and angiogenic ability. However, La-LDH nanohybrid scaffolds lacked sufficient mechanical strength to treat

bone defects. Future work must focus on the preparation of La-based scaffolds with high mechanical strength.

Recently, our group synthesized MgAl-LDHs modified PMMA bone cement (PMMA&LDH) for promoting osseointegration (refers to the direct combination between the implant and bone tissue, without any combination other than bone such as connective tissue).[69] The addition of LDHs improved mechanical and physical properties of PMMA. Transcriptome sequencing demonstrated four key osteogenic pathways of PMMA&LDH: p38 mitogen activated protein kinase (p38 MAPK), extracellular signal-regulated kinases (ERK)/MAPK, transforming growth factor-β (TGF-β), and fibroblast growth factor (FGF), which were further confirmed by quantitative polymerase chain reaction (qPCR), ingenuity pathway analysis (IPA) and Western blot assays. Moreover, alizarin red S (ARS) and alkaline phosphatase (ALP) staining assays showed the significantly enhanced osteogenic ability of PMMA&LDH. The superior osseointegration performance of PMMA&LDH was also confirmed *in vivo*, with an 18.34-fold increment in bone growth volume compared to PMMA at 2 months, postoperatively. Hence, PMMA&LDH is a promising biomaterial for bone growth and has potential application in orthopedic surgeries.

In order to further improve the bioavailability of LDH-based tissue engineering materials, it is necessary to introduce drugs (e.g., analgesic, anti-inflammatory, anti-bone resorption drugs), growth factors, or antimicrobial agents for enhancing the clinical effect.[449-453] Alendronate (AL), an anti-osteoporosis drug, can prevent osteoclast-mediated bone resorption and therefore helps to maintain the microstructure of bone tissue. However, large doses are required for the desired therapeutic effect, which unfortunately also causes significant side effects. To achieve sustained drug release, our group synthesized Yb-doped MgAl-LDH monolayer nanosheets through a bottom-up method, and further loaded with AL (AL/LDHs) for the treatment of femoral head necrosis.[454] MgAl-LDH gave a high loading content (197%) for AL with an encapsulation efficiency of 98.6%. *In vitro* and *in vivo* experiments showed that AL/LDHs not only promoted osteogenic differentiation and bone regeneration more effectively than free AL, but also increased the bone mass density (BMD) of the femoral

head, which could be ascribed to the sustained release of AL from AL/LDHs. Similarly, Piao *et al.* encapsulated AL into MgAl-LDHs *via* ion exchange.[455] Based on the strong electrostatic interaction between the deprotonated phosphate group of AL and the positively charged LDH layers, the controlled and sustained release of AL from AL-LDH was successfully achieved.

Besides, Fu *et al.* proposed another therapeutic strategy for osteoporosis without AL.[456] They constructed a nanocatalytic medicine by synthesizing CaAl-LDHs functionalized with calcein (CaAl-LDHs-calcein, denoted as CALC). Weakly alkaline CaAl-LDH could neutralize the acidic microenvironment to reduce osteoclast activity, accompanied with Ca^{2+} release. The released Ca^{2+} could react with endogenous phosphate cations to form calcium phosphate nanoparticles (CAPs), leading to anti-inflammatory differentiation of bone macrophages and enhancement of regulatory T cells activity. Due to the dual functions of acid neutralization and immunomodulation, CALC exhibited excellent therapeutic effects on osteoporosis *in vitro* and *in vivo*. In order to alleviate the intense pain during bone grafting procedures, Bernardo *et al.* prepared sodium naproxen (NAP, an anti-inflammatory drug)-intercalated MgAl-LDH.[457] The release of NAP was monitored under simulated physiological conditions, and the results showed that free NAP dissolved immediately, while NAP intercalated into LDH was released slowly over 48 h. This could potentially be applied to effectively relieve pain for an extended period of time from a single dose.

In addition to promoting bone regeneration and allowing controlled drug release, LDHs can also be applied in neurogenesis, corneal stroma regeneration, dental repair, and wound healing. Zhu *et al.* evaluated the neuro-regenerative and immunomodulatory functions of MgAl-LDH nanoparticles and revealed the immune-related mechanisms (Fig. 17d).[458] It was found that LDH achieved remarkable effects in accelerating neural stem cells (NSCs) migration and neural differentiation. RNA sequencing (RNA-seq) and IPA demonstrated that transforming growth factor-β receptor 2 (TGFBR2) is a key gene for LDH to suppress inflammatory responses and promote neural regeneration. *In vivo* experiments verified the regeneration of NSCs and neurons in the lesion site of mice with spinal cord injury after LDH implantation. Most recently, Wang *et al.*

reported a neuroprotective agent composed of Gd-doped MgAl-LDHs, ferritin heavy subunit (FTH, a blood-brain barrier transport agent) and atorvastatin (ATO, a neuroprotective drug) (denoted as AFGd-LDH) for alleviating brain reperfusion injury.[459] The space-confinement effect of LDHs toward FTH and ATO enhanced the ROS scavenging efficiency. As a result, AFGd-LDH could effectively reduce neuron apoptosis and oxidative damage in mouse cerebral cortex, thus providing a feasible and safe neuroprotective therapy for the treatment of ischemic-reperfusion injury.

The corneal stroma is an indispensable part of the cornea, which is composed of an organized extracellular matrix (highly oriented and orthogonal collagen fibrils), and damage to it can lead to blindness. Corneal transplantation is currently used in clinical treatment for damaged cornea. Unfortunately, suitable donor corneas are in short supply. Therefore, the development of functional corneal stroma substrates to reconstruct corneal stromal tissue is urgent. Moghanizadeh-Ashkezari *et al.* synthesized vitamin C (VC)-loaded poly(urethane-urea)/ZnAl-LDH nanohybrid scaffolds (PUU-VC-LDH) for corneal stroma tissue regeneration.[460] Vitamin C functioned as a signaling molecule to stimulate the resident keratocytes to synthesize the extracellular matrix collagen. It was found that PUU-VC-LDH exhibited excellent biocompatibility, high biodegradation, tunable mechanical properties, and allowed significant proliferation ability of stromal keratocyte cells, giving rise to great potential for biomedicine application. In other applications, Bernardo *et al.* formulated smart dental materials by intercalating phosphate into ZnAl-LDHs *via* the reconstruction method for preventing damage from caries.[461] The expected sustained release of phosphate markedly improved protection against caries. In combination with other mineralizing elements, the smart materials could also contribute to the remineralization of tooth tissues to protect against dental health problems. Munhoz *et al.* designed an innovative wound dressing (ALG-MgAl-LDH/SDZ) based on alginate (ALG) films loaded with silver sulfadiazine (SDZ, a topical antibiotic)-incorporated MgAl-LDH.[462] ALG-MgAl-LDH/SDZ synergized the reproducibility/non-toxicity of ALG and the antibacterial properties of SDZ, allowing for broad application in wound healing.

In conclusion, for the field of tissue engineering, the excellent biocompatibility and

intercalation chemistry of LDHs enable them to achieve multiple functions, such as controlled drug release, accelerated tissue regeneration and efficient tissue repair. Other applications of LDHs in tissue engineering are summarized in Table 3.[463-476] However, further research effort should be devoted to evaluating the clinical application of LDHs in regenerative medicine comprehensively.

6. Conclusions and outlooks

In this article, we have reviewed the state-of-the-art progress on the synthesis, surface modification and biomedical applications of LDH-based nanomaterials. Based on their components, LDH-based nanomaterials can be classified into pristine LDHs, LDH-based composites, and LDH-derived nanomaterials. Various methods have been developed for preparation of LDH-based nanomaterials. Among them, the co-precipitation method is the most widely used for the controlled synthesis of bulk LDHs, while bottom-up direct synthesis is the most effective method to prepare LDH nanosheets. Owing to their favorable characteristics, LDH-based nanomaterials are have shown great promising in diverse biomedical applications like drug delivery, imaging diagnosis, cancer therapy, biosensing, tissue engineering, *etc*. Success in translating LDH-based particles to first-in-human clinical trials has demonstrated their excellent biosafety and clinical potential.[477] However, there are still many remaining challenges to be addressed in the upcoming research, meanwhile lot of works can be done in the near future in this promising field.

For the synthesis of LDH-based nanomaterials, the existing synthesis methods normally produce nanomaterials without precise control of their size, usually in the range of tens to hundreds of nanometers. Such a relatively wide size distribution limits the precise control of pharmacokinetic behavior, cellular uptake, and release kinetics of LDH-based nanomedicine. Therefore, the synthesis methods must first be improved to produce highly uniform and reproducible LDH-based nanomaterials. Recently, Jose *et al.* manufactured an expandable microreactor with adjustable shear rates, which provides a new way to control crystallinity and particle size for the synthesis of LDHs and represents an important step in the direction of more precise synthesis of LDHs.[478] New methods for drug loading or surface modification should be explored, which

minimize the influence of synthetic environment (such as pH value and temperature) on the properties of the product.

The quantity or density of surface modifiers and their effect on the biological functions of LDHs is also worthy of more in-depth exploration. Although the surface functionalization of LDHs or changes in their particle morphology can influence drug targeting to a certain extent, the interaction between LDHs and cells needs to be studied in more detail, to develop more targeted pathways for enhanced drug delivery. LDH-based composites which respond to endogenous stimuli have been designed for targeted therapy. To further enhance the selectivity of LDHs for maximizing efficiency and mitigating off-target toxicity, it is necessary to employ additional stimuli and/or increase the sensitivity to the stimuli used to date.

In terms of drug delivery and sustained release, LDHs can deliver both hydrophilic and hydrophobic drugs using electrostatic interaction and/or hydrogen bonds, which is an advantage of LDHs over other nanomaterials. Nevertheless, avoiding the early release of drugs during the delivery process and reducing the damage to other tissues and organs is a priority issue which needs to be considered. To address this problem, organic polymers or silica may be used for secondary packaging of LDHs to reduce the drug release rate; alternatively, some bioactive substances including cell membranes and exosomes, may be applied in secondary loading of LDHs for targeted drug release. Recently, the direct synthesis of drugs at the lesion site through biorthogonal chemistry is expected to realize selective targeted therapy,[479] which is of great significance for reducing the toxicity caused by drug delivery. As excipients for several orally-administered drugs, LDH materials can increase the blood concentration and half-life of drugs, thereby enhancing their efficacy. For many diseases, however, oral medications are not as effective as intravenously administered therapies.

Unfortunately, LDH-based nanocomposites tend to aggregate due to their insufficient dispersion and stability. This could potentially result in clotting or blood vessel blockage, and could cause serious side effects. Therefore, intravenous drug delivery systems based on LDHs have not yet been applied in clinical practice. A compromise is to load drugs onto LDHs and combine them with biodegradable hydrogels to

construct a dual sustained-release system. By injecting the hydrogel system into the disease site, its long-acting and sustained-release performance can be utilized to achieve long-term treatment and prevention recurrence of diseases. Especially for some chronic diseases that require regular oral or injection of drugs, a single injection of a high-dose gel system can significantly reduce patient compliance, which has broad prospects in promoting the clinical application of LDH-based injectable drugs.

In imaging diagnosis and cancer therapy, there are also several factors that restrict the clinical application of LDHs. Firstly, for bioimaging applications, introducing metal ions with imaging functions onto LDH matrix or intercalating imaging functional agents into LDH interlayer or loading on LDH surface can achieve multi-modal imaging. However, the biosafety of using some of the transition elements and rare earth metal ions is still need to further explored toward practical biomedical applications. Another approach to mitigate biosafety concerns is to use LDHs to deliver commercialized imaging agents to enhance imaging performance or realize targeted imaging at the lesion site.

Secondly, the current research on using LDH-based nanocomposites to achieve cancer therapy is still in the preliminary stage. LDH-based PDT, PTT, CDT, *etc.* still need further exploration. For example, to solve the problem of insufficient visible light penetration of tissue for PDT applications, defect-rich LDHs can be constructed. Defects can effectively reduce the band gap of LDHs to match the bandgap range of ROS generation, which can not only promote electron-hole separation, but also increase the absorption of long-wavelength light with deep penetration. In this way, LDHs could potentially utilize the more deeply penetrating NIR light to produce electrons which can combine with oxygen to generate ROS, thus realizing NIR-stimulated PDT. In view of the need to strengthen the photothermal performance of NIR-I PTT, the photothermal conversion efficiency can be enhanced by adjusting the metal composition of LDHs, or by preparing TMCs using sulfidation/selenization of LDHs. The adjustment of elemental composition can increase the molar extinction coefficient (which is related to the light absorption capacity of the material) of LDHs or TMCs in NIR-II, thereby increasing the efficiency of NIR-II PTT.

In addition, LDHs have significant advantages over other materials in CDT based on the tunability of their metal elements. However, CDT generally suffers from low chemical reaction rate, which restricts the further development of CDT. LDH-based single-atom catalysts possess ultra-high catalytic efficiency,[480,481] which is promising to conquer the mentioned obstacle of CDT. Thirdly, the construction of LDH-based theranostic platform can also facilitate real-time monitoring of the treatment process and effect to fulfill the practical application requirement. However, a key question here is how to evaluate the synergies between imaging and treatment. Moreover, whether the combination of multiple components may limit the extent or efficiency of each component also should be investigated.

For biosensing applications, although present LDH-based biosensors have shown excellent detection performance towards a variety of biomarkers, there are still some challenges to be overcome. To date, the sensitivity and selectivity of detection of most biomolecules are not high enough. Moreover, the deposition of active substances or reaction intermediates in solution may block the surface of the working electrode. Therefore, it is necessary to further improve the detection limit, response time, selectivity, stability of LDH-based biosensors, and enhance their detection sensitivity in complex environments. In addition, the development of non-invasive, portable, flexible and inexpensive detection equipment is also particularly important. We believe that with the continuous development of LDH-based biosensors, their performance will be significantly improved. In the future, there will be broad application prospects in the clinical analysis of small molecule metabolites *in vitro*. In terms of anti-bacterial activity, on the basis of previous studies, LDH materials containing specific metal ions with antibacterial properties can be combined with commercial antibacterial drugs such as vancomycin and gentamicin. The resulting complex could potentially display synergistic antibacterial performance sufficient for clinical applications.

In the field of tissue engineering, Mg-based LDHs exhibit excellent osteogenic properties. Compared with high-purity Mg alloys and MgO, Mg-based LDHs can effectively compensate for the potential biotoxicity and rapid degradation of the former two, displaying broad application prospects in tissue engineering. Nevertheless, the

application of Mg-based LDHs as bone repair materials still needs significant advances in the following three aspects: (1) To take full advantage of the excellent drug-loading performance of Mg-based LDHs to prepare multifunctional materials. For instance, some osteoporosis drugs and various growth factors could be loaded. The slow release of these drugs can effectively alleviate the symptoms of osteoporosis while promoting bone formation. (2) Development of injectable Mg-LDH based bone repair materials. A desirable strategy is to combine Mg-based LDHs with temperature-sensitive hydrogels to obtain bone fillers. After loading of drugs, the composite hydrogel system could be injected into bone tissue and solidified *in situ* based on the temperature-sensitive effect, therefore achieving bone repair and simultaneously increasing the drug's action cycle through the gradual release of the drug. (3) Rational design of Mg-based LDH composites with the properties of inhibiting osteoarthritis and promoting cartilage regeneration. Based on the intrinsic cartilage regeneration ability of high concentration Mg ions, using Mg-LDHs as the host matrix to construct composites with outstanding osteoarthritis therapeutic properties will effectively expand the application scope and scale of Mg-based LDHs, since LDH matrix can gradually degrade and release Mg ions.

Given that the practical biomedical applications of LDH-based nanomaterials are preferentially dependent on their biosafety, the metabolic pathways and degradation mechanisms of LDH-based nanomaterials *in vivo* are crucial to ensure their long-term biosafety. Over the past decade, most nanomedicine research has been aimed at the pursuit of high therapeutic efficiency, ignoring the need for comprehensive biosafety evaluation. Although it has been demonstrated that LDHs with high biocompatibility can be metabolized and excreted through the liver and kidney, as detected in feces and urine.[47,50,54] However, the long-term side effects of LDH-based nanomaterials *in vivo* are not fully understood. Meanwhile, the degradation mechanism, biodistribution and metabolic pathways of LDH-based nanomaterials have not been well studied. Moreover, multiple evaluation techniques and toxicological parameters, as well as underlying mechanism issues should be also considered.

Author Contributions

T.H. drafted the manuscript in consultation with all the other authors. M.S. and J.Z. arranged all the figures. Z.G., G.R.W and Z.Z. helped to revise the manuscript. X.Z., C.T. and R.L. supervised the project and finalized the manuscript.

Conflicts of interest

There are no conflicts to declare.

Acknowledgements

R.L. thanks the funding support from National Natural Science Foundation of China (NSFC: 21971007) and the Beijing Natural Science Foundation (2212044). C.T. thanks the funding support from the National Natural Science Foundation of China (Project Nos. 22005259 and 52122002), the Start-Up Grant (Project No. 9610495) and Grants (Projects Nos. 9680297 and 7020013) from City University of Hong Kong.

References

1 M. Xu and M. Wei, *Adv. Funct. Mater.*, 2018, **28**, 1802943.

2 Q. Wang and D. O'Hare, *Chem. Rev*., 2012, **112**, 4124−4155.

3 F. Song and X. Hu, *Nat. Commun*., 2014, **5**, 4477.

4 Z. Gu, J. J. Atherton and Z. P. Xu, *Chem. Commun*., 2015, **51**, 3024−3036.

5 H. Yan, M. Wei, J. Ma and X. Duan, *Particuology*, 2010, **8**, 212–220.

6 C. Hochstetter, *J. Prakt. Chem*., 1842, **27**, 376.

7 W. Feitknecht and M. Gerber, *Helv. Chim. Acta*, 1942, **25**, 131.

8 R. Allmann and H. P. Jepsen, *Neues Jahrb. Mineral. Monasth.*, 1966, **12**, 544.

9 S. Miyata, T. Kumura, H. Hatori and K. Tannabe, *Nippon Kagaku Zasshi*, 1971, **92**, 514−519.

10 L. Wang, Y. Zhou, Y. Lin and X. Duan, *Chem. Bull.*, 2011, **74**, 1074–1083.

11 X. Xu, Y. Lin, D. G. Evans and X. Duan, *Sci. China Chem.*, 2010, **53**, 1461–1469.

12 M. Laipan, J. Yu, R. Zhu, J. Zhu, A. T. Smith, H. He, D. O'Hare and L. Sun, *Mater. Horiz.*, 2020, **7**, 715−745.

13 C. Taviot-Guého, V. Prévot, C. Forano, G. Renaudin, C. Mousty and F. Leroux, *Adv. Funct. Mater.*, 2018, **28**, 1703868.

14 G. Fan, F. Li, D. G. Evans and X. Duan, *Chem. Soc. Rev.*, 2014, **43**, 7040−7066.

15 Y. Wang, D. Yan, S. E. Hankari, Y. Zou and S. Wang, *Adv. Sci.*, 2018, **5**, 1800064.

16 L. Lv, Z. Yang, K. Chen, C. Wang and Y. Xiong, *Adv. Energy Mater.*, 2019, **9**, 1803358.

17 H. Yi, S. Liu, C. Lai, G. Zeng, M. Li, X. Liu, B. Li, X. Huo, L. Qin, L. Li, M. Zhang, Y. Fu, Z. An and L. Chen, *Adv. Energy Mater.*, 2021, **11**, 2002863.

18 C. Forano, F. Bruna, C. Mousty and V. Prevot, *Chem. Rec.*, 2018, **18**, 1150−1166.

19 M. Halma, C. Mousty, C. Forano, M. Sancelme, P. Besse-Hoggan and V. Prevot, *Colloids Surf. B Biointerfaces*, 2015, **126**, 344−350.

20 V. Prevot, S. Touati and C. Mousty, *Front. Chem.*, 2020, **8**, 561975.

21 L. Sobhana, M. Sarakha, V. Prevot and P. Fardim, *Appl. Clay. Sci.*, 2016, **134**, 120−127.

22 J. H. Choy, S. Y. Kwak, J. S. Park, Y. J. Jeong and J. Portier, *J. Am. Chem. Soc.*, 1999, **121**, 1399−1400.

23 Z. Liu, J. T. Robinson, X. Sun and H. Dai, *J. Am. Chem. Soc.*, 2008, **130**, 10876−10877.

24 L. Feng, L. Wu and X. Qu, *Adv. Mater.*, 2013, **25**, 168−186.

25 Y. Chen, D. Ye, M. Wu, H. Chen, L. Zhang, J. Shi and L. Wang, *Adv. Mater.*, 2014, **26**, 7019−7026.

26 T. Liu, C. Wang, X. Gu, H. Gong, L. Cheng, X. Shi, L. Feng, B. Sun and Z. Liu, *Adv. Mater.*, 2014, **26**, 3433−3440.

27 H. Wang, X. Yang, W. Shao, S. Chen, J. Xie, X. Zhang, J. Wang and Y. Xie, *J. Am. Chem. Soc.*, 2015, **137**, 11376−11382.

28 L. Yan, S. Gonca, G. Zhu, W. Zhang and X. Chen, *J. Mater. Chem. B*, 2019, **7**, 5583−5601.

29 Z. Cao, B. Li, L. Sun, L. Li, Z. P. Xu and Z. Gu, *Small Methods*, 2020, **4**, 1900343.

30 K. N. Andrade, A. Pérez and G. Arízaga, *Appl. Clay Sci.*, 2019, **181**, 105214.

31 S. Miyata, *US Pat.*, 1985, **5**, 389.

32 W. Jettka, B. Gajdos and M. D. Benedik, *Eur. Pat.*, 1996, **715**, 846.

33 D. G. Evans and X. Duan, *Chem. Commun.*, 2006, **11**, 485−496.

34 W. Jin, S. Ha, J.-H. Myung, B. C. Kim and D.-H. Park, *J. Korean Ceram. Soc.*, 2020, **57**, 597−607.

35 M. Asif, A. Aziz, M. Azeem, Z. Wang, G. Ashraf, F. Xiao, X. Chen and H. Liu, *Adv. Colloid Interface Sci.*, 2018, **262**, 21−38.

36 J. Tan, P. Balan and N. Birbilis, *Appl. Clay Sci.*, 2021, **202**, 105948.

37 V. Shirin, R. Sankar, A. P. Johnson, H. V. Gangadharappa and K. Pramod, *J. Control. Release*, 2021, **330**, 398−426.

38 V. Prevot and Y. Tokudome, *J. Mater. Sci.*, 2017, **52**, 11229−11250.

39 J. H. Choy, S. Y. Kwak, Y. J. Jeong and J. S. Park, *Angew. Chem. Int. Ed.*, 2000, **39**, 4041.

40 J. H. Choy, J. S. Jung, J. M. Oh, M. Park, J. Jeong, Y. K. Kang and O. J. Han, *Biomaterials*, 2004, **25**, 3059−3064.

41 Z. Gu, B. E. Rolfe, Z. P. Xu, J. H. Campbell, G. Q. Lu and A. C. Thomas, *Adv. Healthcare Mater.*, 2012, **1**, 669−673.

42 J.-K. Lin, J.-Y. Uan, C.-P. Wu and H.-H. Huang, *J. Mater. Chem.*, 2011, **21**, 5011−5020.

43 A. Li, L. Qin, W. Wang, R. Zhu, Y. Yu, H. Liu and S. Wang, *Biomaterials*, 2011, **32**, 469−477.

44 R. Liang, R. Tian, L. Ma, L. Zhang, Y. Hu, J. Wang, M. Wei, D. Yan, D. G. Evans and X. Duan, *Adv. Funct. Mater.*, 2014, **24**, 3144.

45 B. Li, Z. Gu, N. Kurniawan, W. Chen and Z. P. Xu, *Adv. Mater.*, 2017, **29**, 1700373.

46 R. Gao, X. Mei, D. Yan, R. Liang and M. Wei, *Nat. Commun.*, 2018, **9**, 2798.

47 L. Peng, X. Mei, J. He, J. Xu, W. Zhang, R. Liang, M. Wei, D. G. Evans and X. Duan, *Adv. Mater.*, 2018, **30**, 1707389.

48 Z. Cao, L. Zhang, K. Liang, S. Cheong, C. Boyer, J. J. Gooding, Y. Chen and Z. Gu, *Adv. Sci.*, 2018, **5**, 1801155.

49 X. Mei, T. Hu, H. Wang, R. Liang, W. Bu and M. Wei, *Biomaterials*, 2020, **258**, 120257.

50 W. Shen, T. Hu, X. Liu, J. Zha, F. Meng, Z. Wu, Z. Cui, Y. Yang, H. Li, Q. Zhang, L. Gu, R. Liang and C. Tan, *Nat. Commun.*, 2022, **13**, 3384.

51 W. Jin and D.-H. Park, *Nanomaterials*, 2019, **9**, 1404.

52 L. Yan, Y. Wang, T. Hu, X. Mei, X. Zhao, Y. Bian, L. Jin, R. Liang, X. Weng and M. Wei, *J. Mater. Chem. B*, 2020, **8**, 1445−1455.

53 T. Zhan, J. Kang, X. Li, L. Pan, G. Li and W. Hou, *Sens. Actuators B Chem.*, 2018, **255**, 2635−2642.

54 Y. Zhu, Y. Wang, G. R. Williams, L. Fu, J. Wu, H. Wang, R. Liang, X. Weng and M. Wei, *Adv. Sci.*, 2020, **7**, 2000272.

55 X. Mei, J. Ma, X. Bai, X. Zhang, S. Zhang, R. Liang, M. Wei, D. G. Evans and X. Duan, *Chem. Sci.*, 2018, **9**, 5630−5639.

56 J. Zhou, M. Min, Y. Liu, J. Tang and W. Tang, *Sens. Actuators B Chem.*, 2018, **260,** 408−417.

57 S. Moolayadukkam, S. Thomas, R. C. Sahoo, C. H. Lee, S. U. Lee and H. S. S. R. Matte, *ACS Appl. Mater. Interfaces*, 2020, **12**, 6193−6204.

58 M. Shao, F. Ning, J. Zhao, M. Wei, D. G. Evans and X. Duan, *J. Am. Chem. Soc.*, **2012**, 134, 1071−1077.

59 M. Asif, W. Haitao, D. Shuang, A. Aziz, G. Zhang, F. Xiao and H. Liu, *Sens. Actuators B Chem.*, 2017, **239**, 243−252.

60 Y. Wang, D. Zhang, D. Lv and Y. Sun, *J. Taiwan Inst. Chem. E.*, 2015, **57**, 160−166.

61 S.-J. Choi, H.-J. Paek and J. Yu, *Int. J. Nanomed.*, 2015, **10**, 3217−3229.

62 F. Deng, H. Zhou, J. Chen, H. Huang, J. Tian, Q. Huang, Y. Wen, M. Liu, X. Zhang and Y. Wei, *Mater. Sci. Eng. C*, 2019, **104**, 109976.

63 S. Guan, R. Liang, C. Li, D. Yan, M. Wei, D. G. Evans and X. Duan, *J. Mater. Chem. B*, 2016, **4**, 1331.

64 J. Li, B. Li, J. Wang, L. He and Y. Zhao, *Acta Chim. Sinica*, 2021, **79**, 238−256.

65 G. Choi, S. Eom, A. Vinu and J.-H. Choy, *Chem. Rec.*, 2018, **18**, 1033−1053.

66 L.-X. Zhang, J. Hu, Y.-B. Jia, R.-T. Liu, T. Cai and Z. P. Xu, *Nanoscale*, 2021, **13**, 7533−7549.

67 F. Peng, D. Wang, D. Zhang, H. Cao and X. Liu, *Appl. Clay Sci.*, 2018, **165**, 179−187.

68 F. Barahuie, M. Z. Hussein, P. Arulselvan, S. Fakurazi and Z. Zainal, *J. Solid State Chem.*, 2014, **217**, 31−41.

69 Y. Wang, S. Shen, T. Hu, G. R. Williams, Y. Bian, B. Feng, R. Liang and X. Weng, *ACS Nano*, 2021, **15**, 9732−9745.

70 T. Li, X. Hao, S. Bai, Y. Zhao and Y.-F. Song, *Acta Phys. -Chim. Sin.*, 2020, **36**, 1912005.

71 S. Mallakpour, M. Hatami and C. M. Hussain, *Adv. Colloid Interface Sci.*, 2020, **283**, 102216.

72 H. Chi, J. Wang, H. Wang, S. Li, M. Yang, S. Bai, C. Li, X. Sun, Y. Zhao and Y.-F. Song, *Adv. Funct. Mater.*, 2022, **32**, 2106645.

73 G. Mishra, B. Dash and S. Pandey, *Appl. Clay Sci.*, 2018, **153**, 172−186.

74 K. N. Andrade, G. G. C. Arízaga and J. A. R. Mayorga, *Processes*, 2020, **8**, 462.

75 M. S. Usman, M. Z. Hussein, A. U. Kura, S. Fakurazi, M. J. Masarudin and F. F. Ahmad Saad, *Mater. Chem. Phys.*, 2020, **240**, 122232.

76 J.-M. Oh, S.-H. Hwang and J.-H. Choy, *Solid State Ionics*, 2002, **151**, 285−291.

77 L. Wang, S.-M. Xu, X. Yang, S. He, S. Guan, G. I. N. Waterhouse and S. Zhou, *ACS Appl. Mater. Interfaces*, 2020, **12**, 54916−54926.

78 L. Xu, M. Lian, X. Chen, Y. Lu and W. Yang, *Microchim. Acta*, 2017, **184**, 3989−3996.

79 D. G. Evans and R. C. T. Slade, in *Layered double hydroxides*, ed. X. Duan and D. G. Evans, Springer, Berlin, Germany, 2006, vol. 119, p. 1−87.

80 J. An, T. Shen, W. Chang, Y. Zhao, B. Qi and Y.-F. Song, *Inorg. Chem. Front.*, 2021, **8**, 996−1004.

81 G. Liu, Z. Wang, T. Shen, X. Zheng, Y. Zhao and Y.-F. Song, *Nanoscale*, 2021, **13**, 1869−1874.

82 J. Song, X. Xu, Y. Lin, D. Li and X. Duan, *China Patent*, ZL200910084976.0.

83 L. Li, R. Ma, Y. Ebina, N. Iyi and T. Sasaki, *Chem. Mater.*, 2005, **17**, 4386−4391.

84 R. Ma, Z. Liu, L. Li, N. Iyi and T. Sasaki, *J. Mater. Chem.*, 2006, **16**, 3809−3813.

85 Z. Wang, S.-M. Xu, Y. Xu, L. Tan, X. Wang, Y. Zhao, H. Duan and Y.-F. Song, *Chem. Sci.*, 2019, **10**, 378−384.

86 L. Tan, S. Xu, Z. Wang, Y. Xu, X. Wang, X. Hao, S. Bai, C. Ning, Y. Wang, W. Zhang, Y. K. Jo, S.-J. Hwang, X. Cao, X. Zheng, H. Yan, Y. Zhao, H. Duan and Y.-F. Song, *Angew. Chem. Int. Ed.*, 2019, **58**, 11860−11867.

87 M. Meyn, K. Beneke and G. Lagaly, *Inorg. Chem.*, 1990, **29**, 5201−5207.

88 J. M. Hidalgo, C. Jimenez-Sanchidrian, M. Mora and J. R. Ruiz, *J. Nanosci. Nanotechnol.*, 2010, **10**, 6562−6566.

89 J. Yu, Q. Wang, D. O'Hare and L. Sun, *Chem. Soc. Rev.*, 2017, **46**, 5950−5974.

90 L. Chen, B. Sun, X. Wang, F. Qiao and S. Ai, *J. Mater. Chem. B*, 2013, **1**, 2268−2274.

91 Z. Liu, R. Ma, M. Osada, N. Iyi, Y. Ebina, K. Takada and T. Sasaki, *J. Am. Chem. Soc.*, 2006, **128**, 4872−4880.

92 L. Li, R. Ma, Y. Ebina, N. Iyi and T. Sasaki, *Chem. Mater.*, 2005, **17**, 4386−4391.

93 Q. Wu, A. Olafsen, O. B. Vistad, J. Roots and P. Norby, *J. Mater. Chem.*, 2005, **15**, 4695−4700.

94 A. Aziz, M. Asif, M. Azeem, G. Ashraf, Z. Wang, F. Xiao and H. Liu, *Anal. Chim. Acta*, 2019, **1047**, 197−207.

95 H. Chi, J. Dong, T. Li, S. Bai, L. Tan, J. Wang, T. Shen, G. Liu, L. Liu, L. Sun, Y. Zhao and Y.-F. Song, *Green Energy Environ.*, 2022, DOI: 10.1016/j.gee.2020.12.013.

96 Q. Wang and D. O'Hare, *Chem. Commun.*, 2013, **49**, 6301−6303.

97 J. Yu, K. Ruengkajorn, D.-G. Crivoi, C. Chen, J.-C. Buffet and D. O'Hare, *Nat. Commun.*, 2019, **10**, 2398.

98 R. Liu, Y. Wang, D. Liu, Y. Zou and S. Wang, *Adv. Mater.*, 2017, **29**, 1701546.

99 Y. Wang, Y. Zhang, Z. Liu, C. Xie, S. Feng, D. Liu, M. Shao and S. Wang, *Angew. Chem. Int. Ed.*, 2017, **56**, 5867−5871.

100 G. Hu, N. Wang, D. O'Hare and J. Davis, *Chem. Commun.*, 2006, **3**, 287−289.

101 J. Yu, B. R. Martin, A. Clearfield, Z. Luo and L. Sun, *Nanoscale*, 2015, **7**, 9448−9451.

102 J. Yu, J. Liu, A. Clearfield, J. E. Sims, M. T. Speiegle, S. L. Suib and L. Sun, *Inorg. Chem.*, 2016, **55**, 12036−12041.

103 T. Hu, L. Yan, Z. Wang, W. Shen, R. Liang, D. Yan and M. Wei, *Chem. Sci.*, 2021, **12**, 2594−2603.

104 J. Wu, G. R. Williams, Y. Zhu, T. Hu, H. Wang, W. Zhao, R. Liang, X. Weng and M. Wei, *Biomaterials*, 2021, **273**, 120807.

105 H. Zhang, Z. Cao, Q. Zhang, J. Xu, S. L. J. Yun, K. Liang and Z. Gu, *Small*, 2020, **16**, 2002732.

106 Y. Yan, Q. Liu, J. Wang, J. Wei, Z. Gao, T. Mann, Z. Li, Y. He, M. Zhang and L. Liu, *J. Colloid Interface Sci.*, 2012, **371**, 15−19.

107 Y. Zhang, H. Li, N. Du, R. Zhang and W. Hou, *Colloids Surf. A Physicochem. Eng. Aspects*, 2016, **501**, 49−54.

108 Y. Qin, B. Wang, Y. Qiu, X. Liu, G. Qi, S. Zhang, A. Han, J. Luo and J. Liu, *Chem. Commun.*, 2021, **57**, 2752−2755.

109 W. Wang, H. Yan, U. Anand and U. Mirsaidov, *J. Am. Chem. Soc.*, 2021, **143**, 1854−1862.

110 C. Zhang, M. Shao, L. Zhou, Z. Li, K. Xiao and M. Wei, *ACS Appl. Mater. Interfaces*, 2016, **8**, 33697−33703.

111 T. Yan, R. Li, T. Yang and Z. Li, *Electrochim. Acta*, 2015, **152**, 530−537.

112 K. Chibwe and W. Jones, *J. Chem. Soc. Chem. Commun.*, 1989, **14**, 926−927.

113 Y. Kuroda, Y. Oka, T. Yasuda, T. Koichi, K. Muramatsu, H. Wada, A. Shimojima and K. Kuroda, *Dalton Trans.*, 2018, **47**, 12884−12892.

114 T.-H. Kim, G. J. Lee, J.-H. Kang, H.-J. Kim, T. Kim and J.-M. Oh, *Biomed Res. Int.*, 2014, **2014**, 193401.

115 C. Madhusha, K. Rajapaksha, I. Munaweera, M. Silva, C. Perera, G. Wijesinghe, M. Weerasekera, D. Attygalle, C. Sandaruwan and N. Kottegoda, *ACS Omega*, 2021, **6**, 9600−9608.

116 A. C. Dennis, *J. Electrochem. Soc.*, 1989, **136**, 723−728.

117 Z. Li, M. Shao, H. An, Z. Wang, S. Xu, M. Wei, D. G. Evans and X. Duan, *Chem. Sci.*, 2015, **6**, 6624−6631.

118 Q. Yin, D. Li, J. Zhang, Y. Zhao, J. Luo, M. Shao and J. Han, *J. Alloy. Compd.*, 2020, **813**, 152187.

119 M. Shao, F. Ning, M. Wei, D. G. Evans and X. Duan, *Adv. Funct. Mater.*, 2014, **24**, 580−586.

120 J. Liu, S. Xu, Y. Li, R. Zhang and M. Shao, *Appl. Catal. B Environ.*, 2020, **264**, 118540.

121 J. Guo, C. Mao, R. Zhang, M. Shao, M. Wei and P. Feng, *J. Mater. Chem. A*, 2017, **5**, 11016−11025.

122 L. Zhou, S. Jiang, Y. Liu, M. Shao, M. Wei and X. Duan, *ACS Appl. Energy Mater.*, 2018, **1**, 623−631.

123 M. Shao, Z. Li, R. Zhang, F. Ning, M. Wei, D. G. Evans and X. Duan, *Small*, 2015, **11**, 3530−3538.

124 S. An, N. Shang, B. Chen, Y. Kang, M. Su, C. Wang and Y. Zhang, *J. Colloid Interface Sci.*, 2021, **592**, 205−214.

125 H. Chen, L. Hu, M. Chen, Y. Yan and L. Wu, *Adv. Funct. Mater.*, 2014, **24**, 934−942.

126 J. Zhao, J. Chen, S. Xu, M. Shao, Q. Zhang, F. Wei, J. Ma, M. Wei, D. G. Evans and X. Duan, *Adv. Funct. Mater.*, 2014, **24,** 2938−2946.

127 C. Tang, H.-S. Wang, H.-F. Wang, Q. Zhang, G.-L. Tian, J.-Q. Nie and F. Wei, *Adv. Mater.*, 2015, **27**, 4516−4522.

128 Z. Wang, S. Zeng, W. Liu, X. Wang, Q. Li, Z. Zhao and F. Geng, *ACS Appl. Mater. Interfaces*, 2017, **9**, 1488−1495.

129 X. Wang, Y. Zheng, J. Yuan, J. Shen, J. Hu, A.-J. Wang, L. Wu and L. Niu, *Electrochim. Acta*, 2017, **224**, 628−635.

130 Y. Lu, B. Jiang, L. Fang, S. Fan, F. Wu, B. Hu and F. Meng, *Electroanalysis*, 2017, **29**, 1755−1761.

131 H. Yang, C. Wang, Y. Zhang and Q. Wang, *Sci. China Mater.*, 2019, **62**, 681−689.

132 K. M. Amin, F. Muench, U. Kunz and W. Ensinger, *J. Colloid Interface Sci.*, 2021, **591**, 384−395.

133 M. Shao, F. Ning, J. Zhao, M. Wei, D. G. Evans and X. Duan, *Adv. Funct. Mater.*, 2013, **23**, 3513−3518.

134 J. Sun, H. Liu, X. Chen, D. G. Evans and W. Yang, *Nanoscale.*, 2013, **5**, 7564−7571.

135 B. Wang, X. Han, C. Guo, J. Jing, C. Yang, Y. Li, A. Han, D. Wang and J. Liu, *Appl. Catal. B Environ.*, 2021, **298**, 120580.

136 S.-Y. Jung, G.-H. Gwak, J. K. Park and J.-M. Oh, *RSC Adv.*, 2020, **10**, 5838−5844.

137 M. Yang, G. Zhang, C. Wu, Z. Chang, X. Sun and X. Duan, *Chinese J. Chem.*, 2012, **30**, 2183−2188.

138 J. M. Oh, D. H. Park and J. H. Choy, *Chem. Soc. Rev.*, 2011, **40**, 583−595.

139 C. Zhang, J. Zhao, L. Zhou, Z. Li, M. Shao and M. Wei, *J. Mater. Chem. A*, 2016, **4**, 11516−11523.

140 Y. Dou, T. Pan, S. Xu, H. Yan, J. Han, M. Wei, D. G. Evans and X. Duan, *Angew. Chem. Int. Ed.*, 2015, **54**, 9673−9678.

141 L. Li, W. Y. Gu, J. Liu, S. Y. Yan and Z. P. Xu, *Nano Res.*, 2015, **8**, 682−694.

142 J. Wang, J. D. Zhou, Z. S. Li, Y. C. Song, Q. Liu, Z. H. Jiang and M. L. Zhang, *Chem. Eur. J.*, 2010, **16**, 14404−14144.

143 L. Li, R. Zhang, W. Gu and Z. P. Xu, *Nanomed. Nanotechnol.*, 2018, **14**, 2355−2364.

144 T. Hu, J. He, S. Zhang, X. Mei, W. Zhang, R. Liang, M. Wei, D. G. Evans and X. Duan, *Chem. Commun.*, 2018, **54**, 5760−5763.

145 Q. Yue, Y. Zhang, Y. J. Jiang, J. L. Li, H. W. Zhang, C. Z. Yu, A. A. Elzatahry, A. Alghamdi, Y. H. Deng and D. Y. Zhao, *J. Am. Chem. Soc.*, 2017, **139**, 4954−4961.

146 J. Liu, S. Z. Qiao, S. B. Hartono and G. Q. Lu, *Angew. Chem. Int. Ed.*, 2010, **49**, 4981−4985.

147 D. A. Li, Y. T. Zhang, M. Yu, J. Guo, D. Chaudhary and C. C. Wang, *Biomaterials*, 2013, **34**, 7913−7922.

148 M. F. Shao, F. Y. Ning, J. W. Zhao, M. Wei, D. G. Evans and X. Duan, *J. Am. Chem. Soc.*, 2012, **134**, 1071−1077.

149 L. Wang, H. Xing, S. Zhang, Q. Ren, L. Pan, K. Zhang, W. Bu, X. Zheng, L. Zhou, W. Peng, Y. Hua and J. Shi, *Biomaterials*, 2013, **34**, 3390−3401.

150 C. P. Chen, P. Gunawan, X. W. Lou and R. Xu, *Adv. Funct. Mater.*, 2012, **22**, 780−787.

151 T. Jia, Z. Wang, Q. Sun, S. Dong, J. Xu, F. Zhang, L. Feng, F. He, D. Yang, P. Yang and J. Lin, *Small*, 2020, **16**, 2001343.

152 J. Wang, W. Zhang, L. Hao, J. Sun, W. Zhang, C. Guo, Y. Mu, W. Ji, C. Yu and F. Yuan, *J. Mater. Res.*, 2019, **34**, 3747−3756.

153 L. Markov and K. Petrov, *Solid State Ionics*, 1990, **39**, 187−193.

154 S. T. Zhang, Y. Dou, J. Zhou, M. Pu, H. Yan, M. Wei, D. G. Evans and X. Duan, *ChemPhysChem*, 2016, **17**, 2754−2766.

155 J. Wu, S. Zhang, X. Mei, N. Liu, T. Hu, R. Liang, D. Yan and M. Wei, *ACS Appl. Mater. Interfaces*, 2020, **12**, 48310−48320.

156 S. Wang, T. Hu, G. Wang, Z. Wang, D. Yan, R. Liang and C. Tan, *Chem. Eng. J.*, 2021, **419**, 129458.

157 R. P. Wang, Z. S. He, P. J. Cai, Y. Zhao, L. Gao, W. Z. Yang, Y. L. Zhao, X. Y. Gao and F. P. Gao, *ACS Appl. Mater. Interfaces*, 2019, **11**, 13964−13972.

158 N. Yang, Y. P. Ding, Y. L. Zhang, B. Wang, X. Zhao, K. M. Cheng, Y. X. Huang, M. Taleb, J. Zhao, W. F. Dong, L. R. Zhang and G. J. Nie, *ACS Appl. Mater. Interfaces*, 2018, **10**, 22963−22973.

159 X. C. Gao, R. X. Cui, G. F. Ji and Z. L. Liu, *Nanoscale*, 2018, **10**, 6205−6211.

160 Y. S. Yoon, B. I. Lee, K. S. Lee, G. H. Im, S. H. Byeon, J. H. Lee and I. S. Lee, *Adv. Funct. Mater.*, 2009, **19**, 3375−3380.

161 Z. Cao, N. N. M. Adnan, G. Wang, A. Rawal, B. Shi, R. Liu, K. Liang, L. Zhao, J. J. Gooding, C. Boyer and Z. Gu, *J. Colloid Interface Sci.*, 2018, **521**, 242−251.

162 Y. Zhang, H. Li, N. Du, S. Song and W. Hou, *Appl. Clay Sci.*, 2017, **143**, 336−344.

163 M. Yan, Z. Zhang, S. Cui, M. Lei, K. Zeng, Y. Liao, W. Chu, Y. Deng and C. Zhao, *Int. J. Nanomed.*, 2014, **9**, 4867.

164 Z. Gu, H. L. Zuo, L. Li, A. H. Wu and Z. P. Xu, *J. Mater. Chem. B*, 2015, **3**, 3331−3339.

165 Y. Tokudome, M. Fukui, N. Tarutani, S. Nishimura, V. Prevot, C. Forano, G. Poologasundarampillai, P. D. Lee and M. Takahashi, *Langmuir*, 2016, **32**, 8826−8833.

166 A. Y. Park, H. Kwon, A. J. Woo and S. J. Kim, *Adv. Mater.*, 2005, **17**, 106−109.

167 J. M. Oh, S. J. Choi, G. E. Lee, S. H. Han and J. H. Choy, *Adv. Funct. Mater.*, 2009, **19**, 1617−1624.

168 Y. M. Kuo, Y. Kuthati, R. K. Kankala, P. R. Wei, C. F. Weng, C. L. Liu, P. J. Sung, C. Y. Mou and C. H. Lee, *J. Mater. Chem. B*, 2015, **3**, 3447−3458.

169 L. X. Zhang, X. X. Xie, D. Q. Liu, Z. P. Xu and R. T. Liu, *Biomaterials*, 2018, **174**, 54−66.

170 W. Chen, B. Zhang, T. Mahony, W. Gu, B. Rolfe and Z. P. Xu, *Small*, 2016, **12**, 1627−1639.

171 Z. Gu, B. E. Rolfe, A. C. Thomas, J. H. Campbell, G. Q. Lu and Z. P. Xu, *Biomaterials*, 2011, **32**, 7234–7240.

172 K. Ladewig, M. Niebert, Z. P. Xu, P. P. Gray and G. Q. Lu, *Biomaterials*, 2010, **31**, 1821–1829.

173 G. Choi, S. Y. Kim, J. M. Oh and J. H. Choy, *J. Am. Ceram. Soc.*, 2012, **95**, 2758−2765.

174 L. Yan, Z. Wang, X. Chen, X. J. Gou, Z. Zhang, X. Zhu, M. Lan, W. Chen, G. Zhu and W. Zhang, *Chem. Commun.*, 2017, **53**, 2339−2342.

175 Z. Wang, H. Zhu, F. He, D. Yan, T. Jia, Q. Sun, X. Wang, X. Wang, D. Yang, S. Gai and P. Yang, *Chem. Eng. J.*, 2020, **382**, 122847.

176 S. G. Choi and J. H. Choy, *J. Mater. Chem.*, 2011, **21**, 5547−5554.

177 L. Yan, M. Zhou, X. Zhang, L. Huang, W. Chen, V. A. L. Roy, W. Zhang and X. Chen, *ACS Appl. Mater. Interfaces*, 2017, **9**, 34185−34193.

178 H. Zhang, L. Zhang, Z. Cao, S. Cheong, C. Boyer, Z. Wang, S. L. J. Yun, R. Amal and Z. Gu, *Small*, 2022, **18**, 2200299.

179 Q. Bao, P. Hu, W. Ren, Y. Guo and J. Shi, *Chem*, 2020, **6**, 2283−2299.

180 W. Zheng, T. Yin, Q. Chen, X. Qin, X. Huang, S. Zhao, T. Xu, L. Chen and J. Liu, *Acta Biomater.*, 2016, **31**, 197−210.

181 V. Ambrogi, Gi. Fardella, G. Grandolini and L. Perioli, *Int. J. Pharmaceut.*, 2001, **220**, 23−32.

182 Z. Gu, A. Wu, L. Li and Z. P. Xu, *Pharmaceutics*, 2014, **6**, 235−248.

183 Z. Gu, A. C. Thomas, Z. P. Xu, J. H. Campbell and G. Q. Lu, *Chem. Mater.*, 2008, **20**, 3715−3722.

184 X. Gao, L. Chen, J. Xie, Y. Yin, T. Chang, Y. Duan and N. Jiang, *Mater. Sci. Eng. C*, 2014, **39**, 56−60.

185 R. Rojas, M. C. Palena, A. F. Jimenez-Kairuz, R. H. Manzo and C. E. Giacomelli, *Appl. Clay Sci.*, 2012, **62**, 15−20.

186 S. Senapati, R. Thakur, S. P. Verma, S. Duggal, D. P. Mishra, P. Das, T. Shripathi, M. Kumar, D. Rana and P. Maiti, *J. Control. Release*, 2016, **224**, 186−198.

187 H. Zhang, K. Zou, S. Guo and X. Duan, *J. Solid State Chem.*, 2006, **179**, 1792−1801.

188 B. Li, J. Tang, W. Chen, G. Hao, N. Kurniawan, Z. Gu and Z. P. Xu, *Biomaterials*, 2018, **177**, 40−51.

189 M. Ebadi, K. Buskaran, S. Bullo, M. Z. Hussein, S. Fakurazi and G. Pastorin, *Alex. Eng. J.*, 2021, **60**, 733−747.

190 P. K. Sahoo, H. S. Panda and D. Bahadur, *Mater. Chem. Phys.*, 2013, **142**, 106−112.

191 Y. Li, H. Y. Bi, H. Li, X. M. Mao and Y. Q. Liang, *Mater. Sci. Eng. C*, 2017, **78**, 886−891.

192 T. R. R. Timóteo, C. G. Melo, L. J. A. Danda, L. C. P. B. B. Silva, D. A. F. Fontes, P. C. D. Silva, C. S. B. Aguilera, L. P. Siqueira, L. A. Rolim and P. J. R. Neto, *Appl. Clay Sci.*, 2019, **180**, 105197.

193 M. Yasaei, M. Khakbiz, E. Ghasemi and A. Zamanian, *Appl. Surf. Sci.*, 2019, **467**, 782−791.

194 A. D. Leão, V. V. Oliveira, F. A. Marinho, A. G. Wanderley, J. S. Aguiar, T. G. Silva, M. F. R. Soares and J. L. S. Sobrinho, *Appl. Clay Sci.*, 2019, **181**, 105218.

195 Y. Salguero, L. Valenti, R. Rojas and M. C. García, *Mater. Sci. Eng. C*, 2020, **111**, 110859.

196 Á. Deák, E. Csapó, Á. Juhász, I. Dékány and L. Janovák, *Appl. Clay Sci.*, 2018, **156**, 28−35.

197 T. Xu, J. Zhang, H. Chi and F. Cao, *Acta Biomater.*, 2016, **36**, 152−163.

198 S. B. Khan, K. A. Alamry, N, A. Alyahyawi and A. M. Asiri, *Int. J. Nanomed.*, 2018, **13**, 3203−3222.

199 Z. Liu, L. Jin, J. Chen, Q. Fang, S. Ablameyko, Z. Yin and Y. Xu, *Comput. Biol. Med.*, 2021, **134**, 104523.

200 Q. Wang and L. Zhang, *ACS Nano*, 2021, **15**, 149−174.

201 A. B. E. Attia, G. Balasundaram, M. Moothanchery, U. S. Dinish, R. Bi, V. Ntziachristos and M. Olivo, *Photoacoustics*, 2019, **16**, 100144.

202 V. Jayanthi, A. B. Das and U. Saxena, *Biosens. Bioelectron.*, 2017, **91**, 15−23.

203 W. M. Burke, J. Orr, M. Leitao, E. Salom, P. Gehrig, A. B. Olawaiye, M. Brewer and D. Boruta, *Gynecol. Oncol.*, 2014, **134**, 385−392.

204 W. Xu, D. Wang and B. Z. Tang, *Angew. Chem. Int. Ed.*, 2021, **60**, 7476−7487.

205 J. Ouyang, A. Xie, J. Zhou, R. Liu, L. Wang, H. Liu, N. Kong and W. Tao, *Chem. Soc. Rev.*, 2022, **51**, 4996−5041.

206 T. H. Shin, Y. Choi, S. Kim and J. Cheon, *Chem. Soc. Rev.*, 2015, **44**, 4501−4516.

207 C. Chi, Y. Du, J. Ye, D. Kou, J. Qiu, J. Wang, J. Tian and X. Chen, *Theranostics*, 2014, **4**, 1072−1084.

208 J. Ge, Q. Zhang, J. Zeng, Z. Gu and M. Gao, *Biomaterials*, 2020, **228**, 119553.

209 J. V. Frangioni, *Curr. Opin. Chem. Biol.*, 2003, **7**, 626−634.

210 C. Chen, L. K. Yee, H. Gong, Y. Zhang and R. Xu, *Nanoscale*, 2013, **5**, 4314−4320.

211 X. Jin, M. Zhang, G. Gou and J. Ren, *J. Pharm. Sci.*, 2016, **105**, 1751−1761.

212 R. Ma, R. Li, X. Liu, P. Zhang, X. Yang and J. Lu, *Adv. Optical Mater.*, 2020, **8**, 1902019.

213 R. Tian, D. Yan, C. Li, S. Xu, R. Liang, L. Guo, M. Wei, D. G. Evans and X. Duan, *Nanoscale*, 2016, **8**, 9815−9821.

214 W. Liu, S. Xu, S. Guan, R. Liang, M. Wei, D. G. Evans and X. Duan, *Adv. Mater.*, 2018, **30**, 1704376.

215 C.-G. Liu, H.-X. Tang, X. Zheng, D.-Y. Yang, Y. Zhang, J.-T. Zhang, R. K. Kankala, S.-B. Wang, G. Liu and A.-Z. Chen, *ACS Appl. Mater. Interfaces*, 2020, **12**, 40673−40683.

216 N. Zhang, Y. Wang, C. Zhang, Y. Fan, D. Li, X. Cao, J. Xia, X. Shi and R. Guo, *Theranostics*, 2020, **10**, 2791−2802.

217 F. S. Vajedi, H. Dehghani and A. Zarrabi, *Mater. Sci. Eng. C*, 2021, **119**, 111627.

218 H. Zuo, W. Chen, B. Li, K. Xu, H. Cooper, Z. Gu and Z. P. Xu, *Chem. Eur. J.*, 2017, **23**, 14299−14306.

219 Q. Zhang, D. Zhou, G. Fang, H. Lu, J. Zeng and Z. Gu, *Adv. Mater. Interfaces*, 2022, **9**, 2101914.

220 C. Zhang, L. Li, F. Y. Han, X. Yu, X. Tan, C. Fu, Z. P. Xu and A. K. Whittaker, *Small*, 2019, **15**, 1902309.

221 L. Wang, Y. Wang and X. Wang, *Materials*, 2017, **10**, 1140.

222 S. Shi, B. C. Fliss, Z. Gu, Y. Zhu, H. Hong, H. F. Valdovinos, R. Hernandez, S. Goel, H. Luo, F. Chen, T. E. Barnhart, R. J. Nickles, Z. P. Xu and W. Cai, *Sci. Rep.*, 2015, **5**, 16930.

223 H.-J. Kim, J. Y. Lee, T.-H. Kim, G.-H. Gwak, J. H. Park and J.-M. Oh, *Appl. Clay Sci.*, 2020, **186**, 105454.

224 D.-E. Lee, H. Koo, I.-C. Sun, J. H. Ryu, K. Kim and I. C. Kwon, *Chem. Soc. Rev.*, 2012, **41**, 2656−2672.

225 S. Guan, R. Liang, C. Li and M. Wei, *Talanta*, 2017, **165**, 297−303.

226 H. Lin, Y. Chen and J. Shi, *Chem. Soc. Rev.*, 2018, **47**, 1938−1958.

227 F. Bray, J. Ferlay, I. Soerjomataram, R. L. Siegel, L. A. Torre and A. Jemal, *CA-Cancer J. Clin.*, 2018, **68**, 394−424.

228 T. Hu, X. Mei, Y. Wang, X. Weng, R. Liang and M. Wei, *Sci. Bull.*, 2019, **64**, 1707−1727.

229 V. Schirrmacher, *Int. J. Oncol.*, 2018, **54**, 407−419.

230 Z. Zhou, X. Wang, H. Zhang, H. Huang, L. Sun, L. Ma, Y. Du, C. Pei, Q. Zhang, H. Li, L. Ma, L. Gu, Z. Liu, L. Cheng and C. Tan, *Small*, 2021, **17**, 2007486.

231 Z. Zhou, B. Li, C. Shen, D. Wu, H. Fan, J. Zhao, H. Li, Z. Zeng, Z. Luo, L. Ma and C. Tan, *Small*, 2020, **16**, 2004173.

232 C. Tan, L. Zhao, P. Yu, Y. Huang, B. Chen, Z. Lai, X. Qi, M. H. Goh, X. Zhang, S. Han, X.-J. Wu, Z. Liu, Y. Zhao and H. Zhang, *Angew. Chem. Int. Ed.*, 2017, **56**, 7842−7846.

233 H. Huang, J. Zha, S. Li and C. Tan, *Chin. Chem. Lett.*, 2022, **33**, 163−176.

234 Z. Zhou, Y. Wang, F. Peng, F. Meng, J. Zha, L. Ma, Y. Du, N. Peng, L. Ma, Q. Zhang, L. Gu, W. Yin, Z. Gu and C. Tan, *Angew. Chem. Int. Ed.*, 2022, **61**, e202115939.

235 C. Chang, W. Chen, Y. Chen, Y. Chen, Y. Chen, F. Ding, C. Fan, H. J. Fan, Z. Fan, C. Gong, Y. Gong, Q. He, X. Hong, S. Hu, W. Hu, W. Huang, Y. Huang, W. Ji, D. Li, L.-J. Li, Q. Li, L. Lin, C. Ling, M. Liu, N. Liu, Z. Liu, K. P. Loh, J. Ma, F. Miao, H. Peng, M. Shao, L. Song, S. Su, S. Sun, C. Tan, Z. Tang, D. Wang, H. Wang, J. Wang, X. Wang, X. Wang, A. T. S. Wee, Z. Wei, Y. Wu,

Z.-S. Wu, J. Xiong, Q. Xiong, W. Xu, P. Yin, H. Zeng, Z. Zeng, T. Zhai, H. Zhang, H. Zhang, Q. Zhang, T. Zhang, X. Zhang, L.-D. Zhao, M. Zhao, W. Zhao, Y. Zhao, K.-G. Zhou, X. Zhou, Y. Zhou, H. Zhu, H. Zhang and Z. Liu, *Acta Phys.-Chim. Sin.*, 2021, **37**, 2108017.

236 C. Liu, S. Sun, Q. Feng, G. Wu, Y. Wu, N. Kong, Z. Yu, J. Yao, X. Zhang, W. Chen, Z. Tang, Y. Xiao, X. Huang, A. Lv, C. Yao, H. Cheng, A. Wu, T. Xie and W. Tao, *Adv. Mater.*, 2021, **33**, 2102054.

237 D. Chimene, D. L. Alge and A. K. Gaharwar, *Adv. Mater.*, 2015, **27**, 7261−7284.

238 Z. Tang, X. Zhang, Y. Shu, M. Guo, H. Zhang and W. Tao, *Nano Today*, 2021, **36**, 101019.

239 D. Zhang, D. Zhong, J. Ouyang, J. He, Y. Qi, W. Chen, X. Zhang, W. Tao and M. Zhou, *Nat. Commun.*, 2022, **13**, 1413.

240 B. Yang and J. Shi, *J. Am. Chem. Soc.*, 2020, **142**, 21775−21785.

241 B. Yang and J. Shi, *Angew. Chem. Int. Ed.*, 2020, **59**, 21829−21838.

242 B. Yang, Y. Chen and J. Shi, *Angew. Chem. Int. Ed.*, 2020, **59**, 9693−9701.

243 L. Qin, M. Xue, W. Wang, R. Zhu, S. Wang, J. Sun, R. Zhang and X. Sun, *Int. J. Pharmaceut.*, 2010, **388**, 223−230.

244 R. Zhu, Q. Wang, Y. Zhu, Z. Wang, H. Zhang, B. Wu, X. Wu and S. Wang, *Acta Biomater.*, 2016, **29**, 320−332.

245 Y. Zhu, R. Zhu, M. Wang, B. Wu, X. He, Y. Qian and S. Wang, *Adv. Sci.*, 2016, **3**, 1600229.

246 H. Asiabi, Y. Yamini, M. Alipour, M. Shamsayei and S. Hosseinkhani, *Mater. Sci. Eng. C*, 2019, **97**, 96−102.

247 A. Hakeem, G. Zhan, Q. Xu, T. Yong, X. Yang and L. Gan, *J. Mater. Chem. B*, 2018, **6**, 5768−5774.

248 N. Ge, D. Wang, F. Peng, J. Li, Y. Qiao and X. Liu, *ACS Appl. Mater. Interfaces*, 2016, **8**, 24491−24501.

249 G. Li, Y. Fan, L. Lin, R. Wu, M. Shen and X. Shi, *Sci. China Chem.*, 2021, **64**, 817−826.

250 S. Saha, S. Ray, S. Ghosh and J. Chakraborty, *J. Am. Ceram. Soc.*, 2018, **101**, 3924−3935.

251 A. Bhattacharjee, S. H. Rahaman, S. Saha, M. Chakraborty and J. Chakraborty, *Appl. Clay Sci.*, 2019, **168**, 31−35.

252 D. Wang, N. Ge, J. Li, Y. Qiao, H. Zhu and X. Liu, *ACS Appl. Mater. Interfaces*, 2015, **7**, 7843−7854.

253 C. Ma, Z. Wang, T. Xu, Z. He and Y. Wei, *Biotechnol. Adv.*, 2020, **40**, 107502.

254 Y. Xiao, Z. Tang, X. Huang, W. Chen, J. Zhou, H. Liu, C. Liu, N. Kong and W. Tao, *Chem. Soc. Rev.*, 2022, **51**, 3828−3845.

255 N. Kong, R. Zhang, G.Wu, X. Sui, J. Wang, N. Y. Kim, S. Blake, D. De, T. Xie, Y. Cao and W. Tao, *Proc. Natl. Acad. Sci. U.S.A.*, 2022, **119**, e2112696119.

256 W. Tao and N. A. Peppas, *Matter*, 2022, **5**, 775−777.

257 M. L. Edelstein, M. R. Abedi and J. Wixon, *J. Gene Med.*, 2007, **9**, 833−842.

258 M. A. Thyveetil, P. V. Coveney, H. C. Greenwell and J. L. Suter, *J. Am. Chem. Soc.*, 2008, **130**, 12485−12495.

259 S. Li, J. Li, C. J. Wang, Q. Wang, M. Z. Cader, J. Lu, D. G. Evans, X. Duan and D. O'Hare, *J. Mater. Chem. B*, 2013, **1**, 61−68.

260 Y. Wong, H. M. Cooper, K. Zhang, M. Chen, P. Bartlett and Z. P. Xu, *J. Colloid Interface Sci.*, 2012, **369**, 453−459.

261 M. Chen, H. M. Cooper, J. Z. Zhou, P. F. Bartlett and Z. P. Xu, *J. Colloid Interface Sci.*, 2013, **390**, 275−281.

262 Z. Yu, P. Hu, Y. Xu, Q. Bao, D. Ni, C. Wei and J. Shi, *Small*, 2020, **16**, 1907233.

263 D.-H. Park, J. Cho, O.-J. Kwon, C.-O. Yun and J.-H. Choy, *Angew. Chem. Int. Ed.*, 2016, **55**, 4582−4586.

264 J. Wang, W. Bao, A. Umar, Q. Wang, D. O'Hare and Y. Wan, *J. Biomed. Nanotechnol.*, 2016, **12**, 922−933.

265 L. Li, W. Gu, J. Chen, W. Chen and Z. P. Xu, *Biomaterials*, 2014, **35**, 3331−3339.

266 R. Ma, Y. Wang, L. Yan, L. Ma, Z. Wang, H. C. Chan, S.-K. Chiu, X. Chen and G. Zhu, *Chem. Commun.*, 2015, **51**, 7859−7862.

267 J. K. Tom, T. J. Albin, S. Manna, B. A. Moser, R. C. Steinhardt and A. P. Esser-Kahn, *Trends Biotechnol.*, 2019, **37**, 373−388.

268 A. W. Purcell, J. McCluskey and J. Rossjohn, *Nat. Rev. Drug Discov*., 2007, **6**, 404−414.

269 C. J. Melief and S. H. Burg, *Nat. Rev. Cancer.*, 2008, **8**, 351−360.

270 Y. Xia, J. Wu, W. Wei, Y. Du, T. Wan, X. Ma, W. An, A. Guo, C. Miao, H. Yue, S. Li, X. Cao, Z. Su and G. Ma, *Nat. Mater.*, 2018, **17**, 187−194.

271 A. A. Itano and M. K. Jenkins, *Nat. Immunol.*, 2003, **4**, 733−739.

272 U. H. Andrian and T. R. Mempel, *Nat. Rev. Immunol.*, 2003, **3**, 867−878.

273 L. X. Zhang, X. M. Sun, Y. B. Jia, X. G. Liu, M. Dong, Z. P. Xu and R. T. Liu, *Nano Today*, 2020, **35**, 100923.

274 W. Chen, H. Zuo, B. Li, C. Duan, B. Rolfe, B. Zhang, T. J. Mahony and Z. P. Xu, *Small*, 2018, **14**, 1704465.

275 G. R. Williams, K. Fierens, S. G. Preston, D. Lunn, O. Rysnik, S. De Prijck, M. Kool, H. C. Buckley, B. N. Lambrecht, D. O'Hare and J. M. Austyn, *J. Exp. Med.*, 2014, **211**, 1019−1025.

276 A. Li, L. Qin, D. Zhu, R. Zhu, J. Sun and S. Wang, *Biomaterials*, 2010, **31**, 748−756.

277 S. Yan, W. Gu, B. Zhang, B. E. Rolfe and Z. P. Xu, *Dalton Trans.*, 2018, **47**, 2956−2964.

278 L. X. Zhang, Y. B. Jia, Y. R. Huang, H. N. Liu, X. M. Sun, T. Cai, R. T. Liu and Z. P. Xu, *Nano Res.*, 2021, **14**, 1326−1334.

279 Z. P. Xu, M. Niebert, K. Porazik, T. L. Walker, H. M. Cooper, A. P. J. Middelberg, P. P. Gray and P. F. Bartlett, *J. Control. Release.*, 2008, **130**, 86−94.

280 W. Chen, H. Zuo, T. J. Mahony, B. Zhang, B. Rolfe and Z. P. Xu, *Sci. Rep.*, 2017, **7**, 13367.

281 L. X. Zhang, D. Q. Liu, S. W. Wang, X. L. Yu, M. Ji, X. X. Xie, S. Y. Liu and R. T. Liu, *J. Mater. Chem. B*, 2017, **5**, 6266.

282 W. Chen, H. Zuo, B. Rolfe, M. A. Schembri, R. N. Cobbold, B. Zhang, T. J. Mahony and Z. P. Xu, *J. Control. Release.*, 2018, **292**, 196−209.

283 S. Yan, B. E. Rolfe, B. Zhang, Y. H. Mohammed, W. Gu and Z. P. Xu, *Biomaterials*, 2014, **35**, 9508−9516.

284 B. Li, G. Hao, B. Sun, Z. Gu and Z. P. Xu, *Adv. Funct. Mater.*, 2020, **30**, 1909745.

285 L. Yang, J. Sun, Q. Liu, R. Zhu, Q. Yang, J. Hua, L. Zheng, K. Li, S. Wang and A. Li, *Adv. Sci.*, 2019, **6**, 1802012.

286 P. N. Manghnani, W. Wu, S. Xu, F. Hu, C. Teh and B. Liu, *Nano-Micro Lett.*, 2018, **10**, 61−69.

287 M. Yang, T. Yang and C. Mao, *Angew. Chem. Int. Ed.*, 2019, **58**, 14066−14080.

288 Y. Liu, P. Bhattarai, Z. Dai and X. Chen, *Chem. Soc. Rev.*, 2019, **48**, 2053−2108.

289 C. Xu and K. Pu, *Chem. Soc. Rev.*, 2021, **50**, 1111−1137.

290 B. Yang, Y. Chen and J. Shi, *Chem. Rev.*, 2019, **119**, 4881−4985.

291 P. C. Lo, M. S. Rodriguez-Morgade, R. K. Pandey, D. K. P. Ng, T. Torres and F. Dumoulin, *Chem. Soc. Rev.*, 2020, **49**, 1041−1056.

292 A. Master, M. Livingston and A. S. Gupta, *J. Control. Release.*, 2013, **168**, 88−102.

293 H. S. Jung, P. Verwilst, A. Sharma, J. Shin, J. L. Sessler and J. S. Kim, *Chem. Soc. Rev.*, 2018, **47**, 2280−2297.

294 B. M. Luby, C. D. Walsh and G. Zheng, *Angew. Chem. Int. Ed.*, 2019, **58**, 2558−2569.

295 Z. Yang, J. Wang, S. Ai, J. Sun, X. Mai and W. Guan, *Theranostics*, 2019, **9**, 6809−6823.

296 H. Ding, H. Yu, Y. Dong, R. Tian, G. Huang, D. A. Boothman, B. D. Sumer and J. Gao, *J. Control. Release.*, 2011, **156**, 276−280.

297 T. Hu, Z. Zhou, J. Zha, G. R. Williams, Z. Wu, W. Zhao, W. Shen, H. Li, X. Weng, R. Liang and C. Tan, *Fund. Res.*, 2022, doi:10.1016/j.fmre.2022.06.001.

298 X. S. Li, M. R. Ke, W. Huang, C. H. Ye and J. D. Huang, *Chem. Eur. J.*, 2015, **21**, 3310−3317.

299 X. Li, J. F. Lovell, J. Yoon and X. Chen, *Nat. Rev. Clin. Oncol.*, 2020, **17**, 657−674.

300 X. Li, B. Y. Zheng, M. R. Ke, Y. Zhang, J. D. Huang and J. Yoon, *Theranostics*, 2017, **7**, 2746−2756.

301 K. Khorsandi, R. Hosseinzadeh and M. Fateh, *RSC Adv.*, 2015, **5**, 93987−93994.

302 J. Liu, L. Sun, L. Li, R. Zhang and Z. P. Xu, *ACS Appl. Mater. Interfaces.*, 2021, **13**, 7115−7126.

303 T. Hu, Z. Wang, W. Shen, R. Liang, D. Yan and M. Wei, *Theranostics*, 2021, **11**, 3278−3300.

304 Z. Zhou, J. Song, L. Nie and X. Chen, *Chem. Soc. Rev.*, 2016, **45**, 6597−6626.

305 Y. Ruan, X. Jia, C. Wang, W. Zhen and X. Jiang, *Chem. Commun.*, 2018, **54**, 11729−11732.

306 J. Chen, C. Ning, Z. Zhou, P. Yu, Y. Zhu, G. Tan and C. Mao, *Prog. Mater. Sci.*, 2019, **99**, 1−26.

307 H. Wang, J. Chang, M. Shi, W. Pan, N. Li and B. Tang, *Angew. Chem. Int. Ed.*, 2019, **58**, 1057−1061.

308 C. Li, R. Liang, R. Tian, S. Guan, D. Yan, J. Luo, M. Wei, D. G. Evans and X. Duan, *RSC Adv.*, 2016, **6**, 16608−16614.

309 S. Guan, Y. Weng, M. Li, R. Liang, C. Sun, X. Qu and S. Zhou, *Nanoscale*, 2017, **9**, 10367−10374.

310 D. Wang, N. Ge, T. Yang, F. Peng, Y. Qiao, Q. Li and X. Liu, *Adv. Sci.*, 2018, **5**, 1700782.

311 K. Ma, Y. Li, Z. Wang, Y. Chen, X. Zhang, C. Chen, H. Yu, J. Huang, Z. Yang, X. Wang and Z. Wang, *ACS Appl. Mater. Interfaces.*, 2019, **11**, 29630−39640.

312 J. Liu, K. Liu, L. Zhang, M. Zhong, T. Hong, R. Zhang, Y. Gao, R. Li, T. Xu and Z. P. Xu, *J. Control. Release.*, 2021, **335**, 49−58.

313 W. Xie, Z. Guo, Q. Gao, D. Wang, K. Liang, Z. Gu and L. Y. Zhao, *ACS Appl. Bio Mater.*, 2020, **3**, 5845−5855.

314 Q. Tian, F. Xue, Y. Wang, Y. Cheng, L. An, S. Yang, X. Chen and G. Huang, *Nano Today*, 2021, **39**, 101162.

315 S. L. Li, P. Jiang, F. L. Jiang and Y. Liu, *Adv. Funct. Mater.*, 2021, **31**, 2100243.

316 X. Meng, X. Zhang, M. Liu, B. Cai, N. He and Z. Wang, *Appl. Mater. Today*, 2020, **21**, 100864.

317 W. Wu, Y. Pu and J. Shi, *Adv. Sci.*, 2021, **8**, 2002816.

318 B. Yang, Y. Chen and J. Shi, *Adv. Mater.*, 2019, **31**, 1901778.

319 X. Liu, Y. Jin, T. Liu, S. Yang, M. Zhou, W. Wang and H. Yu, *ACS Biomater. Sci. Eng.*, 2020, **6**, 4834−4845.

320 W. Fan, B. Yung, P. Huang and X Chen, C*hem. Rev.*, 2017, **117**, 13566−13638.

321 L.-H. Fu, C. Qi, Y.-R. Hu, J. Lin and P. Huang, *Adv. Mater.*, 2019, **31**, 1808325.

322 Q. Chu, L. Liao, B. Liu, G. Han and X. Li, *Adv. Funct. Mater.*, 2021, **31**, 2103262.

323 E. P. Komarala, S. Nigam, M. Aslam and D. Bahadur, *New J. Chem*., 2016, **40**, 423−433.

324 J. Wang, L. Sun, J. Liu, B. Sun, L. Li and Z. P. Xu, *J. Nanobiotechnol.*, 2021, **19,** 351.

325 J. Liu, Y. Wu, C. Fu, B. Li, L. Li, R. Zhang, T. Xu and Z. P. Xu, *Small*, 2020, **16**, 2002115.

326 Z. Wang, L. Fu, Y. Zhu, S. Wang, G. Shen, L. Jin and R. Liang, *J. Mater. Chem. B*, 2021, **9**, 710−718.

327 X. Mei, R. Liang, L. Peng, T. Hu and M. Wei, *J. Mater. Chem. B*, 2017, **5**, 3212−3216.

328 L.-X. Zhang, X.-M. Sun, Z. P. Xu and R.-T. Liu, *ACS Appl. Mater. Interfaces*, 2019, **11**, 35566−35576.

329 M. Ferrari, *Nat. Rev. Cancer*, 2005, **5**, 161−171.

330 H. Maeda, H. Nakamura and J. Fang, *Adv. Drug Deliver. Rev.*, 2013, **65**, 71−79.

331 W. Jiang, Y. H. Huang, Y. An and B. Y. S. Kim, *ACS Nano*, 2015, **9**, 8689−8696.

332 H. Maeda, T. Sawa and T. Konno, *J. Control. Release*, 2001, **74**, 47−61.

333 H. Maeda, G. Y. Bharate and J. Daruwalla, *Eur. J. Pharm. Biopharm.*, 2009, **71**, 409−419.

334 Y. Matsumura and H. Maeda, *Cancer Res.*, 1986, **46**, 6387−6392.

335 G. Choi, O. J. Kwon, Y. Oh, C. O. Yun and J. H. Choy, *Sci. Rep.*, 2015, **4**, 4430.

336 G. Choi, T. H. Kim, J. M. Oh and J. H. Choy, *Coord. Chem. Rev.*, 2018, **359**, 32−51.

337 X. Mei, S. Xu, T. Hu, L. Peng, R. Gao, R. Liang, M. Wei, D. Evans and X. Duan, *Nano Res.*, 2018, **11**, 195−205.

338 E. Blanco, H. Shen and M. Ferrari, *Nat. Biotechnol.*, 2015, **33**, 941−951.

339 F. M. Kievit and M. Q. Zhang, *Adv. Mater.*, 2011, **23**, H217−H247.

340 W. R. Sanhai, J. H. Sakamoto, R. Canady and M. Ferrari, *Nat. Nanotechnol.*, 2008, **3**, 242−244.

341 H. Zuo, W. Chen, H. M. Cooper and Z. P. Xu, *ACS Appl. Mater. Interfaces*, 2017, **9**, 20444−20453.

342 R. Zhu, Z. Wang, P. Liang, X. He, X. Zhuang, R. Huang, M. Wang, Q. Wang, Y. Qian and S. Wang, *Acta Biomater.*, 2017, **63**, 163−180.

343 H. Chen, W. Zhang, G. Zhu, J. Xie and X. Chen, *Nat. Rev. Mater.*, 2017, **2**, 17024.

344 J. Mu, J. Lin, P. Huang and X. Chen, *Chem. Soc. Rev.*, 2018, **47**, 5554−5573.

345 E.-K. Lim, T. Kim, S. Paik, S. Haam, Y.-M. Huh and K. Lee, *Chem. Rev.*, 2015, **115**, 327−394.

346 L. Cheng, X. Wang, F. Gong, T. Liu and Z. Liu, *Adv. Mater.*, 2020, **32**, 1902333.

347 Y. Zhu, P. Xu, X. Zhang and D. Wu, *Chem. Soc. Rev.*, 2022, **51**, 1377−1414.

348 Z. Lei, W. Zhu, X. Zhang, X. Wang and P. Wu, *Adv. Funct. Mater.*, 2021, **31**, 2008020.

349 J. Zhao, H. Wu, J. Zhao, Y. Yin, Z. Zhang, S. Wang and K. Lin, *J. Nanobiotechnol*., 2021, **19**, 36.

350 X. Ji, L. Ge, C. Liu, Z. Tang, Y. Xiao, W. Chen, Z. Lei, W. Gao, S. Blake, D. De, B. Shi, X. Zeng, N. Kong, X. Zhang and W. Tao, *Nat. Commun.*, 2021, **12**, 1124.

351 X. Mei, W. Wang, L. Yan, T. Hu, R. Liang, D. Yan, M. Wei, D. G. Evans and X. Duan, *Biomaterials*, 2018, **165**, 14−24.

352 Y. Weng, S. Guan, H. Lu, X. Meng, A. Y. Kaassis, X. Ren, X. Qu, C. Sun, Z. Xie and S. Zhou, *Talanta*, 2018, **184,** 50−57.

353 X. Zuo, C. Fan and H.-Y. Chen, *Nat. Biomed. Eng.*, 2017, **1**, 0091.

354 Y. Chen, S. Zhou, L. Li and J.-J. Zhu, *Nano Today*, 2017, **12**, 98−115.

355 E. Cesewski and B. N. Johnson, *Biosens. Bioelectron.*, 2020, **159**, 112214.

356 G. Li, C. Liu, X. Zhang, P. Luo, G. Lin and W. Jiang, *Food Chem.*, 2021, **355**, 129443.

357 M. Li, J. Zhao, H. Chu, Y. Mi, Z. Zhou, Z. Di, M. Zhao and L. Li, *Adv. Mater.*, 2019, **31**, 1804745.

358 R. Ranjan, E. N. Esimbekova and V. A. Kratasyuk, *Biosens. Bioelectron.*, 2017, **87**, 918−930.

359 W. He, Z. Zhou, Z. Han, S. Li, Z. Zhou, L. Ma and S. Zang, *Angew. Chem. Int. Ed.*, 2021, **60**, 8505−8509.

360 S. Su, Q. Sun, X. Gu, Y. Xu, J. Shen, D. Zhu, J. Chao, C. Fan and L. Wang, *Trends Anal. Chem.*, 2019, **119**, 115610.

361 H. Ju, *Appl. Mater. Today*, 2018, **10**, 51−71.

362 C. M. G. Aymard, M. Halma, A. Comte, C. Mousty, V. Prevot, L. Hecquet, F. Charmantray, L. J. Blum and B. Doumeche, *Anal. Chem.*, 2018, **90**, 9241−9248.

363 M. Halma, B. Doumeche, L. Hecquet, V. Prevot, C. Mousty and F. Charmantray, *Biosens. Bioelectron.*, 2017, **87**, 850−857.

364 Y. Tian, F. Wang, Y. Liu, F. Pang and X. Zhang, *Electrochim. Acta*, 2014, **146**, 646−653.

365 A. Aziz, M. Asif, G. Ashraf, M. Azeem, I. Majeed, M. Ajmal, J. Wang and H. Liu, *Microchim. Acta*, 2019, **186**, 61.

366 Y. Zhang, X. Chen, J. Wang and W. Yang, *Electrochem. Solid-State Lett.*, 2008, **11**, 19.

367 D. Shan, S. Cosnier and C. Mousty, *Anal. lett.*, 2003, **36**, 909−922.

368 Y. Wang, Z. Wang, Y. Rui and M. Li, *Biosens. Bioelectron.*, 2015, **64**, 57−62.

369 B. Habibi, F. F. Azhar, J. Fakkar and Z. Rezvani, *Anal. Methods*, 2017, **9**, 1956−1964.

370 Y. Sun, H. Xu, L. Wang, C. Yu, J. Zhou, Q. Chen, G. Sun and W. Huang, *J. Mater. Chem. B*, 2021, **9**, 983−991.

371 X. Ge, C. Gu, Z. Yin, X. Wang, J. Tu and J. Li, *Nano Energy*, 2016, **20**, 185−193.

372 W. Ma, R. Ma, C. Wang, J. Liang, X. Liu, K. Zhou and T. Sasaki, *ACS Nano*, 2015, **9**, 1977−1984.

373 B. Bode and T. Battelino, *Int. J. ClinPractice*, 2010, **64**, 11−15.

374 S. Wild, G. Roglic, A. Green, R. Sicree and H. King, *Diab. Care*., 2004, **27**, 1047−1053.

375 M. Sivakumar, R. Madhu, S.-M. Chen, V. Veeramani, A. Manikandan, W. H. Hung, N. Miyamoto and Y.-L. Chueh, *J. Phys. Chem. C*, 2016, **120**, 25752−25759.

376 D. L. Williams, A. R. Doig and A. Korosi, *Anal. Chem.*, 1970, **42**, 118−121.

377 Q. Xue, Z. Li, Q. Wang, W. Pan, Y. Chang and X. Duan, *Nanoscale Horiz.*, 2020, **5**, 934−943.

378 Y. Zhou, S. D. Uzun, N. J. Watkins, S. Li, W. Li, A. L. Briseno, K. R. Carter and J. J. Watkins, *ACS Appl. Mater. Interfaces*, 2019, **11**, 1821−1828.

379 J. Tang, Y. Wang, J. Li, P. Da, J. Geng and G. Zheng, *J. Mater. Chem. A*, 2014, **2**, 6153−6157.

380 S. Cosnier, C. Mousty, C. Gondran and A. Lepellec, *Mater. Sci. Eng. C*, 2006, **26**, 442−447.

381 H. Shen, Z. Zhou, W. He, H. Chao, P. Su, J. Song and Y. Yang, *ACS Appl. Mater. Interfaces*, 2021, **13**, 14995−15007.

382 L. Lin, J. Yan and J. Li, *Anal. Chem.*, 2014, **86**, 10546−10551.

383 Z. Wen, S. Ci and J. Li, *J. Phys. Chem. C*, 2009, **113**, 13482−13487.

384 K. Tian, M. Prestgard and A. Tiwari, *Mater. Sci. Eng. C*, 2014, **41**, 100−118.

385 D. Luo, L. Wu and J. Zhi, *ACS Nano*, 2009, **3**, 2121−2128.

386 Z. Shami, S. M. Amininasab and P. Shakeri, *ACS Appl. Mater. Interfaces*, 2016, **8**, 28964−28973.

387 N. Shishegari, A. Sabahi, F. Manteghi, A. Ghaffarinejad and Z. Tehrani, *J. Electroanal. Chem.*, 2020, **871**, 114285.

388 S. Fu, G. Fan, L. Yang and F. Li, *Electrochim. Acta*, 2015, **152**, 146−154.

389 D. Chu, F. Li, X. Song, H. Ma, L. Tan, H. Pang, X. Wang, D. Guo and B. Xiao, *J. Colloid Interface Sci*., 2020, **568,** 130−138.

390 J. Cui, Z. Li, K. Liu, J. Li and M. Shao, *Nanoscale Adv.*, 2019, **1**, 948−952.

391 X. Zan, H. Bai, C. Wang, F. Zhao and Duan H. *Chem. Eur. J*., 2016, **22**, 5204−5210.

392 H. Abdolmohammad-Zadeh and M. Zamani-Kalajahi, *Microchem. J*., 2020, **155**, 104704.

393 C.-G. Qian, S. Zhu, P.-J. Feng, Y.-L. Chen, J.-C. Yu, X. Tang, Y. Liu and Q.-D. Shen, *ACS Appl. Mater. Interfaces*, 2015, **7**, 18581−18589.

394 Z. Zhu, L. Qu, Y. Guo, Y. Zeng, W. Sun and X. Huang, *Sens. Actuators B Chem.*, 2010, **151**, 146−152.

395 M. Annalakshmi, S. Kumaravel, S. Chen and T. Chen, *J. Mater. Chem. B*, 2020, **8**, 8249−8260.

396 M. Li, J. Zhu, L. Zhang, X. Chen, H. Zhang, F. Zhang, S. Xu and D. G. Evans, *Nanoscale*, 2011, **3**, 4240−4246.

397 M. Asif, A. Aziz, H. Wang, Z. Wang, W. Wang, M. Ajmal, F. Xiao, X. Chen and H. Liu, *Microchim. Acta*, 2019, **186**, 61.

398 F. Vajedi and H. Dehghani, *Talanta*, 2020, **208**, 120444.

399 D. Shan, Y. Wang, M. Zhu, H. Xue, S. Cosnier and C. Wang, *Biosens. Bioelectron.*, 2009, **24**, 1171−1176.

400 X. Wang, X. Chen, D. G. Evans and W. Yang, *Sens. Actuators B Chem.*, 2011, **160**, 1444−1449.

401 B. Rezaei, H. Khosropour, A. A. Ensafi, M. Dinari and A. Nabiyan, *RSC Adv.*, 2015, **5**, 75756−75765.

402 A. T. E. Vilian, K. S. Ranjith, S. J. Lee, R. Umapathi, S. K. Hwang, C. W. Oh, Y. S. Huh and Y. K. Han, *Electrochim. Acta*, 2020, **354**, 136723.

403 Y. Zhang, Z. Zhang, Z. Wang, H. Pan, Y. Lin and D. Chang, *Biosens. Bioelectron.*, 2021, **190**, 113437.

404 M. M. Khalil, W. M. A. Rouby and M. A. Korany, *Mater. Sci. Eng. C*, 2019, **100**, 186−195.

405 S. Li, S. Dong, W. Xu, S. Tu, L. Yan, C. Zhao, J. Ding and X. Chen, *Adv. Sci.*, 2018, **5**, 1700527.

406 A. Zipperer, M. C. Konnerth, C. Laux, A. Berscheid, D. Janek, C. Weidenmaier, M. Burian, N. A. Schilling, C. Slavetinsky, M. Marschal, M. Willmann, H. Kalbacher, B. Schittek, H. Brotz-Oesterhelt, S. Grond, A. Peschel and B. Krismer, *Nature*, 2016, **535**, 511−516.

407 K. E. Boehle, J. Gilliand, C. R. Wheeldon, A. Holder, J. A. Adkins, B. J. Geiss, E. P. Ryan and C. S. Henry, *Angew. Chem. Int. Ed.*, 2017, **129**, 6990−6994.

408 H. Chen, X. He, Z. Zhou, Z. Wu, H. Li, X. Peng, Y. Zhou, C. Tan and J. Shen, *J. Nanobiotechnol.*, 2022, **20**, 136.

409 M. Li, L. Li and S. Lin, *Chin. Chem. Lett.*, 2020, **31**, 1511−1515.

410 W. Zhang, Y. Zhao, W. Wang, J. Peng, Y. Li, Y. Shangguan, G. Ouyang, M. Xu, S. Wang, J. Wei, H. Wei, W. Li and Z. Yang, *Adv. Healthcare Mater.*, 2020, **9**, 2000092.

411 Y. Zhao, P. Chen, B. Zhang, D. S. Su, S. Zhang, L. Tian, J. Lu, Z. Li, X. Cao, B. Wang, M. Wei, D. G. Evans and X. Duan, *Chem. Eur. J.*, 2012, **18**, 11949−11958.

412 M. Lobo-Sanchez, G. Najera-Melendez, G. Luna, V. Segura-Perez, J. A. Rivera and G. Fetter, *Appl. Clay Sci.*, 2018, **153**, 61−69.

413 D. S. Karaman, U. K. Ercan, E. Bakay, N. Topaloglu and J. M. Rosenholm, *Adv. Funct. Mater.*, 2020, **30**, 1908783.

414 S. A. A. Moaty, A. A. Farghali and R. Khaled, *Mater. Sci. Eng. C*, 2016, **68**, 184−193.

415 Y. Zhao, C. J. Wang, W. Gao, B. Li, Q. Wang, L. Zheng, M. Wei, D. G. Evans, X. Duan and D. O'Hare, *J. Mater. Chem. B*, 2013, **1**, 5988−5994.

416 M. Li, Z. P. Xu, Y. Sultanbawa, W. Chen, J. Liu and G. Qian, *Colloids Surf. B Biointerfaces*, 2019, **181**, 585−592.

417 Y. Hao, B. Liu, L. Tian, F. Li, J. Ren, S. Liu, Y. Liu, J. Zhao and X. Wang, *ACS Appl. Mater. Interfaces*, 2017, **9**, 12687−12693.

418 W. Li, B. Li, M. Meng, Y. Cui, Y. Wu, Y. Zhang, H. Dong and Y. Feng, *Appl. Surf. Sci.*, 2019, **487**, 1008−1017.

419 C. Chen, Y. Wang, D. Zhang and J. Wang, *J. Ind. Eng. Chem.*, 2022, **105**, 291−302.

420 J. Sun, H. Fan, N. Wang and S. Ai, *J. Nanopart. Res.*, 2014, **16**, 2597.

421 G. Mishra, B. Dash and S. Pandey, *Appl. Clay. Sci.*, 2019, **181**, 105230.

422 X. Liu, T. Hu, G. Lin, X. Wang, Y. Zhu, R. Liang, W. Duan and M. Wei, *RSC Adv.*, 2020, **10**, 9786−9790.

423 H. Cheng, X. Gao, K. Zhang, X. Wang, W. Zhou, S. Li, X. Cao and D. Yan, *New J. Chem.*, 2019, **43**, 19408−19414.

424 L. Tang, H. Cheng, S. Cui, X. Wang, L. Song, W. Zhou and S. Li, *Colloids Surf. B Biointerfaces*, 2018, **165**, 111−117.

425 D. Wang, F. Peng, J. Li, Y. Qiao, Q. Li and X. Liu, *Mater. Today*, 2017, **20**, 238−257.

426 S. Du, N. Zhou, G. Xie, Y. Chen, H. Suo, J. Xu, J. Tao, L. Zhang and J. Zhu, *Nano Energy*, 2021, **85**, 106004.

427 G. Mishra, B. Dash, S. Pandey and P. P. Mohanty, *J. Environ. Chem. Eng.*, 2013, **1**, 1124−1130.

428 J. Sun, J. Li, H. Fan and S. Ai, *J. Mater. Chem. B*, 2013, **1**, 5436−5442.

429 F. Xiao, X. Liu, Y. Xiao, F. Chen and Y. Wu, *New J. Chem.*, 2017, **41**, 7260−7266.

430 R. Langer and J. P. Vacanti, *Science*, 1993, **260**, 920−926.

431 H. Ramaraju, R. E. Akman, D. L. Safranski and S. J. Hollister, *Adv. Funct. Mater.*, 2020, **30**, 2002014.

432 J. Zhang, H. Chen, M. Zhao, G. Liu and J. Wu, *Nano Res.*, 2020, **13**, 2019−2034.

433 Y. Li, B.-F. Liu and X. Zhang, *Mater. Today*, 2021, **51**, 273−293.

434 J. Ouyang, Q. Bu, N. Tao, M. Chen, H. Liu, J. Zhou, J. Liu, B. Deng, N. Kong, X. Zhang, T. Chen, Y. Cao and W. Tao, *Bioact. Mater.*, 2022, **18**, 446−458.

435 J. Zhou, Z. Zhang, J. Joseph, X. Zhang, B. E. Ferdows, D. N. Patel, W. Chen, G. Banfi, R. Molinaro, D. Cosco, N. Kong, N. Joshi, O. C. Farokhzad, C. Corbo and W. Tao, *Exploration*, 2021, **1**, 20210011.

436 X. Zhang, L. Li, J. Ouyang, L. Zhang, J. Xue, H. Zhang and W. Tao, *Nano Today*, 2021, **39**, 101196.

437 X. Zhang, S. Ko, J. H. Kim, X. Huang, N. Kong, L. Zhang, J. Zhou, J. Xue, M. B. Harris, W. Tao and J. S. Kim, *Matter*, 2021, **4**, 2727−2764.

438 L. Li, X. Zhang, J. Zhou, L. Zhang, J. Xue and W. Tao, *Small*, 2022, **18**, 2107705.

439 S. Torgbo and P. Sukyai, *Appl. Mater. Today*, 2018, **11**, 34−49.

440 Z. Zhang, J. Zhou, C. Liu, J. Zhang, Y. Shibata, N. Kong, C. Corbo, M. B. Harris and Wei Tao, *Trends Chem.*, 2022, **4**, 420−436.

441 D. B. Raina, L.-M. Matuszewski, C. Vater, J. Bolte, H. Isaksson, L. Lidgren, M. Tägil and S. Zwingenberger, *Sci. Adv.*, 2020, **6**, 1779.

442 X. Zhang, Z. Li, P. Yang, G. Duan, X. Liu, Z. Gu and Y. Li, *Mater. Horiz.*, 2021, **8**, 145−167.

443 K. Y. Morgan, D. Sklaviadis, Z. L. Tochka, K. M. Fischer, K. Hearon, T. D. Morgan, R. Langer and L. E. Freed, *Adv. Funct. Mater.*, 2016, **26**, 5873−5883.

444 F. Mammoli, S. Castiglioni, S. Parenti, C. Cappadone, G. Farruggia, S. Iotti, P. Davalli, J. Maier, A. Grande and C. Frassineti, *Int. J. Mol. Sci.*, 2019, **20**, 385.

445 H. R. Kang, C. J. C. Fernandes, R. A. Silva, V. R. L. Constantino, I. H. J. Koh and W. F. Zambuzzi, *Adv. Healthcare Mater.*, 2017, **7**, 1700693.

446 Q. Li, D. Wang, J. Qiu, F. Peng and X. Liu, *Biomater. Sci.*, 2018, **6**, 1227−1237.

447 D. Zhang, S. Cheng, J. Tan, J. Xie, Y. Zhang, S. Chen, H. Du, S. Qian, Y. Qiao, F. Peng and X. Liu, *Bioact. Mater.*, 2022, **17**, 394−405.

448 M. Chu, Z. Sun, Z. Fan, D. Yu, Y. Mao and Y. Guo, *Theranostics*, 2021, **11**, 6717−6734.

449 G. L. Koons, M. Diba and A. G. Mikos, *Nat. Rev. Mater.*, 2020, **5**, 584−603.

450 L. Yang, X. He, G. Jing, H. Wang, J. Niu, Y. Qian and S. Wang, *ACS Appl. Mater. Interfaces*, 2021, **13**, 48386−48402.

451 M. H. Kim, W. Hur, G. Choi, H. S. Min, T. H. Choi, Y. B. Choy and J.-H. Choy, *Adv. Healthcare Mater.*, 2016, **5**, 2765.

452 M. Cámara-Torres, S. Duarte, R. Sinha, A. Egizabal, N. Álvarez, M. Bastianini, M. Sisani, P. Scopece, M. Scatto, A. Bonetto, A. Marcomini, A. Sanchez, A. Patelli, C. Mota and L. Moroni, *Bioact. Mater.*, 2021, **6**, 1073.

453 H. Kang, M. Kim, Q. Feng, S. Lin, K. Wei, R. Li, C. J. Choi, T. Kim, G. Li, J. Oh and L. Bian, *Biomaterials*, 2017, **149**, 12−28.

454 Y. Wang, X. Mei, Y. Bian, T. Hu, X. Weng, R. Liang and M. Wei, *Nanoscale*, 2020, **12**, 19075−19082.

455 H. Piao, M. H. Kim, M. Cui, G. Choi and J. Choy, *J. Korean Med. Sci.*, 2019, **34**, e37.

456 H. Fu, L. Wang, Q. Bao, D. Ni, P. Hu and J. Shi, *J. Am. Chem. Soc.*, 2022, **144**, 8987–8999.

457 M. P. Bernardo, B. C. S. Rodrigues, T. D. Oliveira, A. P. M. Guedes, A. A. Batista and L. H. C. Mattoso, *Clays Clay Miner.*, 2020, **68**, 623−631.

458 R. Zhu, X. Zhu, Y. Zhu, Z. Wang, X. He, Z. Wu, L. Xue, W. Fan, R. Huang, Z. Xu, X. Qi, W. Xu, Y. Yu, Y. Ren, C. Li, Q. Cheng, L. Ling, S. Wang and L. Cheng, *ACS Nano*, 2021, **15**, 2812−2830.

459 L. Wang, B. Zhang, X. Yang, S. Guo, G. I. N. Waterhouse, G. Song, S. Guan, A. Liu, L. Cheng and S. Zhou, *Bioact. Mater.*, 2022, **20**, 126−136.

460 M. Moghanizadeh-Ashkezari, P. Shokrollahi, M. Zandi, F. Shokrolahi, M. J. Daliri, M. R. Kanavi and S. Balagholi, *ACS Appl. Mater. Interfaces*, 2019, **11**, 35525−35539.

461 M. P. Bernardo and C. Ribeiro, *J. Mater. Res. Tech.*, 2019, **8**, 1250−1257.

462 D. R. Munhoz, M. P. Bernardo, J. O. D. Malafatti, F. K. V. Moreira and L. H. C. Mattoso, *Int. J. Biol. Macromol.*, 2019, **141**, 504−510.

463 S. Cheng, D. Zhang, M. Li, X. Liu, Y. Zhang, S. Qian and F. Peng, *Bioact. Mater.*, 2021, **6**, 91−105.

464 S. Mallakpour and M. Hatami, *Mater. Chem. Phys.*, 2020, **250**, 123044.

465 M. P. Figueiredo, G. Layrac, A. Hébraud, L. Limousy, J. Brendle, G. Schlatter and V. R. L. Constantino, *Eur. Polym. J.*, 2020, **131**, 109675.

466 T. baradaran, S. S. Shafiei, S. Mohammadi and F. Moztarzadeh, *Mater. Today Commun.*, 2020, **23**, 100913.

467 J. Tan, D. Wang, H. Cao, Y. Qiao, H. Zhu and X. Liu, *ACS Appl. Mater. Interfaces*, 2018, **10**, 42018−42029.

468 F. Fayyazbakhsh, M. Solati-Hashjin, A. Keshtkar, M. A. Shokrgozar, M. M. Dehghan and B. Larijani, *Mater. Sci. Eng. C*, 2017, **76**, 701−714.

469 D. Cao, Z. Xu, Y. Chen, Q. Ke, C. Zhang and Y. Guo, *J. Biomed. Mater. Res. Part B Appl. Biomater.*, 2018, **106**, 863−873.

470 L. S. Costard, D. C. Kelly, R. N. Power, C. Hobbs, S. Jaskaniec, V. Nicolosi, B. L. Cavanagh, C. M. Curtin and F. J. O'Brien, *Pharmaceutics*, 2020, **12**, 1219.

471 Y. Wang, L. Zhou, L. Fang and F. Cao, *Acta Biomater.*, 2020, **104**, 104−114.

472 X. Yu, T. Wen, P. Cao, L. Shan and L. Li, *J. Colloid Interface Sci.*, 2019, **556**, 258−265.

473 X. Li, P. Gong, Y. Li, J. Yu, F. Wang, X. Li, Z. Fan and Z. Wang, *Mater. Lett.*, 2019, **243**, 1−4.

474 M. P. Figueiredo, A. Borrego-Sánchez, F. García-Villén, D. Miele, S. Rossi, G. Sandri, C. Viseras and V. R. L. Constantino, *Pharmaceutics*, 2020, **12**, 1130.

475 P. J. Shiny, M. V. Devi, S. J. G. Felciya, G. Ramanathan, P. Fardim and U. T. Sivagnanam, *Int. J. Biol. Macromol.*, 2021, **168**, 46−58.

476 P. Liu, M. Li, H. Yu, H. Fang, J. Yin, D. Zhu, Q. Yang, Q. Ke, Y. Huang, Y. Guo, Y. Gao and C. Zhang, *Chem. Eng. J.*, 2021, **418**, 129531.

477 A. Koch, Impact of Excipients on Pharmacokinetics of OXPzero(TM) Ibuprofen, https://clinicaltrials.gov/ct2/show/NCT02974361, (accessed May 2017).

478 N. A. Jose, H. C. Zeng and A. A. Lapkin, *Nat. Commun.*, 2018, **9**, 4913.

479 H. Maslah, C. Skarbek, C. Gourson, M.-A. Plamont, S. Pethe, L. Jullien, T. L. Saux and R. Labruère, *Angew. Chem. Int. Ed.*, 2021, **60**, 24043−24047.

480 J. Jin, X. Han, Y. Fang, Z. Zhang, Y. Li, T. Zhang, A. Han and J. Liu, *Adv. Funct. Mater.*, 2022, **32**, 2109218.

481 H. Sun, C. Tung, Y. Qiu, W. Zhang, Q. Wang, Z. Li, J. Tang, H. Chen, C. Wang and H. M. Chen, *J. Am. Chem. Soc.*, 2022, **144**, 1174−1186.

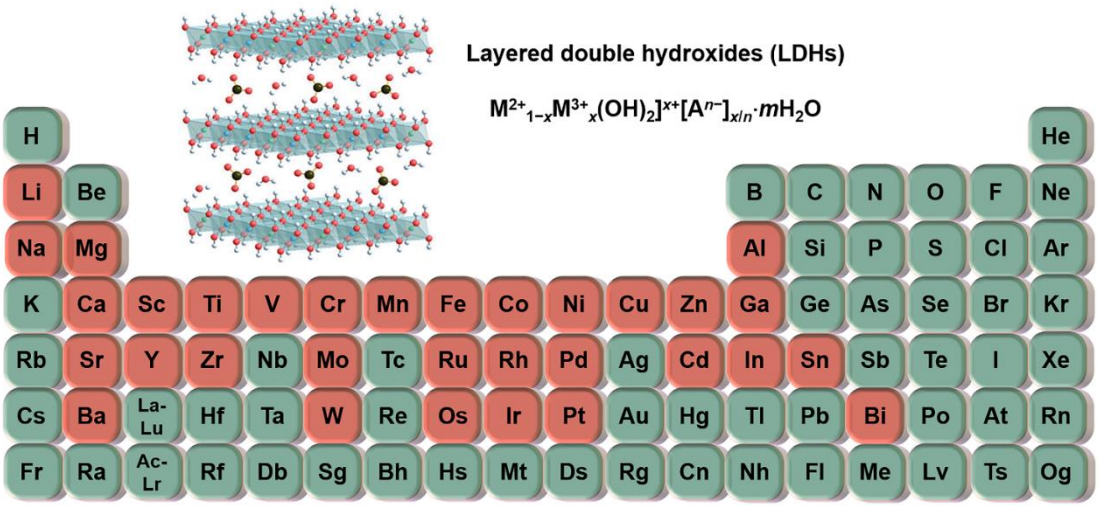

Fig. 1 Schematic diagram of LDHs structure (top) and the periodic table (bottom). Metal elements that have been reported to enter or anchor on the LDH layers are highlighted in red.

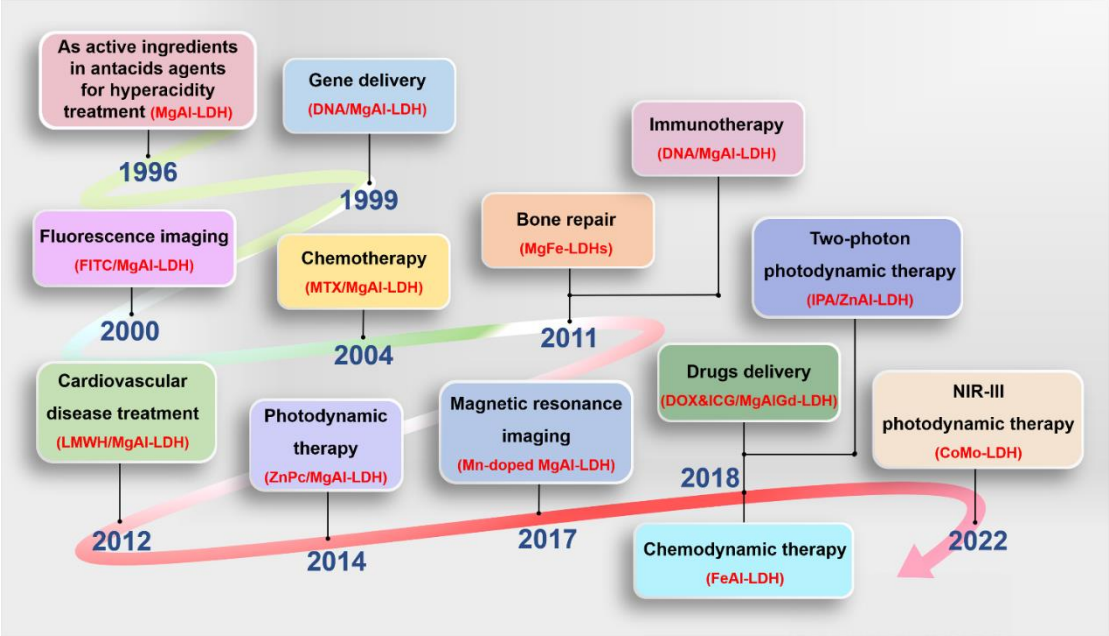

Fig. 2 Diagrammatic representation of LDHs in various biomedical applications in chronological order.

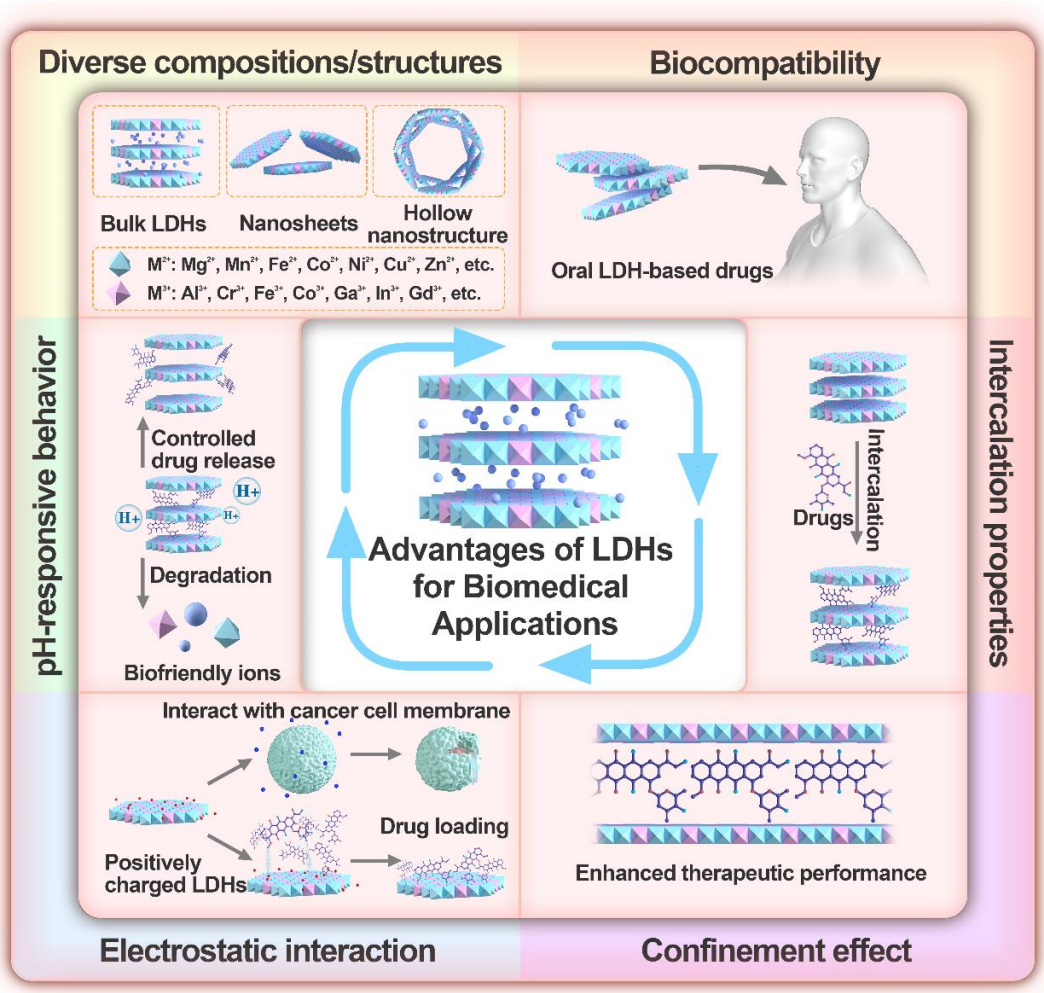

Fig. 3 Schematic demonstration of the properties and advantages of LDH-based nanomaterials for biomedical applications.

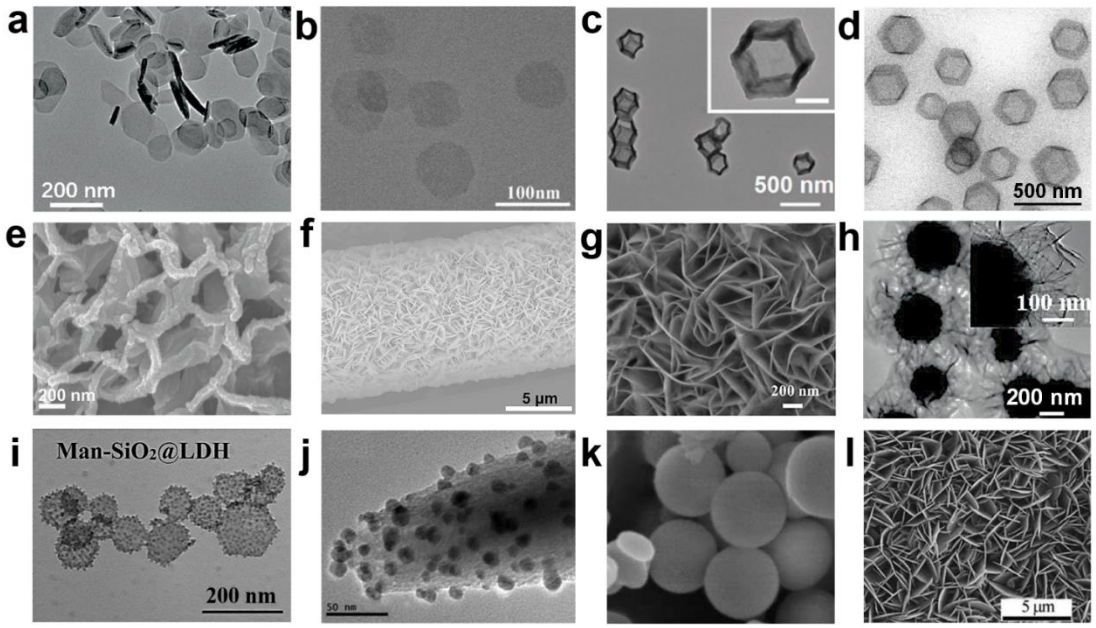

Fig. 4 Different structures of LDHs and their nanocomposites prepared by various synthetic methods. (a) TEM image of bulk CoMn-LDHs synthesize by separate nucleation and aging steps. Reproduced with permission from ref. 78. Copyright 2017, Royal Society of Chemistry. (b) TEM image of Gd^{3+}-doped monolayered MgAl-LDH nanosheets acquired through a bottom-up method. Reproduced with permission from ref. 47. Copyright 2018, Wiley-VCH. (c) TEM image of hollow-structured NiFe-LDH obtained by template etching. Reproduced with permission from ref. 108. Copyright 2021, Royal Society of Chemistry. (d) TEM image of hollow-structured ZnCo-LDHs obtained by template etching. Reproduced with permission from ref. 109. Copyright 2021, American Chemical Society. (e) SEM image of CuO/CoNi-LDHs prepared by *in-situ* electrodeposition. Reproduced with permission from ref. 124. Copyright 2021, Elsevier. (f) SEM image of NiCo-LDH nanosheets array on carbon cloth prepared by co-precipitation approach. Reproduced with permission from ref. 129. Copyright 2017, Elsevier. (g) High-magnification SEM images of NiFe-LDH/NF acquired by *in-situ* hydrothermal synthesis. Reproduced with permission from ref. 130. Copyright 2017, Wiley-VCH. (h) TEM image of Fe_3O_4@SiO_2@NiAl-LDH microspheres acquired by template-oriented assembly. Reproduced with permission from ref. 58. Copyright 2012, American Chemical Society. (i) TEM image of Man-SiO_2@LDH synthesized by hydrothermal treatment. Reproduced with permission from ref. 143. Copyright 2018,

Elsevier. (j) SEM image of Ag-coated MgAl-LDH obtained by surface deposition. Reproduced with permission from ref. 150. Copyright 2012, Wiley-VCH. (k) SEM image of LDH@MS prepared by the surfactant-assistant sol-gel coating method. Reproduced with permission from ref. 152. Copyright 2019, Springer International Publishing. l) SEM image of MgAl-MMO films on Al substrate acquired by topological transformation. Reproduced with permission from ref. 60. Copyright 2015, Elsevier.

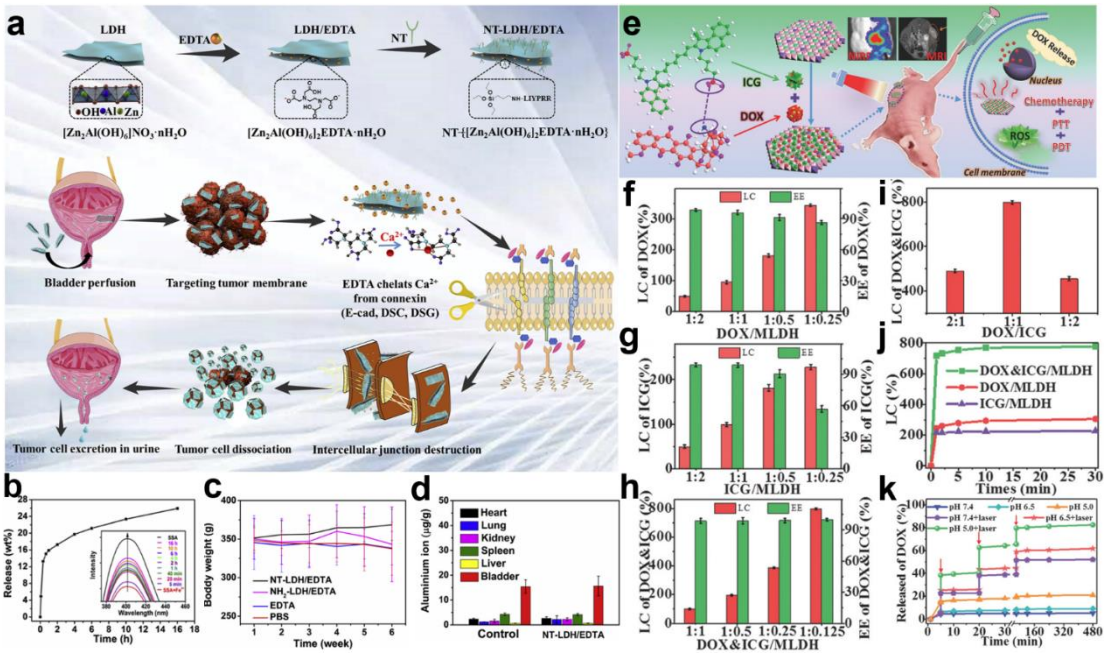

Fig. 5 LDH-based nanomaterials for controlled release of drugs. (a) Schematic diagram of the synthesis of NT-LDH/EDTA nanosheets and its therapeutic mechanism. (b) EDTA release from NT-LDH/EDTA in PBS (pH 6.5) within 16 h and corresponding fluorescence spectrograms. (c) Body weight curves of bladder carcinoma-bearing mice after different treatments. (d) Bio-distributions of NT-LDH/EDTA in bladder and main organs of mice with different treatments. Reproduced with permission from ref. 179. Copyright 2020, Elsevier. (e) Schematic representation of DOX&ICG/MLDH nanosheets for drug delivery. Loading content and encapsulation efficiency of: (f) DOX, (g) ICG, and (h) DOX&ICG onto MLDH nanosheets with different mass ratios. (i) Loading content of DOX&ICG onto MLDH nanosheets with different mass ratios of DOX:ICG. (j) Adsorption curves of ICG, DOX, and DOX&ICG onto MLDH nanosheets. (k) Release profile of DOX from DOX&ICG/MLDH in PBS (pH 7.4, 6.5, and 5.0) with or without laser irradiation; the arrows indicate the time points of laser irradiation. Reproduced with permission from ref. 47. Copyright 2018, Wiley-VCH.

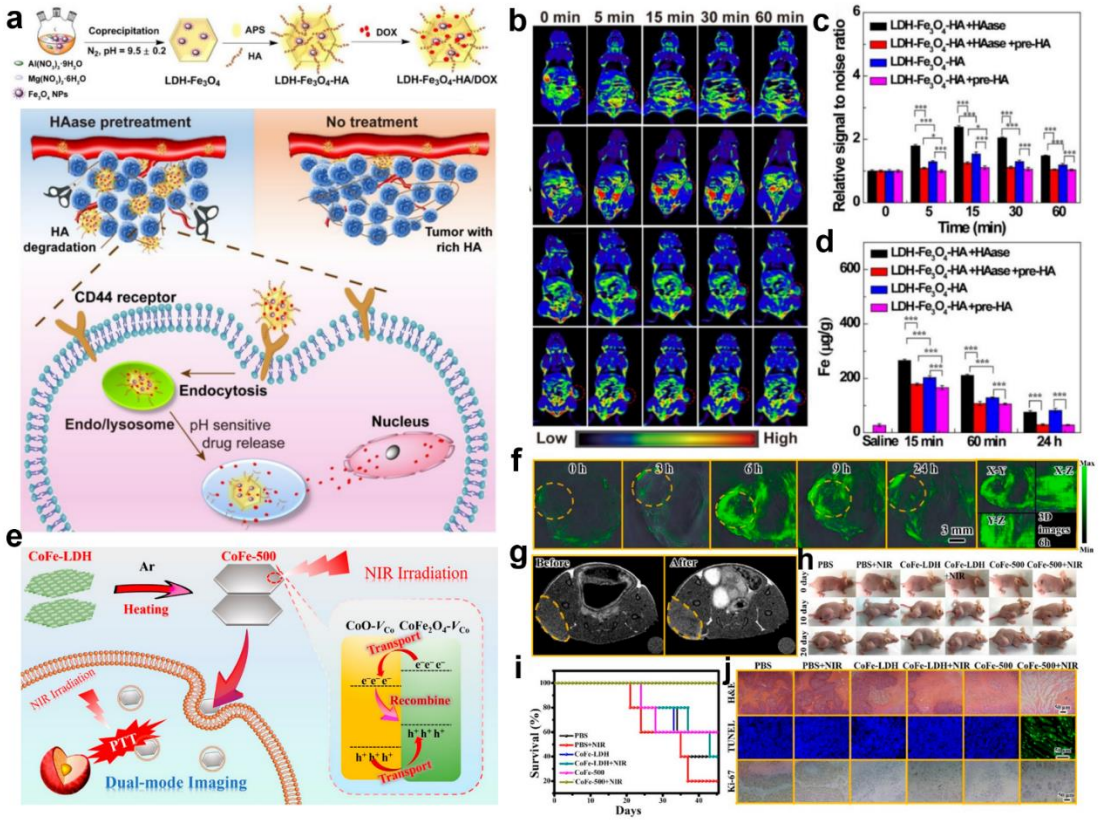

Fig. 6 LDH-based nanomaterials for tumor imaging. (a) Schematic illustration of synthetic procedure of LDH-Fe_3O_4-HA/DOX nanoplatforms, along with its theranostic mechanism. (b) Tumor T_1-weighted MR images, and (c) the corresponding MR signal intensity. (d) The Fe content in tumors at different post-injection time points after various treatments. Reproduced with permission from ref. 216. Copyright 2020, Ivyspring International Publisher. (e) Schematic diagram of the preparation of CoFe-500, along with CoFe-500-driven PA/MR/NIR imaging-guided PTT. (f) *In vivo* PA images at different post-injection time points and tumor 3D images at 6 h post-injection. (g) *In vivo* T_1-weighted MR imaging of mice injected with and without CoFe-500. (h) Mice photographs at different post-injection time points after various treatments. (i) Survival of mice after various treatments as indicated. (j) Immunostaining images of tumor sections for the different sets. Reproduced with permission from ref. 77. Copyright 2020, American Chemical Society.

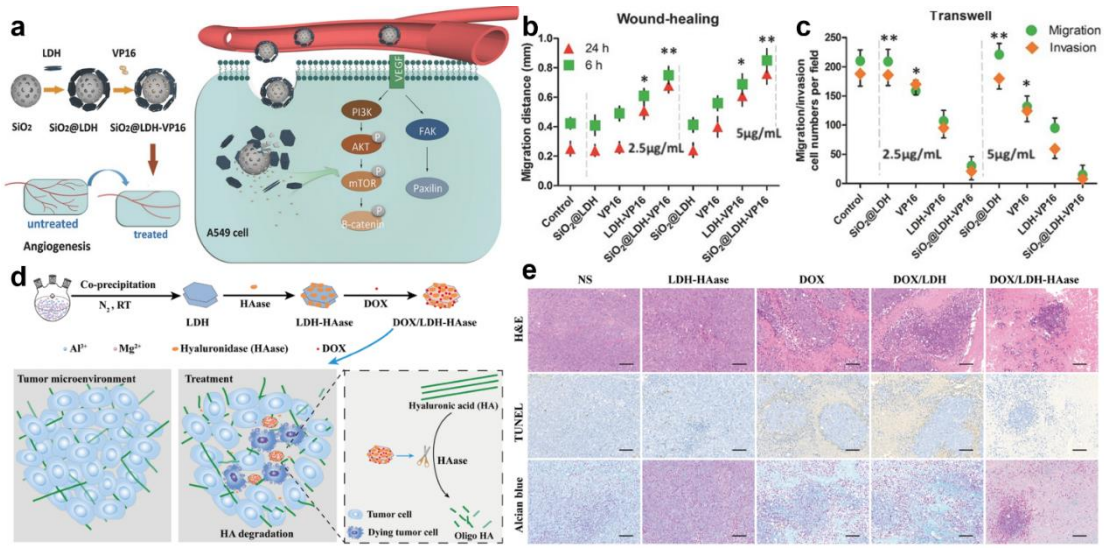

Fig. 7 LDH-based nanomaterials for chemotherapy. (a) Schematic diagram of the synthesis of SiO_2@LDH-VP16 and its chemotherapeutic mechanism. (b) Distance migrated by A549 cells at different time points after various treatments. (c) Number of migrating and invading A549 cells after various treatments. Reproduced with permission from ref. 245. Copyright 2016, Wiley-VCH. (d) Preparation of DOX/LDH-HAase for chemotherapy. (e) Histological staining of tumor sections after different treatments (scale bar: 100 μm). Reproduced with permission from ref. 249. Copyright 2021, Springer International Publishing.

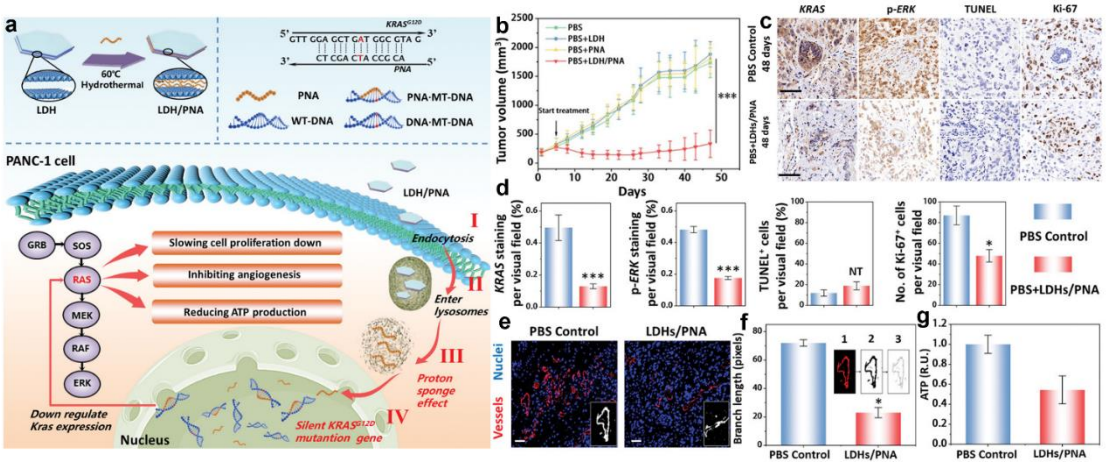

Fig. 8 LDH-based nanomaterials for gene therapy. (a) Schematic diagram of the preparation of LDHs/PNA and the mechanism of cancer cell proliferation suppression. (b) Tumor growth curves of mice from different groups. (c) Immunolabeling of tumor sections at the 48th day (scale bar: 100 μm), and (d) corresponding quantitative analysis data. (e) CD31 staining of the vessels in tumor sections after different treatments, and (f) corresponding quantification of branch lengths. (g) Adenosine triphosphate (ATP) relative levels of tumor tissues. Reproduced with permission from ref. 262. Copyright 2020, Wiley-VCH.

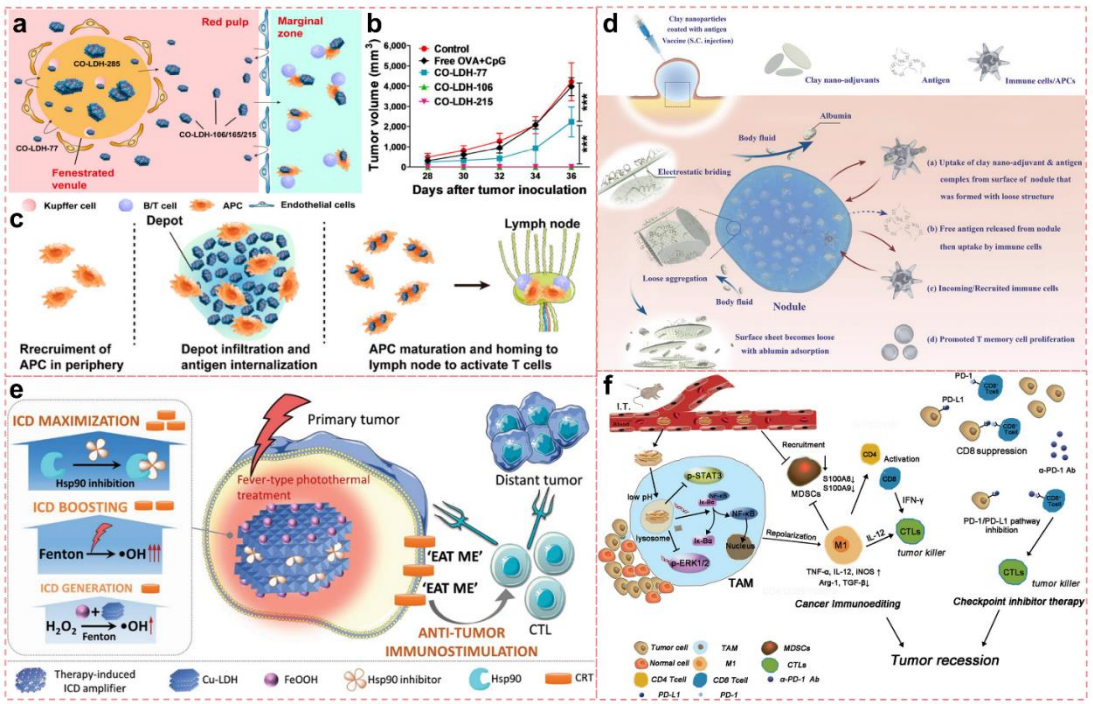

Fig. 9 LDH-based nanomaterials for immunotherapy. (a) Schematic representation of the spleen enrichment capacity of CO-LDH nanovaccines. (b) The average tumor volume of mice after various treatments. (c) Antigen delivery process of CO-LDH-215 *via* subcutaneous vaccination route. Reproduced with permission from ref. 278. Copyright 2021, Springer International Publishing. (d) Schematic diagram of the immune behavior of IB-loaded MgAl-LDH with loose structure. Reproduced with permission from ref. 274. Copyright 2018, Wiley-VCH. (e) Schematic diagram of the therapeutic mechanism of FeOOH@STA/Cu-LDH nanohybrid. Reproduced with permission from ref. 284. Copyright 2020, Wiley-VCH. (f) Schematic diagram of enhanced immunotherapy by remodeling the immunoenvironment through LDH@155. Reproduced with permission from ref. 285. Copyright 2019, Wiley-VCH.

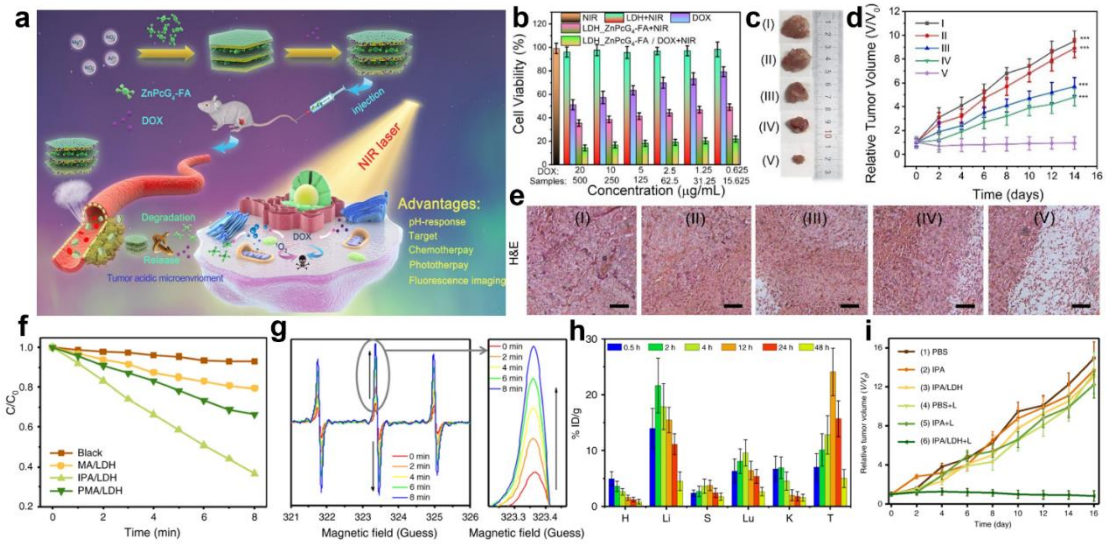

Fig. 10 LDH-based nanomaterials for photodynamic therapy. (a) Schematic illustration of the synthesis and antitumor performance of $ZnPcG_4$-FA/LDHs with upon 650 nm irradiation. (b) The cytotoxicity of HeLa cells after different treatments. (c) The excised tumors and (d) corresponding tumor-growth curves of mice after 14 days treatment from different groups. (e) Histological staining of tumor sections from mice after various treatments on the 14th day (scale bar: 100 μm). Reproduced with permission from ref. 175. Copyright 2020, Elsevier. (f) Normalized absorbance of 1,3-diphenylisobenzofuran (DPBF) after various treatments. (g) Time-dependent electron spin resonance (ESR) spectra of IPA/LDH for $^1O_2$ detection in the presence of 2,2,6,6-tetramethylpiperidine (TEMP). (h) Quantitative biodistribution analysis of IPA/LDH in mice at different time points post-injection. (i) Tumor growth curves of mice after various treatments. Reproduced with permission from ref. 46. Copyright 2018, Nature Publishing Group.

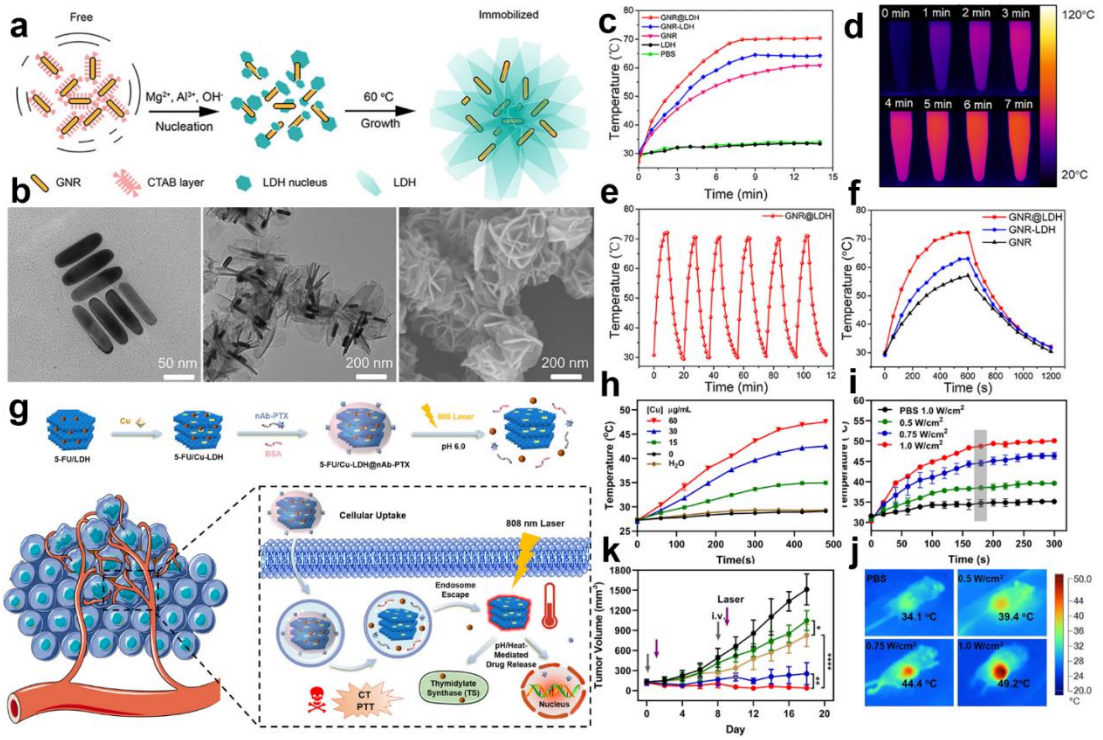

Fig. 11 LDH-based nanomaterials for photothermal therapy. (a) Synthesis scheme of GNR@LDH. (b) TEM images of GNRs (left) and GNR@LDH (middle) as well as SEM image of GNR@LDH (right). (c) Temperature elevation of different samples under 808 nm irradiation. (d) Infrared thermal images of GNR@LDH under 808 nm irradiation. (e) Photothermal stability of GNR@LDH. (f) Temperature profiles of different samples under 808 nm irradiation over 600 s, followed by natural cooling. Reproduced with permission from ref. 311. Copyright 2019, American Chemical Society. (g) Schematic illustration of Cu-LDH based nanomedicine formation process and its proposed mechanism in cancer treatment. (h) Temperature profiles of Cu-LDH with various concentrations under 808 nm irradiation for 8 min. (i) Temperature profiles of mice tumor after different treatments under 808 nm irradiation, and (j) corresponding infrared thermal images. (k) Tumor volume change of different groups of mice after various treatments. Reproduced with permission from ref. 312. Copyright 2021, Elsevier.

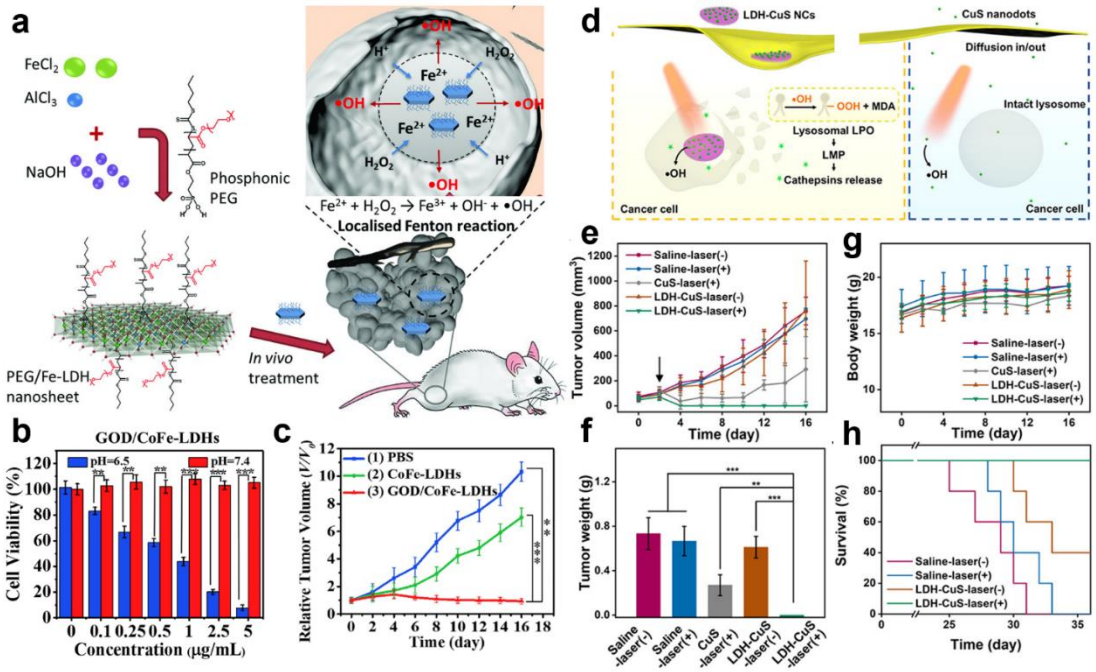

Fig. 12 LDH-based nanomaterials for chemodynamic therapy. (a) Schematic illustration of the therapeutic mechanism of PEG/Fe-LDH nanosheets. Reproduced with permission from ref. 48. Copyright 2018, Wiley-VCH. (b) Cell viability of Hela cells incubated with GOD/CoFe-LDHs at pH = 7.4 and 6.5. (c) Tumor growth tendency of mice after different treatments. Reproduced with permission from ref. 49. Copyright 2020, Elsevier. (d) Schematic illustration for the cellular internalization of CuS nanodots and LDH-CuS NCs. (e) Tumor volume, (f) tumor weight, (g) body weight, and (h) survival of mice after various treatments. Reproduced with permission from ref. 215. Copyright 2020, American Chemical Society.

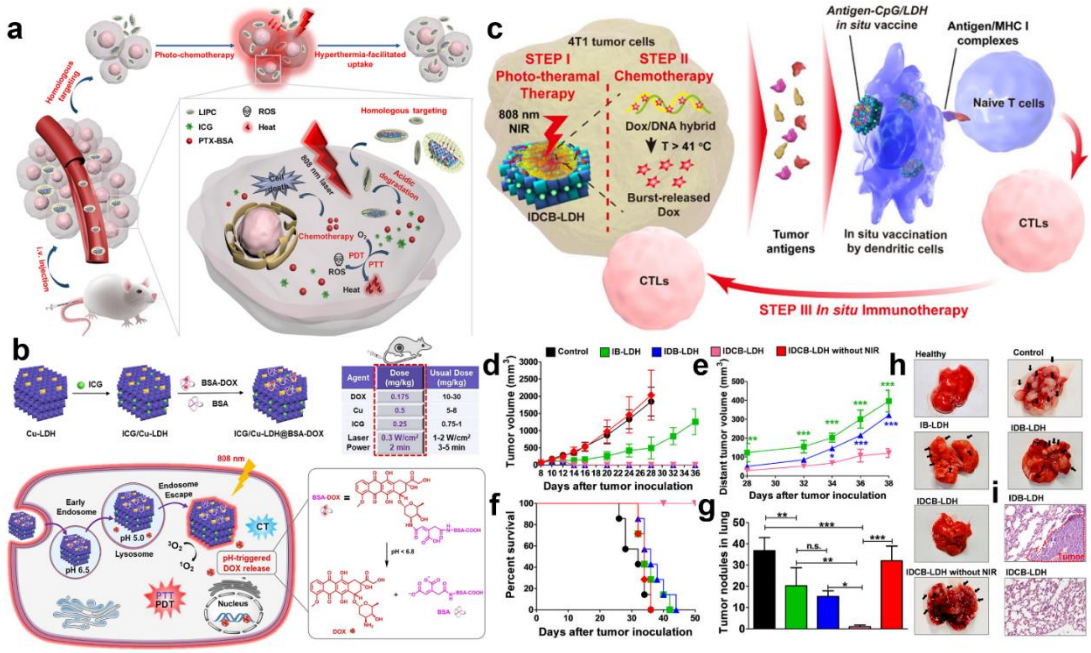

Fig. 13 LDH-based nanomaterials for combination therapy. (a) Schematic representation of CCM-cloaked LDH nanosheets for photo-chemotherapy. Reproduced with permission from ref. 324. Copyright 2021, Springer International Publishing. (b) Schematic illustration of the structure and performance concept of multifunctional ICG/Cu-LDH@BSA-DOX. Reproduced with permission from ref. 302. Copyright 2021, American Chemical Society. (c) Schematic representation of synergistic Chemo/PTT/immunotherapy. Volume change of the (d) primary and (e) distant tumors after different treatments. (f) Survival of mice from different groups. (g) Average tumor nodules in the lung of mice after different treatments. (h) Dissected lungs of mice from different groups. (i) Histological staining of lung sections of mice from different groups. Reproduced with permission from ref. 328. Copyright 2019, American Chemical Society.

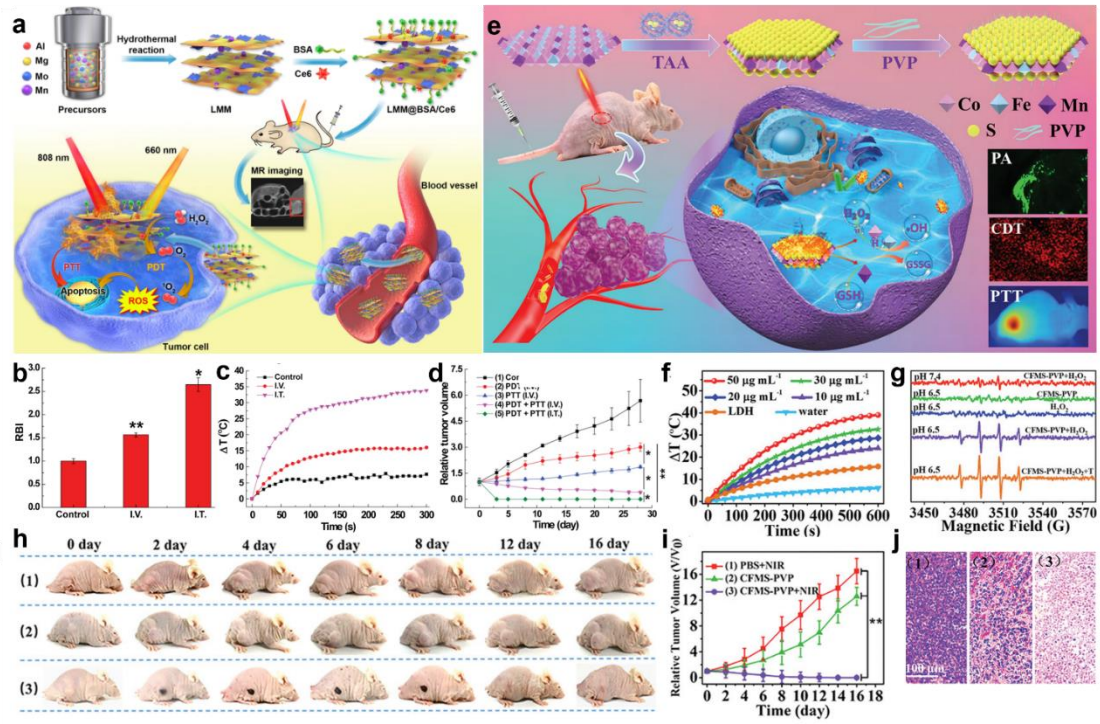

Fig. 14 LDH-based nanomaterials for theranostics. (a) Schematic representation for the synthesis of LMM@Ce6 and its synergistic tumor phototherapy procedure. (b) *In vivo* T_1-weighted MRI intensity of mice tumor after various treatments. (c) Temperature curves of mice tumor under 808 nm irradiation. (d) Tumor growth profile of mice after different treatments. Reproduced with permission from ref. 349. Copyright 2021, Springer International Publishing. (e) Schematic representation for preparing CFMS-PVP NSs to achieve PAI-guided PTT/CDT. (f) Temperature profiles of CFMS-PVP NS at different concentrations. (g) ESR spectra of CFMS-PVP NS with H_2O_2 at different pH and temperatures. (h) Digital photographs of mice from different groups, and (i) corresponding tumor growth profile. (j) Histological staining of tumor sections from mice after various treatments on the 16th day (scale bar: 100 μm). Reproduced with permission from ref. 54. Copyright 2020, Wiley-VCH.

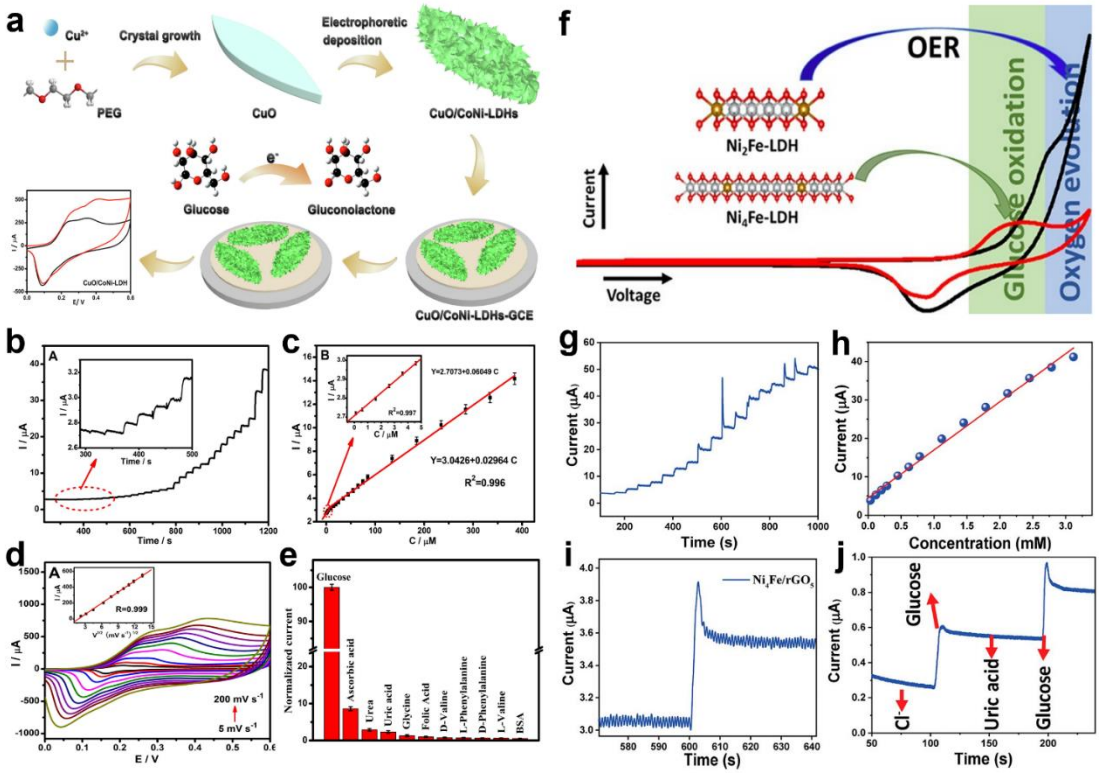

Fig. 15 LDH-based nanomaterials for biosensing. (a) The preparation of CuO/CoNi-LDHs GCE. (b) Typical i-t (current-time) curves of CuO/CoNi-LDHs. (c) Corresponding calibration curve between glucose concentration and current signal. (d) Cyclic voltammetry curves of CuO/CoNi-LDHs with glucose (1.0 mM). (e) Normalized current of CuO/CoNi-LDHs for glucose with various interferences. Reproduced with permission from ref. 124. Copyright 2021, Elsevier. (f) Schematic illustration of NiFe-LDH for glucose detection. (g) Chronoamperometric response of NiFe-LDH/rGO with additions of glucose. (h) Calibration curve for NiFe-LDH/rGO. (i) response time, and (j) selectivity of NiFe-LDH/rGO with addition of uric acid and Cl^- ions. Reproduced with permission from ref. 57. Copyright 2020, American Chemical Society.

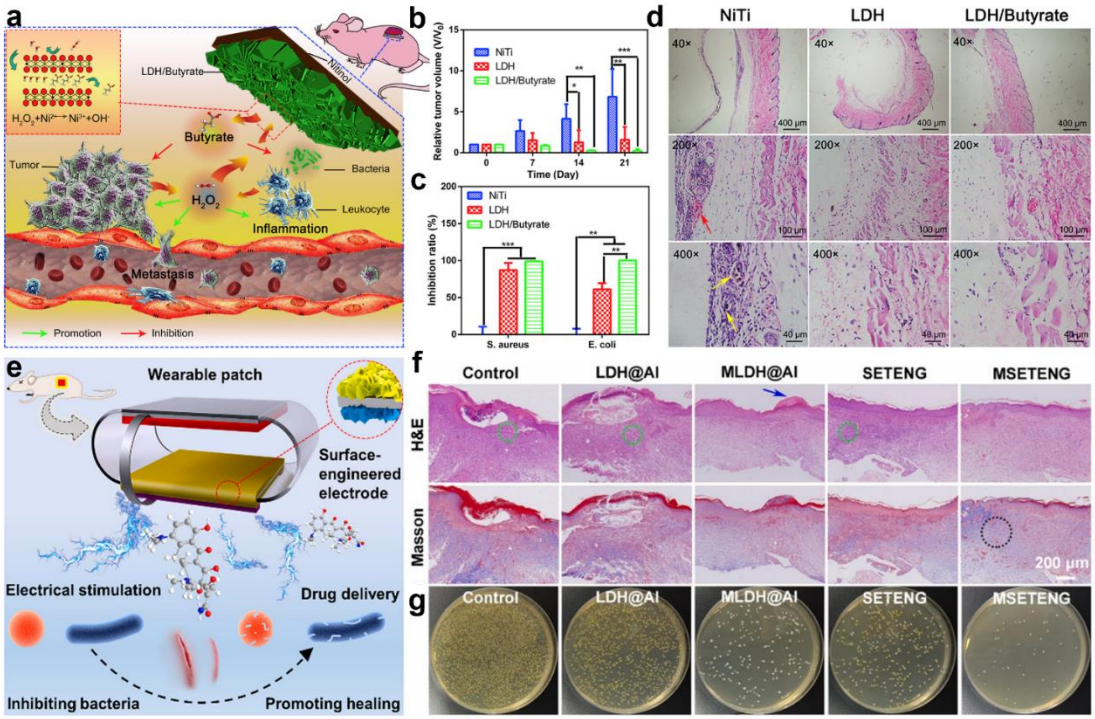

Fig. 16 LDH-based nanomaterials for anti-bacterial applications. (a) Illustration of H_2O_2-mediated bacteria-killing abilities of LDH/Butyrate. (b) Tumor volumes of mice after treatment with different samples. (c) Inhibition ratio of different samples to *E. coli* and *S. aureus*. (d) Histological staining of the wound site tissues with different samples. Reproduced with permission from ref. 425. Copyright 2017, Elsevier. (e) Schematic illustration of the triboelectric nanogenerator patch for the drug loading and infected wounds healing. (f) Histological staining images of the wound site tissues sections on day 10, and (g) *S. aureus* in wound secretions of different groups after treatment for 5 days. Reproduced with permission from ref. 426. Copyright 2021, Elsevier.

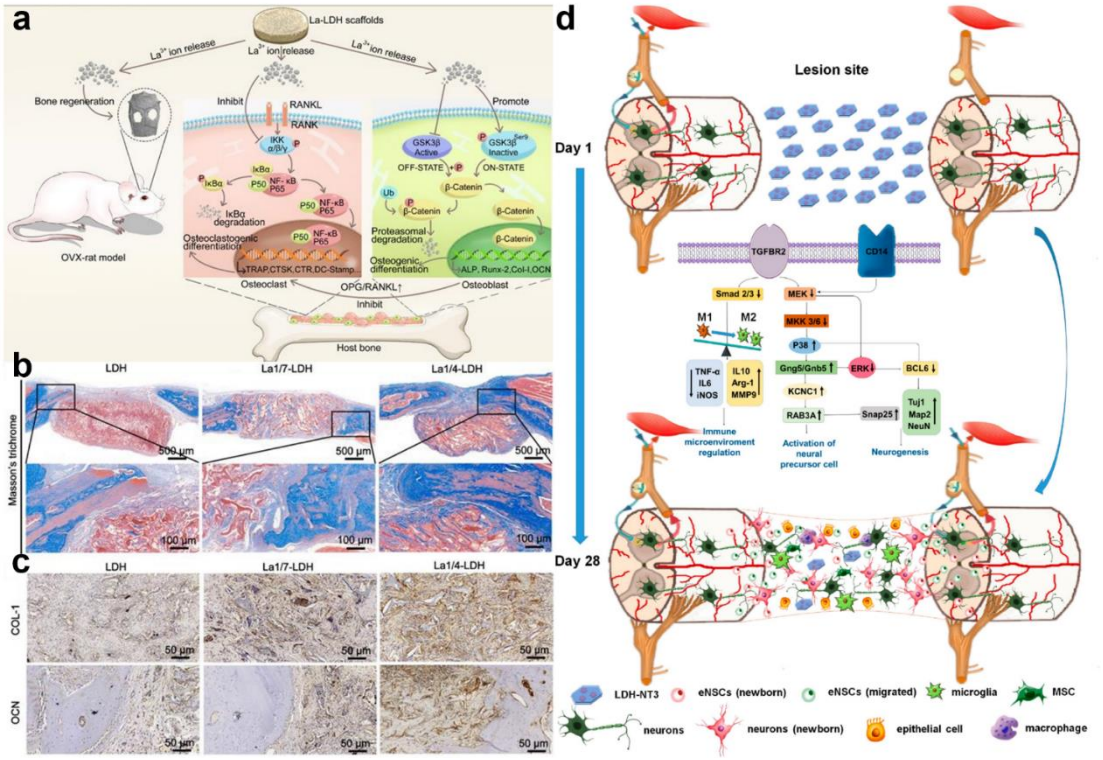

Fig. 17 LDH-based nanomaterials for tissue engineering. (a) Schematic representation of the biological effects of La-LDH scaffolds. (b) Histological staining images of collagen components and (c) immunohistochemical staining images of collagen type I (COL-I) and osteocalcin (OCN) for LDH, La1/7-LDH (Al/La molar ratios of 7:1) and La1/4-LDH (Al/La molar ratios of 4:1) groups. Reproduced with permission from ref. 448. Copyright 2021, Ivyspring International Publisher. (d) Schematic diagram of neural regeneration/neural circuit reconstruction after LDH transplantation in spinal cord injury mice. Reproduced with permission from ref. 458. Copyright 2021, American Chemical Society.

Table 1 Summary of reported LDH-based nanomaterials for controlled drug release applications.

Nanomaterial	Drugs	Release mechanism	Application	Ref.
Sorafenib/ZnAl-LDH	Sorafenib	Corrosion mechanism	Drug delivery for cancer therapy	189
MgAl-Dexa-LDHs	Dexamethasone (Dexa)	Ion exchange/ Corrosion mechanism	Controlled drug release	190
Fe_3O_4@(ENR-MgAl-LDH)	Enrofloxacin (ENR)	Ion exchange mechanism	Sustained release of ENR	191
CaAl-LDH:PZQ	Praziquantel (PZQ)	Corrosion mechanism	Drug delivery for increased dissolution rate of PZQ	192
SIM/ZnAl-LDHs	Simvastatin (SIM)	Ion exchange/ Corrosion mechanism	Sustained release of SIM for bone generation	193
ZnAl-Cl-GLIB; MgAl-Cl-GLIB	Glibenclamide (GLIB)	Corrosion mechanism	Drug delivery for the treatment of diabetes mellitus II	194
ZnAl-LDH-Cip	Ciprofloxacin (Cip)	Ion exchange mechanism	Composite dressings for controlled antimicrobial topical delivery	195
KYNA/MgAl-LDH	Kynurenic acid (KYNA)	Corrosion mechanism	Drug delivery for peptic ulcer diseases.	196
PRN-MgAl-LDH	Pirenoxine sodium (PRN)	Ion exchange mechanism	Ocular drug delivery	197
CD/ZnAl-LDHs	Cefadroxil(CD)	Corrosion mechanism	CD controlled release	198

Table 2 Summary of analytical performance parameters of LDH-based biosensors for biomolecules detection.

Material	Electrode	Target	Linear range	Detection limit	Sensitivity	Sample	Ref.
ZnNiAl-LDH/rGO	GCE	Uric acid	0.0011-0.95 μM	0.9 nM		Human urine	397
		Ascorbic acid	0.5-11 μM	13.5 nM			
DNA/GO/$CoFe_2O_4$/ZnAl-LDH	Fluorine tin oxide (FTO) substrate	Etoposide	0.2~10 μM	0.0010 μM	63.408 μA μM^{-1}	Human blood plasma, serum and urine	398
XnOx/ZnAl-LDHs		Xanthine	1×10^{-6}~2×10^{-4} M	1×10^{-7} M	220 mA M^{-1} cm^{-2}		399
ZnAl-CoTsPc-LDH	GCE	GSH	1~818 μM	0.2 μM	2.16 μA cm^{-2} M^{-1}	Human blood erythrocytes	400
MWCNTs/NiAl-LDH/GO	GCE	Guanine	0.01-45 μM	3 nM		Thermally denatured DNA	401
		Adenine	0.08-45 μM	20 nM			
CNF-NiCo-LDH	GCE	Metronidazole	3~57 nM	0.13 nM	1.294 μA nM^{-1} cm^{-2}	Human plasma, tears, commercial tablets, human urine	402
Ferrocenecarboxylic acid@MgAl-LDH	GCE	Prostate-specific antigen	0.05 pg mL^{-1} ~ 50 ng mL^{-1}	0.034 pg mL^{-1}		Human serum	403
MgAl-LDH/MWCNTs		Bambuterol hydrochloride	1.0×10^{-7}~1.0×10^{-2} M	2.3×10^{-8} M		Human plasma and urine	404
MgAl-LDH/TNT			1.0×10^{-6}~1.0×10^{-2} M	2.5×10^{-7} M			

Table 3 Summary of applications of LDH-based materials in tissue engineering.

Nanomaterial	Functionalization/Scaffold	Application	Ref.
MgAl-LDH	Pure Mg	Protective coating on Mg for orthopedic applications	463
FA-MgAl-LDH	CS	Implant materials, bone and teeth additives, and bone tissue engineering	464
NAP-MgFeAl-LDH	Poly(lactic acid) (PLA)	Polymer dressings	465
MgAl-LDH	PCL	3D scaffolds in bone tissue engineering	466
MgAl-LDH	Pure titanium	Bone regeneration	467
CaAl-LDH	HAP/Gel	Bone regeneration	468
Ag-MgSrFe-LDH	CS	Osteogenic and antibacterial agent	469
MgAl/LDH	Plasmid DNA (PDNA)/miRNA/siRNA	Tissue regeneration	470
Dexamethasone disodium phosphate (DEXP)/MgAl-LDH	Carboxymethyl chitosan (CMCS)	Ocular drug delivery	471
MgAl-LDH	ALG-CS	Oral vaccine delivery	472
MgAl-LDH-enoxacin (ENO)	Polyurethane-polyvinyl alcohol (PU-PVA) hydrogel	Wound dressings	473
NAP/MgFeAl-LDHs; NAP-ZnFeAl-LDHs	Polymer	Wound dressings	474
Bacitracin-MgAl-LDHS	Poly-3-hydroxybutyric acid (P)-sodium alginate (S)-(core-shell) nanofibrous	Healing of cutaneous wound	475
MgAl-LDH	Peptide CK2.1 coated β-glycerophosphate/CS and LL37 modified CS scaffold	The repair of hyaline cartilage and subchondral bone defects	476

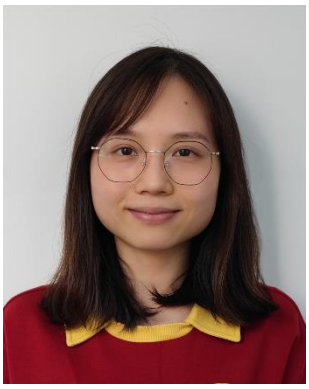

Tingting Hu graduated from Beijing University of Chemical Technology (BUCT) with bachelor degree in 2018. She is now pursuing her PhD degree under the supervision of Prof. Ruizheng Liang at BUCT. Her current interests is on layered double hydroxide (LDH)-based biomaterials for cancer diagnosis and treatment.

Xingcai Zhang is a Harvard/MIT research fellow with expertise in sustainable Nature, bio-derived, inspired, mimetic materials and technologies. He published 100+ peer-reviewed papers in top journals, including *Nat. Rev. Mater.*, *Nat. Nanotechnol.*, *Matter*, *Proc. Natl. Acad. Sci. U. S. A.*, *Nat. Commun.*, *Sci. Adv.*, *J. Am. Chem. Soc.*, *Angew. Chem., Int. Ed.*, *Adv. Mater.*, *Mater. Today*, *Prog. Mater. Sci.*, and *Chem. Soc. Rev*. He has served as a science writer/editor/advisory board member for Nature, Springer, Elsevier, Materials Today, American Chemical Society, The Royal Society of Chemistry, and Wiley. He has also received multiple awards including the Nature Nano Award.

Chaoliang Tan is currently an Assistant Professor in the Department of Electrical Engineering at the City University of Hong Kong. He received his PhD from Nanyang Technological University in 2016. After working as a Research Fellow in the same group for about one year, he then worked as a Postdoctoral Research Fellow at the University of California, Berkeley, for two years. His research focuses on 2D materials for electronics and optoelectronics, and structural engineering of layered materials for biomedicine, energy storage, etc.

Ruizheng Liang received his PhD degree from Beijing University of Chemical Technology (BUCT) in 2015, under the supervision of Prof. Xue Duan and Prof. Min Wei, after which he joined BUCT as the associate professor in the State Key Laboratory of Chemical Resource Engineering. He used to be a visiting student at the University of Oxford (in 2014). He was promoted to professor in 2021. His current interests are mainly focused on: (1) the two-dimensional intercalation chemistry and functional nanomaterials, and (2) the design and fabrication of layered double hydroxide (LDH)-based biomaterials.